2021

Research on Power System State Estimation Problems – Series-Compensated Transmission Line Parameter and Load Model Parameter Estimation

Yiqi Zhang
University of Kentucky, yqz990@gmail.com
Digital Object Identifier: https://doi.org/10.13023/etd.2021.435

STUDENT AGREEMENT:

I represent that my thesis or dissertation and abstract are my original work. Proper attribution has been given to all outside sources. I understand that I am solely responsible for obtaining any needed copyright permissions. I have obtained needed written permission statement(s) from the owner(s) of each third-party copyrighted matter to be included in my work, allowing electronic distribution (if such use is not permitted by the fair use doctrine) which will be submitted to UKnowledge as Additional File.

I hereby grant to The University of Kentucky and its agents the irrevocable, non-exclusive, and royalty-free license to archive and make accessible my work in whole or in part in all forms of media, now or hereafter known. I agree that the document mentioned above may be made available immediately for worldwide access unless an embargo applies.

I retain all other ownership rights to the copyright of my work. I also retain the right to use in future works (such as articles or books) all or part of my work. I understand that I am free to register the copyright to my work.

REVIEW, APPROVAL AND ACCEPTANCE

The document mentioned above has been reviewed and accepted by the student's advisor, on behalf of the advisory committee, and by the Director of Graduate Studies (DGS), on behalf of the program; we verify that this is the final, approved version of the student's thesis including all changes required by the advisory committee. The undersigned agree to abide by the statements above.

Yiqi Zhang, Student

Dr. Yuan Liao, Major Professor

Dr. Daniel Lau, Director of Graduate Studies

Research on Power System State Estimation Problems – Series-Compensated Transmission Line Parameter and Load Model Parameter Estimation

---

DISSERTATION

A dissertation submitted in partial fulfillment of the

requirements for the degree of Doctor of Philosophy in the

College of Engineering

at the University of Kentucky

By

Yiqi Zhang

Lexington, Kentucky

Director: Dr. Yuan Liao, Professor of Electrical and Computer Engineering

Lexington, Kentucky

2021

ABSTRACT OF DISSERTATION

Research on Power System State Estimation Problems – Series-Compensated Transmission Line Parameter and Load Model Parameter Estimation

Transmission line and load model parameters are essential inputs to power system modeling and simulation, control, protection, operation, optimization, and planning. These parameters usually vary over time or under different operating conditions. Thus, reliable estimation methods are desired to ensure the accuracy of those parameters. This research focuses on estimation for transmission line parameters and the ZIP load model. The proposed estimation methods can use both online measurements and historical data of a specified duration. The parameters of long transmission lines with different series-compensation configurations are estimated using linear methods and optimal estimators with bad data detection capability. Additionally, Kalman filter estimation methods have been proposed to improve the estimation accuracy and to track the dynamically changing line parameters under the effect of measurement noises. The estimation methods are tested with data generated using Matlab Simulink. For the ZIP load model parameter estimation, theoretical formulation for the aggregate ZIP load model has been established. The least squares, optimization, neural network, and Kalman filter methods have been investigated to estimate ZIP parameters and been verified based on OpenDSS simulation data.

KEYWORDS: line parameter, Kalman Filter, least squares, neural network, optimization, ZIP load model

Yiqi Zhang

12/02/2021

Research on Power System State Estimation Problems – Series-Compensated Transmission Line Parameter and Load Model Parameter Estimation

By
Yiqi Zhang

Yuan Liao
Director of Dissertation

Daniel Lau
Director of Graduate Studies

12/06/2021
Date

ACKNOWLEDGEMENTS

I would first like to thank my advisor, Dr. Yuan Liao, whose expertise was invaluable in formulating the research problems and methodology. His insightful feedback pushed me to sharpen my thinking and brought my work to a higher level. In addition, I would like to thank my wife and my parents who all have been supportive and caring. I could not have completed this dissertation without the support from them. Finally, I would like to acknowledge the Electrical and Computer Engineering Department of the University of Kentucky for the Teaching Assistantship and LGE&KU for the Research Assistantship I received during my studies.

TABLE OF CONTENTS

LIST OF TABLES

LIST OF FIGURES

CHAPTER 1 INTRODUCTION

1.1 Transmission Line Parameter Estimation

1.1.1 Background

Transmission line and load model parameters are essential inputs to power system modeling and simulation, control, protection, operation, optimization, and planning. These parameters usually vary over time or under different operating conditions. Thus, reliable estimation methods are desired to ensure the accuracy of those parameters.

An electric power system can be divided into three parts: power generation, power transmission, and power consumption. Power transmission can be further divided into two parts: transmission (transmitting power from the power plant to substations) and distribution (distributing power from substation to customer). Transmission line parameters including series impedance, series reactance, and shunt susceptance are required by a variety of power system analysis applications, including power flow and contingency analysis for efficient and reliable operation and optimal planning [2], protective relaying applications [3][4], and impedance-based fault location detection [5][6][7][8][9]. Thus, the accuracy of transmission line parameters is critical, and estimation algorithms with high accuracy are strongly desired.

1.1.2 Review of Transmission Line Parameter Estimation

Transmission line parameter estimation methods can be classified into offline methods and online methods. Offline methods estimate line parameters based on factors such as conductor dimensions and line length under an assumed ambient environment. However, offline methods can

be inaccurate and unreliable due to the discrepancy between the assumed conditions and the actual conditions.

Hence, to estimate transmission line parameters accurately, the estimation methods need to adapt to the changes in conditions. To accommodate the changes in ambient environmental conditions and obtain line parameters in real-time, some online estimation algorithms have been proposed in [1], [11], [12], and [13]-[15]. The authors in [1],[12], and [14] proposed methods based on linear estimation theory. The method that was presented in [1] estimates positive sequence line parameters using the linear least squares method. A linear method was proposed in [12] to estimate transmission line parameters for non-compensated and series-compensated lines. An optimal estimator was also proposed as well to detect and identify possible measurement errors in [12]. The author of [12] proposed a linear estimation method for transposed lines based on distributed parameter line model.

Non-linear estimation methods for estimating positive sequence transmission line parameters have been proposed in [11], [13], and [15]. In [11], methods of using both synchronized and unsynchronized voltage and current measurements to estimate line parameters were proposed. In [13], the author proposed a method for the detection and identification of bad measurements. The author of [15] proposed a non-linear estimation method that can detect and identify bad measurement data and minimize the impact of measurement errors. Moreover, a method of optimizing the scheme of Phasor Measurement Units (PMUs) placement in the system was proposed. The goal is to minimize the number of PMUs that need to be installed.

1.1.3 Motivation and Objectives

First, most existing transmission line estimation methods are developed for non-compensated transmission lines. However, in real power systems, ultra-high voltage transmission

lines are series compensated. Therefore, it is important to develop estimation methods for series compensated transmission lines. This research puts forward an optimal estimator for different series-compensated lines. Considering the potential of the exitance of bad measurements, a bad detection method is introduced. In addition, Kalman filter based approaches are proposed to improve the estimation performance under the effect of measurement noise.

Second, most estimation methods are proposed under the assumption that line parameters are static. However, line parameters are continuously changing over time with varying loading and weather conditions. This research proposes Kalman filtering based methods that employ voltage and current measurements from line terminals and require no extra information to track parameters of long transmission lines dynamically. In addition, the proposed methods are applicable to transmission lines with different series compensation configurations.

1.2 ZIP Load Model Parameter Estimation

1.2.1 Background

Load modeling is important to power system control, planning, and analysis. It describes the relationship between the power and voltage in a load bus using mathematical representation [10]. Constant impedance, constant current, constant power (ZIP) load modeling has been widely used in steady-state and dynamic studies [17]. The ZIP load model is used in the optimal power flow study [18], feeder load forecasting [19], and voltage stability analysis [20]. In [36], the authors proposed an equivalent modeling method for multi-port area load based on the extended generalized ZIP load model. The authors of [65] used the ZIP load model in evaluating the impact of load models on power transfer limits. The ZIP load parameters are also useful for examining the benefits of conservation through voltage reduction (CVR) and voltage and var optimization (VVO) program [21][22][23]. Therefore, it is crucial to have accurate ZIP load model parameters.

1.2.2 Review of ZIP Load Model Parameter Estimation

Various estimation methods have been used to estimate ZIP parameters. An optimization method was proposed in [24] to estimate ZIP parameters. The algorithm is tested on a two-bus system. The least squares method was proposed in [25] to determine the ZIP coefficients for residential appliances. In [26], the time-varying ZIP parameters were estimated using a neural network method with sliding window using the single-phase data at a transformer.

The individual load models are used in power system distribution system analysis such as integrating distributed energy resources with improved power quality and reliability. The household appliances and industrial equipment were tested in the laboratory by varying the voltage to find individual ZIP parameters in [25]. In [29], a method for estimating individual ZIP load model by analyzing the load switching events across the distribution feeder is proposed. In [30], the authors developed a ZIP load model for residential house appliances.

The feeder-level aggregate load model is also very important as it is used in various distribution and transmission system analyses. In [28], the authors proposed a hybrid learning algorithm that combines the genetic algorithm (GA) and the nonlinear Levenberg–Marquardt (L-M) algorithm for the aggregate ZIP load model estimation. In [27], the household and feeder level ZIP parameters are obtained by aggregating the appliance-level ZIP parameters.

1.2.3 Motivation and Objectives

For the aggregate ZIP parameter estimation studies in power systems, it is common to use the three-phase average voltage as the voltage variable for the ZIP load model. However, little research has focused on the theoretical formulation for the aggregate ZIP load and how different factors can contribute to the estimation results. Apparently, the voltage of one phase will not determine the power consumed by a load at another phase. Thus, the use of average voltage can

cause uncertainty in ZIP parameter estimation in unbalanced systems, which should be carefully analyzed. Moreover, the load connection type (star or delta) can also affect the estimation results. The measurement noise, load unbalance, voltage unbalance, and load connection types are examined in detail in this research.

1.3 Dissertation Outline

The remainder of this dissertation is organized as follows:

In Chapter 2, the optimal estimator and bad data detection techniques for transmission line parameter estimation are introduced first. Then, the Kalman filter based transmission line parameter estimation approaches for lines with different series compensated configurations are discussed. Additionally, the Kalman filter based line parameter tracking methods are proposed to track dynamically changing line parameters.

Chapter 3 presents the case studies for the proposed transmission line parameter estimation methods. Different series compensated transmission line models are built in Matlab Simscape Electrical. The proposed estimation methods are implemented in Matlab to estimate line parameters using simulation from the models.

Chapter 4 is dedicated to ZIP load parameter estimation. The different ZIP load model parameter estimation methods (including least squares, optimization, Kalman filter, neural network) are discussed. Then theoretical formulation for aggregate ZIP load model is studied. The analysis for aggregate ZIP load model.

Chapter 5 the case studies for ZIP load model parameter estimation. The IEEE 13-bus and 34-bus systems are simulated in OpenDSS with loads set to ZIP load model. The proposed ZIP

parameter estimation methods are implemented in Matlab to estimate the ZIP load model parameters. The estimation results are analyzed and explained in detail.

Chapter 6 presents the final conclusion for this research.

CHAPTER 2 PROPOSED TRANSMISSION LINE PARAMETER ESTIMATION METHODS

Series compensation is a way of increasing power transfer capacity by connecting series capacitors in series with the line. As discussed before, the series compensator can be installed at different positions of a transmission line.

In Section 2.1 and 2.2, linear estimation methods were proposed for mid-compensated line and two-end compensated line. Additionally in Section 2.1, an optimal estimator method is proposed to estimate the line parameters for the mid-compensated line; a bad data detection method is proposed to eliminate bad measurements. In Section 2.3, the Kalman filter based approaches were proposed for different compensated lines; Also, a Kalman filter based tracking method is introduced to track dynamically changing line parameters.

2.1 Mid-Compensated Line

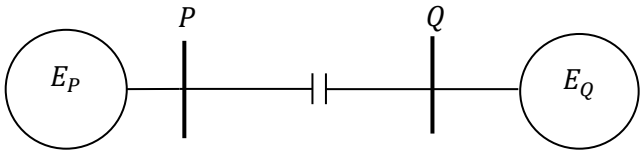

Figure 2.1 The schematic diagram for a two-bus system with a series compensator installed at the middle of the transmission line.

A two-bus system is shown in Figure 2.1, where P is the sending end and Q is the receiving end. E_P and E_Q are the Thevenin equivalent sources. PMUs are installed at both ends for recording the synchronized voltage and current phasors. Line parameters including series resistance, series

reactance, and shunt susceptance, can be obtained based on the line's positive-sequence equivalent π circuit.

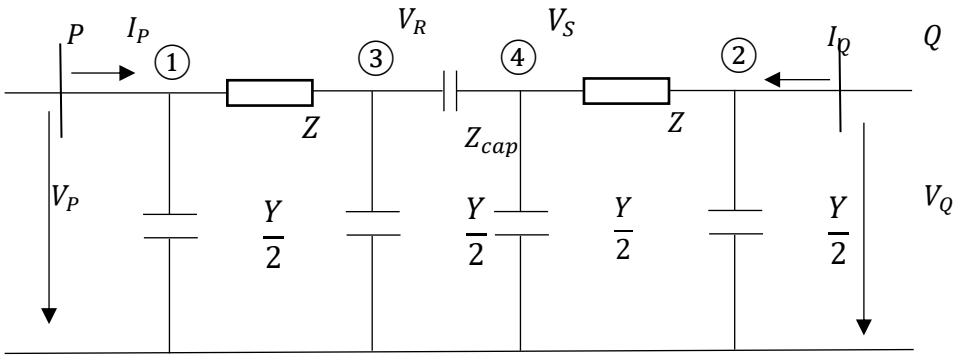

Figure 2.2 The equivalent-π circuit of the positive sequence network of the mid-compensated line with known Z_{cap}.

Figure 2.2 shows the equivalent π circuit of the positive sequence network of a transmission line with a series compensator installed at the middle of the transmission line. In this figure, V_P and I_P are the positive sequence voltage and current at the sending end P, while V_Q and I_Q are the positive sequence voltage and current at the receiving end Q. The voltage and current at both ends are measured by PMUs. In addition, Z and Y represent the positive sequence series impedance and shunt admittance of each equivalent π circuit, and Z_{cap} is the series impedance of the series compensator. Based on the distributed parameter line model in [31], Z and Y can be expressed as follows:

$$Z = Z_c \sinh(\gamma l) \tag{2.1}$$

$$\frac{Y}{2} = \frac{\tanh(\gamma l/2)}{Z_c} \tag{2.2}$$

$$Z_c = \sqrt{z_1/y_1} \tag{2.3}$$

$$\gamma = \sqrt{z_1 y_1} \tag{2.4}$$

where Z_c and γ are the characteristic impedance and the propagation constant of the line respectively, z_1 is the positive sequence series impedance per unit length, y_1 is the positive sequence shunt admittance per unit length, and l is half the length of the line.

2.1.1 Methods for the Case of Known Impedance of Series Compensator

2.1.1.1 Linear Method

For simplicity, we define the unknown variables $a = \frac{Y}{2} + \frac{1}{Z}$ and $b = \frac{1}{Z}$. Assume that Z_{cap} is known and $Y_{cap} = \frac{1}{Z_{cap}}$.

The voltage and current at each node of this power transmission network can be related by the admittance matrix as

$$\begin{bmatrix} I_P \\ I_Q \\ 0 \\ 0 \end{bmatrix} = \begin{bmatrix} a & 0 & -b & 0 \\ 0 & a & 0 & -b \\ -b & 0 & a + Y_{cap} & -Y_{cap} \\ 0 & -b & -Y_{cap} & a + Y_{cap} \end{bmatrix} \begin{bmatrix} V_P \\ V_Q \\ V_R \\ V_S \end{bmatrix} \tag{2.5}$$

Use node elimination technique, the following equation can be obtained

$$\begin{bmatrix} I_P \\ I_Q \end{bmatrix} = \begin{bmatrix} A & \mathrm{B} \\ \mathrm{B} & A \end{bmatrix} \begin{bmatrix} V_P \\ V_Q \end{bmatrix} \tag{2.6}$$

where

$$A = a - \frac{b^2}{a} + \frac{Y_{cap} b^2}{a^2 + 2aY_{cap}} \tag{2.7}$$

$$B = -\frac{b^2 Y_{cap}}{a^2 + 2aY_{cap}} \tag{2.8}$$

Eq. (2.6) can be rewritten as

$$\begin{bmatrix} I_P \\ I_Q \end{bmatrix} = \begin{bmatrix} V_P & V_Q \\ V_Q & V_P \end{bmatrix} \begin{bmatrix} A \\ B \end{bmatrix} \tag{2.9}$$

Hence, A and B can be determined by

$$\begin{bmatrix} A \\ B \end{bmatrix} = \begin{bmatrix} V_P & V_Q \\ V_Q & V_P \end{bmatrix}^{-1} \begin{bmatrix} I_P \\ I_Q \end{bmatrix} \tag{2.10}$$

Consequently, a and b can be calculated as

$$a = \frac{A - B}{1 + B/Y_{cap}} \tag{2.11}$$

$$b = \sqrt{-B\left(a^2 + 2aY_{cap}\right)/Y_{cap}} \tag{2.12}$$

Once a and b are known, Z and $\frac{Y}{2}$ can be obtained by

$$Z = \frac{1}{b} \tag{2.13}$$

$$\frac{Y}{2} = a - b \tag{2.14}$$

Denote c as the product of Z and $\frac{Y}{2}$. From (2.13) and (2.14), we have

$$c = \frac{ZY}{2} = Z_c \sinh(\gamma l) \frac{\tanh(\gamma l/2)}{Z_c} = \sinh(\gamma l) \tanh(\gamma l/2) \tag{2.15}$$

Let $d = \gamma l$ and rewrite (2.15) as

$$e^{2d} - (2 + 2\mathrm{c})e^d + 1 = 0 \tag{2.16}$$

Solving the quadratic equation (2.16) gives two solutions for e^d, from which we can compute two possible values for γ using (2.17). However, only one of them is correct. The real part of the correct value is greater than zero while the real part of the incorrect value is less than zero.

$$\gamma = \frac{1}{l}\ln(e^d) \tag{2.17}$$

Consequently, the characteristic impedance can be calculated based on (2.1) as

$$Z_c = \frac{Z}{\sinh(\gamma l)} \tag{2.18}$$

Finally, the line parameters are solved using (2.3) and (2.4)

$$z_1 = Z_c\gamma \tag{2.19}$$

$$y_1 = \frac{\gamma}{Z_c} \tag{2.20}$$

2.1.1.2 Optimal Estimator and Bad Data Detection

When we have n $(n \geq 2)$ sets of measurements, the optimization of measurements and line parameters can be performed. Define measurement vector M as

$$M = \left[V_{P_1}, I_{P_1}, V_{Q_1}, I_{Q_1}, \dots, V_{P_n}, I_{P_n}, V_{Q_n}, I_{Q_n}\right] \tag{2.21}$$

where $V_{P_i}, I_{P_i}, V_{Q_i}$, and I_{Q_i} are the voltage and current at both ends of the i^{th} set measurement. Define the state to be estimated as

$$X = [x_1, x_2, \dots, x_{8\mathrm{n}}, x_{8n+1}, x_{8n+2}, x_{8n+3}]^T \tag{2.22}$$

where $x_1, \dots, x_{8n}$ represent the magnitude and angle of the total $4n$ measurements, x_{8n+1} represents the series resistance $Re(z_1)$, x_{8n+2} represents series reactance $Im(z_1)$ and x_{8n+3} represents shunt susceptance $Im(y_1)$.

Define F as the function vector. F_{4i-3} to F_{4i} are defined as the real and imaginary part of Eq. (2.7) and Eq. (2.8) for the i^{th} set measurement. The remaining function vectors can be defined as

$$F_{4n+2i-1}(X) = Re\left(x_{2i-1}e^{jx_{2i}}\right), \quad i = 1, \dots, 4n \tag{2.23}$$

$$F_{4n+2i}(X) = Im\left(x_{2i-1}e^{jx_{2i}}\right), \quad i = 1, \dots, 4n \tag{2.24}$$

Define Y as the measurement vector,

$$Y_i = 0, \quad i = 1, \dots, 4n \tag{2.25}$$

$$Y_{4n+2i-1} = Re(M_i), \quad i = 1, \dots, 4n \tag{2.26}$$

$$Y_{4n+2i} = Im(M_i), \quad i = 1, \dots, 4n \tag{2.27}$$

The relationship between the measurement vector and the function vector can be represented by

$$Y = F(X) + \mu \tag{2.28}$$

where μ is the measurement error which depends on meter accuracy.

The optimization is achieved by finding the minimum value of cost function J

$$J = (F(X) - Y)R^{-1}(F(X) - Y) \tag{2.29}$$

where R is the Covariance matrix for all measurements. Then Eq. (2.29) can be solved by using the Newton-Raphson method and the optimal estimation for measurements and line parameters can be obtained.

To detect and identify bad data, we use Chi-Square Test. First, we calculate the expected value of the cost function E_J and the estimated value of the cost function C_J. Then a threshold value

of $\chi^2_{k,\alpha}$ can be obtained based on the number of degrees of freedom k, a desired confidence level α, and the Chi-Square distribution. If $C_J \geq \chi^2_{k,\alpha}$, then there is a probability of $(1-\alpha)$ for the presence of bad data. The bad measurement has the greatest standardized error.

2.1.2 Method for the Case of Known Current Through Series Compensator

In this case, Z_{cap} is considered as an unknown, but the current through the capacitor is considered as known. Note that the voltage at the capacitor location is not known. Figure 2.3 shows the same model as in Figure 2.2 except here we know the current through the capacitor available.

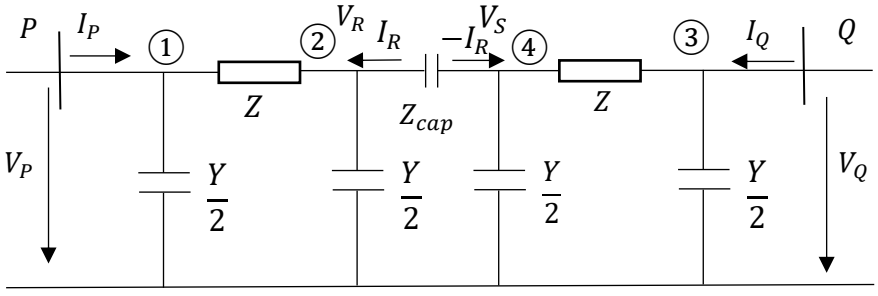

Figure 2.3 The equivalent-π circuit of the positive sequence network of the mid-compensated line with known I_R.

We define the unknown variables $a = \frac{Y}{2} + \frac{1}{Z}$ and $b = \frac{1}{Z}$ as before. Again, we write KCL equations for the four nodes as follows.

For node ①,

$$I_P = \frac{Y}{2}V_P + \frac{1}{Z}(V_P - V_R) = aV_P - bV_R \tag{2.30}$$

For node ②,

$$I_R = \frac{1}{Z}(V_R - V_P) + \frac{Y}{2}V_R = -bV_P + aV_R \tag{2.31}$$

For node ③,

$$I_Q = \frac{Y}{2}V_Q + \frac{1}{Z}(V_Q - V_S) = aV_Q s - bV_S \tag{2.32}$$

For node ④,

$$-I_R = \frac{1}{Z}(V_S - V_Q) + \frac{Y}{2}V_S = -bV_Q + aV_S \tag{2.33}$$

Based on (2.30) and (2.31), V_R can be eliminated

$$aI_P + bI_R = (a^2 - b^2)V_P \tag{2.34}$$

Based on (2.32) and (2.33), V_S can be eliminated

$$aI_Q - bI_R = (a^2 - b^2)V_Q \tag{2.35}$$

Multiply V_Q to (2.34) and V_P to (2.35), then subtract the resultant equations. Then a can be expressed in terms of b,

$$a = \frac{I_R(V_P + V_Q)}{I_Q V_P - I_P V_Q}b \tag{2.36}$$

This indicates that a and b are proportional to each other. Let the proportional constant be C, i.e.,

$$C = \frac{I_R(V_P + V_Q)}{I_Q V_P - I_P V_Q} \tag{2.37}$$

In fact, C is obtained through measurements. Hence, it can be used to determine a and b. To this end, substitute $a = Cb$ for a in (2.34), we get

$$b = \frac{CI_P + I_R}{(C^2 - 1)V_P} \tag{2.38}$$

2.2 Two-End Equivalent Compensated Line

The two-end equivalent compensation is the case where two same series compensators are installed at both ends of a transmission line. Figure 2.4 shows the equivalent π circuit of the positive sequence network of a transmission line with two-end equivalent compensation during normal operations. Y_{cap} is the admittance of each capacitor. In this method, the known quantities are voltages and currents at the two terminals. We will determine Y, Z, and Y_{cap} from the measurements.

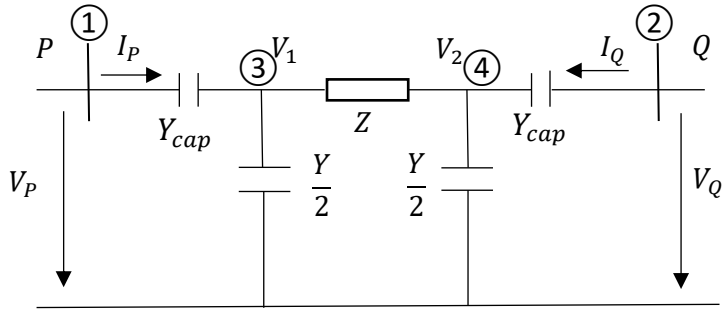

Figure 2.4 The equivalent-π circuit of the positive sequence network of the two-end equivalent compensated line.

Based on Kirchhoff's Current Law(KCL), we can write the following equations for each node.

For node ①,

$$I_P = (V_P - V_1)Y_{cap} = Y_{cap}V_P - Y_{cap}V_1 \tag{2.39}$$

For node ②,

$$I_Q = (V_Q - V_2)Y_{cap} = Y_{cap}V_Q - Y_{cap}V_2 \tag{2.40}$$

For node ③,

$$\begin{aligned} 0 &= Y_{cap}(V_1 - V_P) + \frac{Y}{2}V_1 + \frac{1}{Z}(V_1 - V_2) \\ &= -Y_{cap}V_P + \left(Y_{cap} + \frac{Y}{2} + \frac{1}{Z}\right)V_1 - \frac{1}{Z}V_2 \end{aligned} \tag{2.41}$$

For node ④,

$$\begin{aligned} 0 &= Y_{cap}(V_2 - V_Q) + \frac{Y}{2}V_2 + \frac{1}{Z}(V_2 - V_1) \\ &= -Y_{cap}V_Q + \left(Y_{cap} + \frac{Y}{2} + \frac{1}{Z}\right)V_2 - \frac{1}{Z}V_1 \end{aligned} \tag{2.42}$$

In vector-matrix form, (2.39) – (2.42) become

$$\begin{bmatrix} I_P \\ I_Q \\ 0 \\ 0 \end{bmatrix} = \begin{bmatrix} Y_{cap} & 0 & -Y_{cap} & 0 \\ 0 & Y_{cap} & 0 & -Y_{cap} \\ -Y_{cap} & 0 & \frac{Y}{2} + \frac{1}{Z} + \frac{1}{Z_{cap}} & -\frac{1}{Z} \\ 0 & -Y_{cap} & -\frac{1}{Z} & \frac{Y}{2} + \frac{1}{Z} + \frac{1}{Z_{cap}} \end{bmatrix} \begin{bmatrix} V_P \\ V_Q \\ V_1 \\ V_2 \end{bmatrix} \tag{2.43}$$

Use node elimination technique, (2.43) can be reduced to the following form

$$\begin{bmatrix} I_P \\ I_Q \end{bmatrix} = \begin{bmatrix} A & B \\ B & A \end{bmatrix} \begin{bmatrix} V_P \\ V_Q \end{bmatrix} \tag{2.44}$$

The node elimination process is given below. First, let $a = \frac{Y}{2} + \frac{1}{Z}$ and $b = \frac{1}{Z}$, (2.39) – (2.42) can be rewritten as

$$I_P = Y_{cap}V_P - Y_{cap}V_1 \tag{2.45}$$

$$I_Q = Y_{cap}V_Q - Y_{cap}V_2 \tag{2.46}$$

$$0 = -Y_{cap}V_P + \left(Y_{cap} + a\right)V_1 - bV_2 \tag{2.47}$$

$$0 = -Y_{cap}V_Q + \left(Y_{cap} + a\right)V_2 - bV_1 \tag{2.48}$$

Based on (2.48), V_2 can be expressed in terms of V_Q and V_1

$$V_2 = \frac{Y_{cap}}{Y_{cap} + a}V_Q + \frac{b}{Y_{cap} + a}V_1 \tag{2.49}$$

Substitute (2.49) for V_2, (2.47) can be rewritten as

$$0 = -Y_{cap}V_P + \left(Y_{cap} + a\right)V_1 - b\left(\frac{Y_{cap}}{Y_{cap} + a}V_Q + \frac{b}{Y_{cap} + a}V_1\right) \tag{2.50}$$

Based on (2.50), V_1 can be expressed in terms of V_P and V_Q

$$V_1 = \frac{Y_{cap}\left(Y_{cap} + a\right)}{\left(Y_{cap} + a\right)^2 - b^2}V_P + \frac{Y_{cap}b}{\left(Y_{cap} + a\right)^2 - b^2}V_Q \tag{2.51}$$

Substitute (2.49) for V_2 and then (2.51) for V_1 in (2.45), I_Q can be expressed in terms of V_P and V_Q

$$I_Q = -\frac{{Y_{cap}}^2 b}{\left(Y_{cap} + a\right)^2 - b^2}V_P + \left(Y_{cap} - \frac{{Y_{cap}}^2\left(Y_{cap} + a\right)}{\left(Y_{cap} + a\right)^2 - b^2}\right)V_Q \tag{2.52}$$

Substitute (2.51) for V_1 in (2.45), I_P can be expressed in terms of V_P and V_Q

$$I_P = \left(Y_{cap} - \frac{{Y_{cap}}^2\left(Y_{cap} + a\right)}{\left(Y_{cap} + a\right)^2 - b^2}\right)V_P - \frac{{Y_{cap}}^2 b}{\left(Y_{cap} + a\right)^2 - b^2}V_Q \tag{2.53}$$

In vector-matrix form (2.52) and (2.53) become

$$\begin{bmatrix} I_P \\ I_Q \end{bmatrix} = \begin{bmatrix} Y_{cap} - \dfrac{{Y_{cap}}^2 (Y_{cap} + a)}{(Y_{cap} + a)^2 - b^2} & -\dfrac{{Y_{cap}}^2 b}{(Y_{cap} + a)^2 - b^2} \\ -\dfrac{{Y_{cap}}^2 b}{(Y_{cap} + a)^2 - b^2} & Y_{cap} - \dfrac{{Y_{cap}}^2 (Y_{cap} + a)}{(Y_{cap} + a)^2 - b^2} \end{bmatrix} \begin{bmatrix} V_P \\ V_Q \end{bmatrix} \tag{2.54}$$

Let

$$A = Y_{cap} - \frac{{Y_{cap}}^2 (Y_{cap} + a)}{(Y_{cap} + a)^2 - b^2} \tag{2.55}$$

$$B = -\frac{{Y_{cap}}^2 b}{(Y_{cap} + a)^2 - b^2} \tag{2.56}$$

Then (2.54) is in the form of (2.44). Based on (2.55) and (2.56), (2.54) represents two linear equations,

$$\begin{cases} I_P = AV_P + BV_Q = V_P \cdot A + V_Q \cdot B \\ I_Q = BV_P + AV_Q = V_Q \cdot A + V_P \cdot B \end{cases} \tag{2.57}$$

Therefore, the following equation can be obtained

$$\begin{bmatrix} I_P \\ I_Q \end{bmatrix} = \begin{bmatrix} V_P & V_Q \\ V_Q & V_P \end{bmatrix} \begin{bmatrix} A \\ B \end{bmatrix} \tag{2.58}$$

Consequently, A and B can be determined as

$$\begin{bmatrix} A \\ B \end{bmatrix} = \begin{bmatrix} V_P & V_Q \\ V_Q & V_P \end{bmatrix}^{-1} \begin{bmatrix} I_P \\ I_Q \end{bmatrix} \tag{2.59}$$

Eq. (2.59) is a key equation for line parameter estimation. It allows us to determine A and B from the measurements of V_P, V_Q, I_P, and I_Q. Once A and B are known, the values of a, b, and Y_{cap} can be solved by using the Matlab fsolve function from (2.55) and (2.56). Based on a and b, line parameters including positive sequence series impedance per unit length z_1 and positive sequence

shunt admittance per unit length y_1 can be solved by using the same approach as described in Section 2.1.

2.3 Kalman Filter Estimation Methods for Transmission line Parameters

The Kalman filter method is defined by two steps: prediction and update. Define the state to be estimated as x. In the first step, the priori estimate for the state at time k is predicted based on the state at time $k-1$ by using (2.60); In this case, the line parameters are assumed to be static; Thus, $\hat{x}_k^-$ will be predicted to have the same value as $\hat{x}_{k-1}$; the priori error covariance at time k is calculated based on (2.61):

$$\hat{x}_k^- = \hat{x}_{k-1} \tag{2.60}$$

$$P_k^- = P_{k-1} + Q \tag{2.61}$$

where the subscript k is the instant, the superscript – means priori, $\hat{x}$ means the estimate for x, P is the error covariance, and Q is the process noise covariance. Then the Kalman gain K, the posteriori estimate $\hat{x}$ and the posteriori error covariance P at instant k is calculated by (2.62)-(2.64),

$$K_k = P_k^- H_k^T (H_k P_k^- H_k^T + R)^{-1} \tag{2.62}$$

$$\hat{x}_k = \hat{x}_k^- + K_k(w_k - H_k \hat{x}_k^-) \tag{2.63}$$

$$P_k = (I - K_k H_k) P_k^- \tag{2.64}$$

where R is the observation noise covariance, I is the identity matrix, H is the observation matrix, and w is the observation vector. For the next time step $k+1$, the estimated value $\hat{x}_k$ will be used to compute $\hat{x}_{k+1}^-$ like in (2.60), and so forth.

In the following subsections, the Kalman filter line parameter estimation methods for the non-compensated transmission line and different types of series-compensated transmission lines will be discussed. Since the estimation process is described by the five questions (2.60)–(2.64), the most important task for the following subsections is to define the state to be estimated x_k, the measurement vector w_k, and the measurement matrix H_k. After estimation, the line parameters can be obtained using (2.13) – (2.20).

2.3.1 Kalman Filter for Non-Compensated Transmission Line

The equivalent-π circuit of the non-compensated system is shown in Figure 2.5.

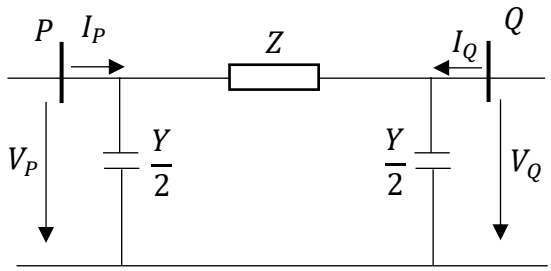

Figure 2.5 The equivalent-π circuit of the positive sequence network of the non-compensated transmission line.

In this circuit, the voltages and currents at the two buses can be related using the admittance matrix of the system.

$$\begin{bmatrix} I_P \\ I_Q \end{bmatrix} = \begin{bmatrix} \frac{1}{Z} + \frac{Y}{2} & -\frac{1}{Z} \\ -\frac{1}{Z} & \frac{1}{Z} + \frac{Y}{2} \end{bmatrix} \begin{bmatrix} V_P \\ V_Q \end{bmatrix} \tag{2.65}$$

Let $a = \frac{1}{Z} + \frac{Y}{2}$ and $b = -\frac{1}{Z}$. Eq. (2.65) becomes

$$\begin{bmatrix} I_P \\ I_Q \end{bmatrix} = \begin{bmatrix} a & b \\ b & a \end{bmatrix} \begin{bmatrix} V_P \\ V_Q \end{bmatrix} \tag{2.66}$$

Eq. (2.66) can be rewritten as,

$$\begin{bmatrix} I_P \\ I_Q \end{bmatrix} = \begin{bmatrix} V_P & V_Q \\ V_Q & V_P \end{bmatrix} \begin{bmatrix} a \\ b \end{bmatrix} \tag{2.67}$$

Define the state to be estimated as $x = \begin{bmatrix} a \\ b \end{bmatrix}$. Assume that N sets of measurements $\left(I_{P_1}, I_{Q_1}, V_{P_1}, V_{Q_1}, \dots, I_{P_N}, I_{Q_N}, V_{P_N}, V_{Q_N}\right)$ are available. Then the k^{th} $(1 \le k \le N)$ true state is denoted as x_k=$\begin{bmatrix} a_k \\ b_k \end{bmatrix}$. In addition, $H_k = \begin{bmatrix} V_{P_k} & V_{Q_k} \\ V_{Q_k} & V_{P_k} \end{bmatrix}$ and $Z_k = \begin{bmatrix} I_{P_k} \\ I_{Q_k} \end{bmatrix}$.

2.3.2 Kalman Filter for One-End Compensated Line

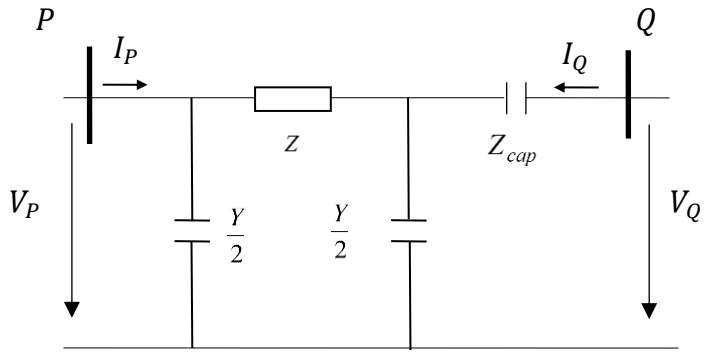

Figure 2.6 The equivalent-π circuit of the positive sequence network of the one-end compensated line.

The circuit diagram of the one-end compensated line is shown in Figure 2.6. The voltage and the current measurements at both ends are related by the admittance matrix,

$$\begin{bmatrix} I_P \\ I_Q \end{bmatrix} = \begin{bmatrix} \frac{Y}{2} + \frac{1}{Z} & -\frac{1}{Z} \\ -\frac{1}{Z} & \frac{Y}{2} + \frac{1}{Z} \end{bmatrix} \begin{bmatrix} V_P \\ V_Q - I_Q Z_{cap} \end{bmatrix} \tag{2.68}$$

Let $a = \frac{Y}{2} + \frac{1}{Z}$ and $b = \frac{1}{Z}$, then (2.68) can be expressed as

$$\begin{bmatrix} I_P \\ I_Q \end{bmatrix} = \begin{bmatrix} a & -b \\ -b & a \end{bmatrix} \begin{bmatrix} V_P \\ V_Q - I_Q Z_{cap} \end{bmatrix} \tag{2.69}$$

Two equations can be obtained from the above,

$$I_P = V_P \cdot a - V_Q \cdot b + I_Q \cdot bZ_{cap} \tag{2.70}$$

$$I_Q = V_Q \cdot a - V_P \cdot b - I_Q \cdot aZ_{cap} \tag{2.71}$$

Rearrange (2.70) and (2.71) in vector-matrix form, we have

$$\begin{bmatrix} I_P \\ I_Q \end{bmatrix} = \begin{bmatrix} V_P & -V_Q & I_Q & 0 \\ V_Q & -V_P & 0 & -I_Q \end{bmatrix} \begin{bmatrix} a \\ b \\ bZ_{cap} \\ aZ_{cap} \end{bmatrix} \tag{2.72}$$

To effectively estimate the line parameters, at least two sets of voltage and current measurements from both ends are required. The first set of measurements are denoted as V_{P_1}, V_{Q_1}, I_{P_1}, I_{Q_1} , and the second set of measurements are denoted as V_{P_2}, V_{Q_2}, I_{P_2}, I_{Q_2}.

For the two sets of measurements, (2.72) can be rewritten as

$$\begin{bmatrix} I_{P_1} \\ I_{Q_1} \\ I_{P_2} \\ I_{Q_2} \end{bmatrix} = \begin{bmatrix} V_{P_1} & -V_{Q_1} & -I_{Q_1} & 0 \\ V_{Q_1} & -V_{P_1} & 0 & -I_{Q_1} \\ V_{P_2} & -V_{Q_2} & -I_{Q_2} & 0 \\ V_{Q_2} & -V_{P_2} & 0 & -I_{Q_2} \end{bmatrix} \begin{bmatrix} a \\ b \\ g \\ h \end{bmatrix} \tag{2.73}$$

where $g = bZ_{cap}$, and $h = aZ_{cap}$.

The problem is formulated as (2.73). For Kalman filter, we define the true state to be estimated as $x = [a \quad b \quad g \quad h]^T$. Assume that we have N $(N \geq 2)$ sets of measurements $\left(I_{P_1}, I_{Q_1}, V_{P_1}, V_{Q_1}, \dots, I_{P_N}, I_{Q_N}, V_{P_N}, V_{Q_N}\right)$. Then the k^{th} $\left(1 \leq k \leq \frac{N}{2}\right)$ true state is denoted as x_k=$[a_k \quad b_k \quad g_k \quad h_k]^T$, which is corresponding to the $(2k-1)^{th}$ and $(2k)^{th}$ measurement sets.

Like previously, we specify the same five equations for the Kalman filter. The difference is in the z_k and H_k, for which we have $z_k = \begin{bmatrix} I_{P_{2k-1}} \\ I_{Q_{2k-1}} \\ I_{P_{2k}} \\ I_{Q_{2k}} \end{bmatrix}$ and $H_k = \begin{bmatrix} V_{P_{2k-1}} & V_{Q_{2k-1}} & -I_{Q_{2k-1}} & 0 \\ V_{Q_{2k-1}} & V_{P_{2k-1}} & 0 & -I_{Q_{2k-1}} \\ V_{P_{2k}} & V_{Q_{2k}} & -I_{Q_{2k}} & 0 \\ V_{Q_{2k}} & V_{P_{2k}} & 0 & -I_{Q_{2k}} \end{bmatrix}$.

After the k^{th} recursion, we can obtain $[\hat{a}_k \quad \hat{b}_k \quad \hat{g}_k \quad \hat{h}_k]^T$. Similarly, the line parameters can be obtained using the same technique as described in Section 2.1.1.

2.3.3 Kalman Filter for Mid-Compensated Line (Known Series Compensator)

The circuit diagram of the mid-compensated line (known series compensator) is shown in Figure 2.2. The problem is formulated as (2.9). Define the state to be estimated as $x = \begin{bmatrix} A \\ B \end{bmatrix}$. Assume that *N* sets of measurements $\left(I_{P_1}, I_{Q_1}, V_{P_1}, V_{Q_1}, \ldots, I_{P_N}, I_{Q_N}, V_{P_N}, V_{Q_N}\right)$ are available. Then the k^{th} $(1 \le k \le N)$ true state is denoted as x_k=$\begin{bmatrix} A_k \\ B_k \end{bmatrix}$. Here, z_k=$\begin{bmatrix} I_{P_k} \\ I_{Q_k} \end{bmatrix}$ and $H_k = \begin{bmatrix} V_{P_k} & V_{Q_k} \\ V_{Q_k} & V_{P_k} \end{bmatrix}$. The estimated state $[\hat{A}_k \quad \hat{B}_k]^T$ can be obtained after the k^{th} recursion. Finally, $\hat{a}_k$ and $\hat{b}_k$ can be obtained using (2.11) and (2.12).

2.3.4 Kalman Filter for Mid-Compensated Line (Known Current Through Series Compensator)

The circuit diagram of the mid-compensated line (known series compensator current) is shown in Figure 2.3. To use the Kalman filter, first, we define the states to be estimated as $x = \begin{bmatrix} a \\ b \end{bmatrix}$. Assume that there are *N* sets of measurements (I_{P_1}, I_{Q_1}, V_{P_1}, V_{Q_1}, V_{Q_1}, I_{R_1}, ..., I_{P_N}, I_{Q_N}, V_{P_N}, V_{Q_N} , I_{R_N}). Then the k^{th} $(1 \le k \le N)$ true state is denoted as $x_k = \begin{bmatrix} a_k \\ b_k \end{bmatrix}$, $H_k = \begin{bmatrix} I_{Q_k}V_{P_k} - I_{P_k}V_{Q_k} & 0 \\ 0 & (\bar{C}_k^2 - 1)V_{P_k} \end{bmatrix}$, and $z_k = \begin{bmatrix} I_{R_k}\left(V_{P_k} + V_{Q_k}\right)\overline{b_k} \\ \overline{C_k}I_{P_k} + I_{R_k} \end{bmatrix}$.

2.3.5 Kalman Filter for Two-End Compensated Line

The circuit diagram of the two-end line is shown in Figure 2.4. Define the state to be estimated as $x = \begin{bmatrix} A \\ B \end{bmatrix}$. Assume that there are N sets of measurements (I_{P_1}, I_{Q_1}, V_{P_1}, V_{Q_1}, ..., I_{P_N}, I_{Q_N}, V_{P_N}, V_{Q_N}). Then the k^{th} $(1 \leq k \leq N)$ true state is denoted as x_k=$\begin{bmatrix} A_k \\ B_k \end{bmatrix}$. Similarly, we build the five equations of the Kalman filter. Here, z_k=$\begin{bmatrix} I_{P_k} \\ I_{Q_k} \end{bmatrix}$ and $H_k = \begin{bmatrix} V_{P_k} & V_{Q_k} \\ V_{Q_k} & V_{P_k} \end{bmatrix}$. Once the estimates of A and B are available, the line parameters can be solved using the following steps. For (2.55) and (2.56), we substitute the three line parameters $r1$, $x1$, and $y1$ for Y and Z using (2.1) – (2.4) . Then separating (2.55) and (2.56) into the real and imaginary parts, we get four new equations. The four equations can be solved using nonlinear equation solving techniques.

2.3.6 Kalman Filter Tracking for Transmission Line Parameters

To dynamically track the state without knowing any information between the states at instant k and $k-1$, it is critical to make the most of measurements. Regular Kalman filtering technique yields slow tracking performance as shown in case studies that will be presented in Section 3. To improve the tracking performance of the Kalman filter, the following two adjustment methods are proposed.

The first solution is to use the adjusted Kalman gain method, which increases the Kalman gain K. While the priori estimate $\hat{x}_k^-$ gets pulled away from the actual value by the previous estimate $\hat{x}_{k-1}$, it is reasonable to add more weight to the current measurements. The concept of adjusting the Kalman gain has already been considered previously (such as in [32]). In our work, a factor D ($D > 1$) is introduced as follows:

$$\hat{x}_k^- = \hat{x}_{k-1} + DK_k(w_k - H\hat{x}_{k-1}) \tag{2.74}$$

The second solution is to use the fast Kalman method, which considers the direction in which the line parameters are moving toward, i.e., taking $(\hat{x}_k^- - \hat{x}_{k-n})$ into account, where $n \geq 1$. Thus,

$$\hat{x}_k = \hat{x}_k^- + K_k(w_k - H_k\hat{x}_k^-) + U(\hat{x}_k - \hat{x}_{k-n}) \tag{2.75}$$

where the variable U is used to adjust the weight of $(\hat{x}_k^- - \hat{x}_{k-n})$. By rearranging the terms, $\hat{x}_k$ can be expressed as

$$\hat{x}_k = \frac{1}{1-U}\hat{x}_k^- + \frac{1}{1-U}K_k(w_k - H\hat{x}_k^-) - \frac{U}{1-U}\hat{x}_{k-n} \tag{2.76}$$

For the first n estimations (when $k - n < 0$), $\hat{x}_{k-n}$ is set to zero. Note that while increasing the value of D and U can increase the ability of dynamic tracking, it also brings instability to the algorithm. In the case studies, the value of D and U are chosen to balance the performance of dynamic tracking and stability. The choice of optimal process noise covariance Q and measurement noise covariance R can be found in [33]–[35].

In the following subsections, Kalman filter formulation is presented for different line configurations with and without series compensators, based on which the states and then the line parameters will be derived.

CHAPTER 3 TRANSMISSION LINE PARAMETER ESTIMATION CASE STUDIES

In this chapter, we will discuss the process of transmission line parameter estimation and present the preliminary results. Based on the equations from the previous chapters, Matlab programs are written to implement the proposed estimation algorithms to estimate the transmission line parameters. The programs take measurement data, which are obtained through simulation of transmission line models in Matlab Simulink, as inputs. In other words, the Matlab Simulink simulation is a way to provide the measurements. As a result, the simulation process includes the following steps (also shown in Figure 3.1):

(1) Build the transmission line model in Matlab Simulink and run the simulation to get the voltages and currents (the measurements).

(2) Use the measured data as input to the program to estimate the desired parameters (If measurement error needs to be considered, we will introduce some noise to certain measurement quantities).

(3) Produce results and calculate the estimation errors.

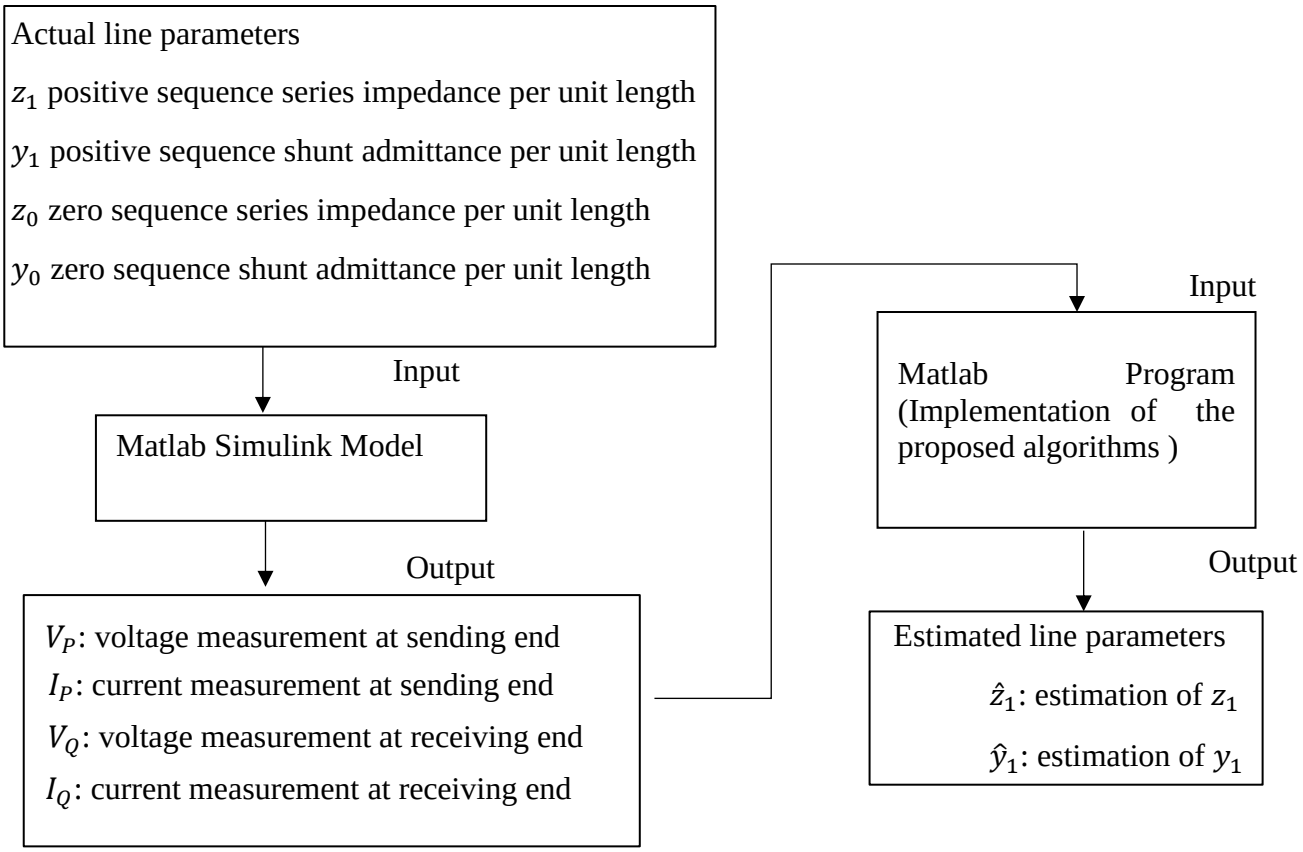

Figure 3.1 The process of line parameter estimation.

The parameters of the simulated transmission line model used in the simulations are displayed in Table 3.1.

Table 3.1 Transmission line parameters used in the simulations

Total Line Length	350 km		
Base Voltage	500 kV		
Base Power	1000MVA		
System Frequency	60 Hz		
Positive Sequence Parameters	R (Ω/mile)	L (H/mile)	C (F/mile)
	0.249168	0.00156277	19.469×10^{-9}

3.1 Estimation Results for the Mid-Compensated Line

In this Section, the line parameters of the transmission line with mid-compensation are estimated using the two methods described in Section 2.3. The estimation results will be given in Section 3.3.1 and Section 3.3.2 respectively.

3.1.1 Estimation Results for the Case of Known Impedance of Series Compensator

First, we test the estimation methods using measurements directly from PMUs. As we can see from Table 3.2, all line parameters can be estimated accurately.

Table 3.2 The estimation results for mid-compensated line with known impedance of the series compensator

Line Parameters	Actual Values	Estimated Values	Estimation Errors
Series Resistance (p.u./mile)	9.9667×10^{-4}	9.9455×10^{-4}	0.85%
Series Reactance (p.u./mile)	2.3566×10^{-3}	2.3570×10^{-3}	0.01%
Shunt Susceptance (p.u./mile)	1.8349×10^{-3}	1.8349×10^{-3}	0.00%

Next, we consider the effect of measurement errors. Table 3.3 shows the line parameter estimation results using one set of measurements for mid-compensated line where there is a 1% current measurement error at the sending end (measurement current magnitude is 99% of the actual current magnitude). In this case, all three parameters can still be estimated accurately.

Table 3.3 The estimation results for mid-compensated line with known impedance of the series compensator with 1% current error

Line Parameters	Actual Values	Estimated Values	Estimation Errors
Series Resistance (p.u./mile)	9.9667×10^{-4}	1.0009×10^{-3}	0.42%
Series Reactance (p.u./mile)	2.3566×10^{-3}	2.3604×10^{-3}	0.16%
Shunt Susceptance (p.u./mile)	1.8349×10^{-3}	1.8360×10^{-3}	0.06%

Table 3.8 shows the line parameter estimation results using one set of measurements for mid-compensated line where there is a 1% voltage measurement error at the sending end (measurement voltage magnitude is 99% of the actual voltage magnitude). In this case, only shunt susceptance can be estimated with a small error.

Table 3.4 The estimation results for mid-compensated line with known impedance of the series compensator with 1% voltage error

Line Parameters	Actual Values	Estimated Values	Estimation Errors
Series Resistance (p.u./mile)	9.9667×10^{-4}	1.0768×10^{-3}	8.04%
Series Reactance (p.u./mile)	2.3566×10^{-3}	2.3041×10^{-3}	-2.23%

Shunt Susceptance (p.u./mile)	1.8349×10^{-3}	1.8446×10^{-3}	0.53%

3.1.2 Estimation Results for the Case of Known Current Through Series Compensator

In this section, we estimate line parameters of mid-compensated transmission line when we have the current measurement at the series compensator. Table 3.5 shows the estimated results are very close to the actual line parameters.

Table 3.5 The estimation results for mid-compensated line with known current at the series compensator

Line Parameters	Actual Values	Estimated Values	Estimation Errors
Series Resistance (p.u./mile)	9.9667×10^{-4}	9.9455×10^{-4}	0.85%
Series Reactance (p.u./mile)	2.3566×10^{-3}	2.3570×10^{-3}	0.01%
Shunt Susceptance (p.u./mile)	1.8349×10^{-3}	1.8349×10^{-3}	0.00%

In practical applications, there may be measurement errors to the parameters. Table 3.6 shows the line parameter estimation results using one set of measurements for mid-compensated line where there is a 1% current measurement error at sending end (measurement current magnitude is 99% of the actual current magnitude). In this situation, only shunt susceptance can be estimated accurately.

Table 3.6 The estimation results for mid-compensated line with known current at the series compensator with 1% current error

Line Parameters	Actual Values	Estimated Values	Estimation Errors
Series Resistance (p.u./mile)	9.9667×10^{-4}	6.8644×10^{-4}	-16.02%
Series Reactance (p.u./mile)	2.3566×10^{-3}	1.6225×10^{-3}	-15.50%
Shunt Susceptance (p.u./mile)	1.8349×10^{-3}	1.8468×10^{-3}	0.32%

Then we apply a 1% error on voltage measurements at the sending end. Table 3.7 shows that only the shunt susceptance can be estimated accurately in this case.

Table 3.7 The estimation results for mid-compensated line with known current at the series compensator with 1% voltage error

Line Parameters	Actual Values	Estimated Values	Estimation Errors
Series Resistance (p.u./mile)	9.9667×10^{-4}	1.1639×10^{-3}	16.77%
Series Reactance (p.u./mile)	2.3566×10^{-3}	2.2519×10^{-3}	-4.44%
Shunt Susceptance (p.u./mile)	1.8349×10^{-3}	1.8453×10^{-3}	0.57%

3.2 Estimation Results for the Two-End Equivalent Compensated Line

In this Section, line parameters of transmission line with two-end compensation is estimated using the proposed algorithm in Section 2.1.2. As discussed, this method uses the Matlab fsolve function, which requires a set of initial inputs of estimated line parameters. In the actual situation, we may have transmission line parameters that are close to their actual values. Here, we assume that we have some difference to the initial inputs within $\pm 10\%$ of the actual values. The initial inputs of series impedance and shunt susceptance are 90% of their actual values, and series reactance and series compensator's admittance are 110% of their actual values. As we can see in Table 3.8, the estimated values are still very accurate with all the estimation errors equal to 0%.

Table 3.8 The estimation results for two-end compensated line

Line Parameters	Actual Values	Estimated Values	Estimation Errors
Series Resistance (p.u./mile)	9.9667×10^{-4}	9.9667×10^{-4}	0.00%
Series Reactance (p.u./mile)	2.3566×10^{-3}	2.3566×10^{-3}	0.00%
Shunt Susceptance (p.u./mile)	1.8349×10^{-3}	1.8349×10^{-3}	0.00%
Series Compensator's Admittance (p.u.)	8.6718	8.6718	0.00%

3.3 Kalman Filter Estimation Results for Transmission Line Parameters

3.3.1 Kalman Filter Estimation Results for Non-Compensated Line

In this section, the proposed method for the non-compensated line is studied. First, no measurement noises are added to voltage and current data. The estimated line parameters are very close to their true values as shown in Table 3.9.

Table 3.9 The estimation results for non-compensated transmission line using Kalman filter

Line Parameters	Actual Values	Estimated Values	Estimation Errors
Series Resistance (p.u./mile)	9.9667×10^{-4}	9.8815×10^{-4}	0.80%
Series Reactance (p.u./mile)	2.3566×10^{-3}	2.3584×10^{-3}	0.08%
Shunt Susceptance (p.u./mile)	1.8349×10^{-3}	1.8348×10^{-3}	0.01%

Then the voltage and current data from the simulation are added with Gaussian white noise to create 20 sets of new measurements. The standard deviation of the magnitude measurement error and the angle measurement error are denoted by σ_{mag} and σ_{theta}. We define $\sigma_{mag} = |measurement| \times 0.5\%$, and $\sigma_{theta} = 0.2°$ (σ_{theta} is selected as the equivalent of $10\mu s$, which is calculated by (3.1)). The estimation results for the two unknown variables a and b are shown in Figure 3.2 – Figure 3.5. Both variables can be estimated accurately while the estimation results of the direct calculation appear to be more greatly affected by measurement noises.

$$10\mu s \times \frac{60\ cycles}{10^6\ \mu s} \times \frac{360°}{1\ cycle} \approx 0.2° \tag{3.1}$$

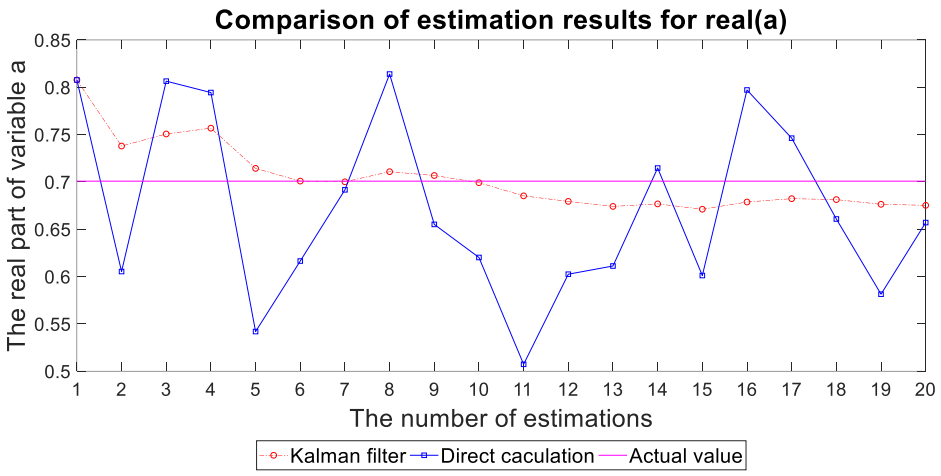

Figure 3.2 The estimation results for the real part of the variable a for non-compensated line.

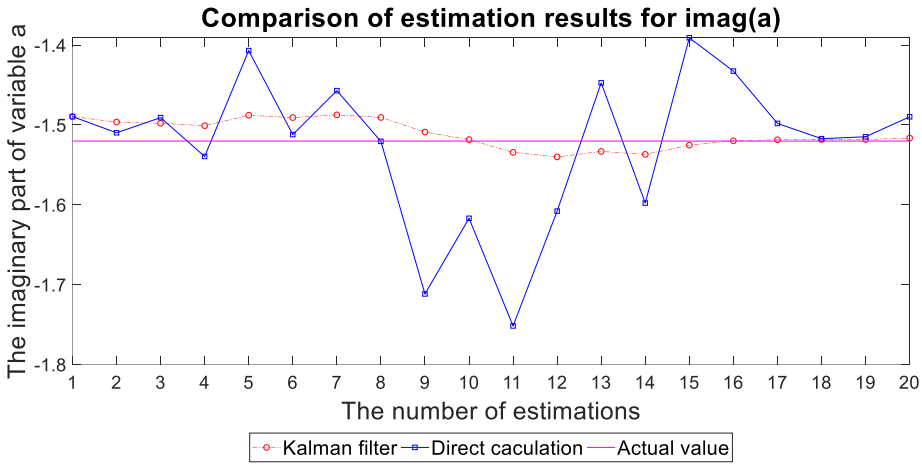

Figure 3.3 The estimation results for the imaginary part of the variable a for non-compensated line.

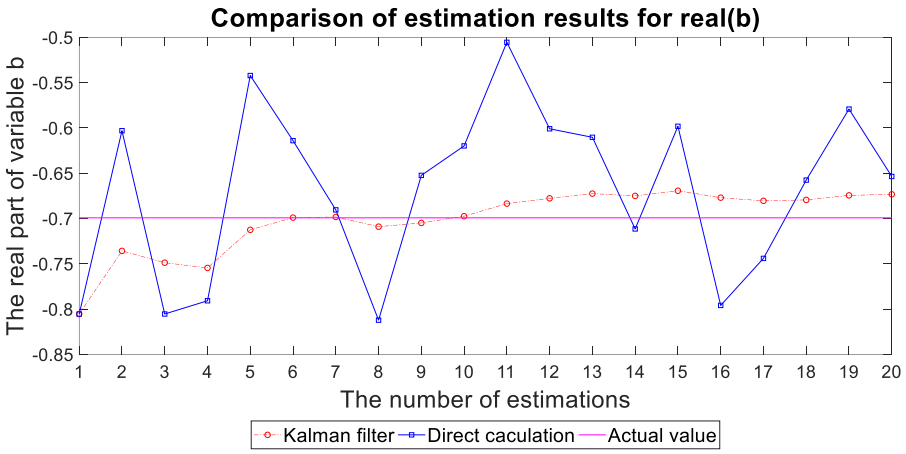

Figure 3.4 The estimation results for the real part of the variable b for non-compensated line.

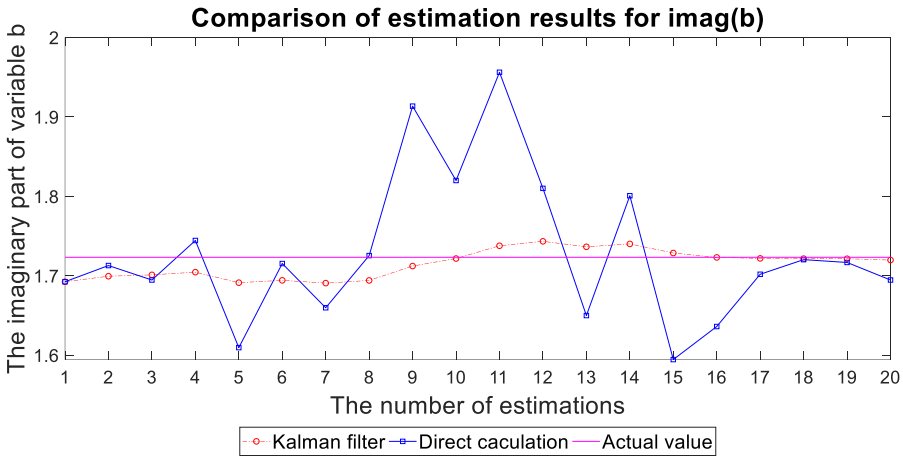

Figure 3.5 The estimation results for the imaginary part of the variable b for non-compensated line.

The estimated a and b are then used to calculate the line parameters. The estimation results for the line parameters are shown in Figure 3.6 – Figure 3.8. We can see that the estimation accuracy of all three line parameters is improved by using the Kalman filter.

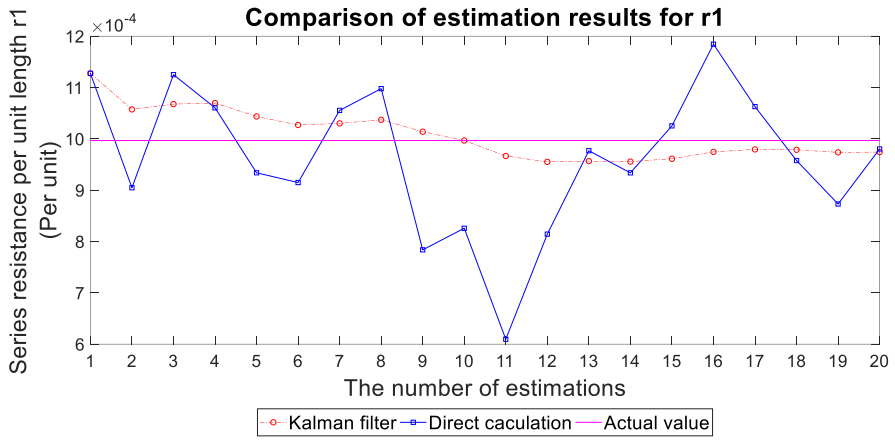

Figure 3.6 The estimation results for $r1$ for the non-compensated line.

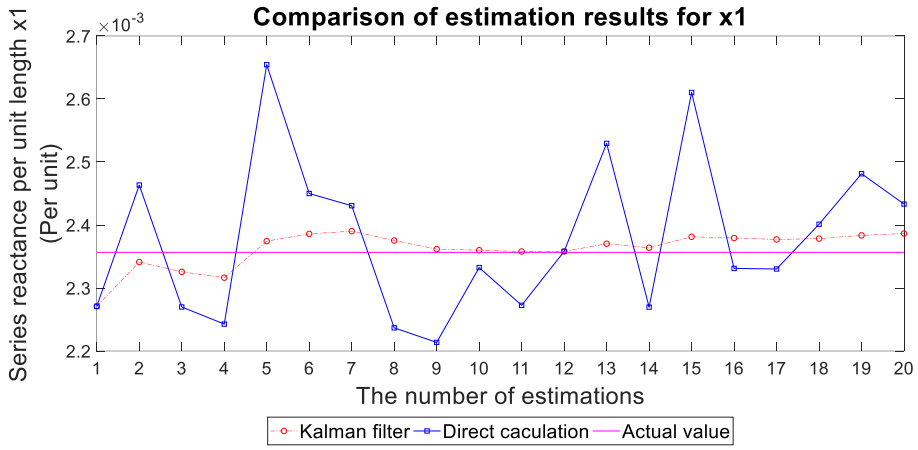

Figure 3.7 The estimation results for $x1$ for the non-compensated line.

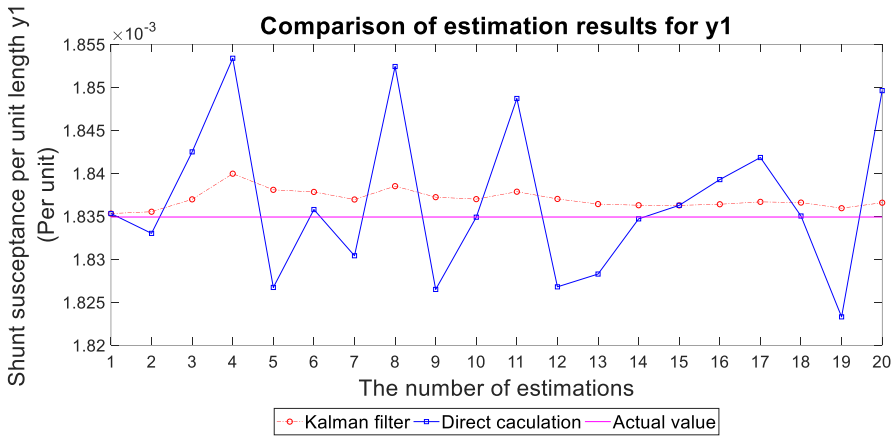

Figure 3.8 The estimation results for $y1$ for the non-compensated line.

The estimated line parameters of the 20th measurements are shown in Table 3.10. It is shown that all the parameters have been estimated reliably.

Table 3.10 Line parameters obtained from the 20th estimation results for the non-compensated line with noises in measurements using the Kalman filter

Line Parameters	Actual Values	Estimated Values	Estimation Errors
Series Resistance (p.u./mile)	9.9667×10^{-4}	9.7420×10^{-4}	2.25%
Series Reactance (p.u./mile)	2.3566×10^{-3}	2.3836×10^{-3}	1.27%
Shunt Susceptance (p.u./mile)	1.8349×10^{-3}	1.8366×10^{-3}	0.09%

3.3.2 Kalman Filter Estimation Results for One End-Compensated Line

The proposed method for the one-end compensated line is studied in this section. First, the estimation is performed for the measurements without any noise. The line parameters estimation results of the Kalman filter are displayed in Table 3.11. It is shown that all the three line parameters and the compensator parameter can be estimated accurately.

Table 3.11 Line parameters obtained from estimation results for the one-end compensated line without noise in measurements using the Kalman filter

Line Parameters	Actual Values	Estimated Values	Estimation Errors
Series Resistance (p.u./mile)	9.9667×10^{-4}	9.8829×10^{-4}	0.84%
Series Reactance (p.u./mile)	2.3566×10^{-3}	2.3581×10^{-3}	0.07%
Shunt Susceptance (p.u./mile)	1.8349×10^{-3}	1.8348×10^{-3}	0.00%
Capacitance of Series Compensator (p.u./mile)	4.6006×10^{-5}	4.6019×10^{-5}	0.03%

Then Gaussian white noises are added to the measurements. The estimates for the real and imaginary parts of the four unknown variables a, b, g, and h are shown in Figure 3.9 – Figure 3.16. We can see that the estimation results of the direct calculation are considerably affected by measurement noises. The estimates of the proposed method are getting very close to the actual values after the initial several estimates.

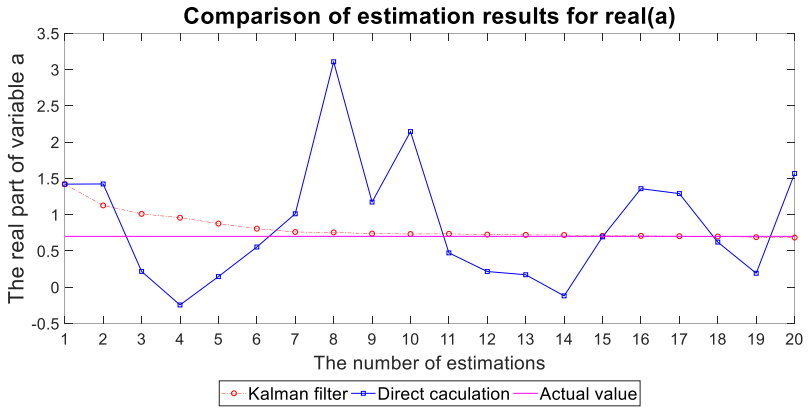

Figure 3.9 The estimation results for the real part of the variable a for one-end compensated line.

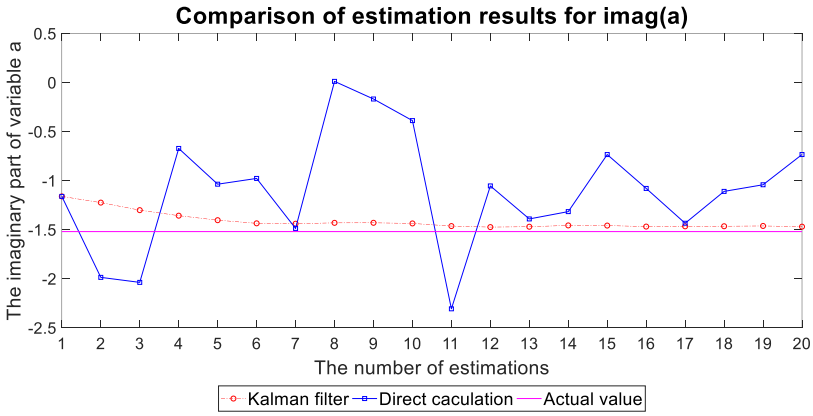

Figure 3.10 The estimation results for the imaginary part of the variable a for one-end compensated line.

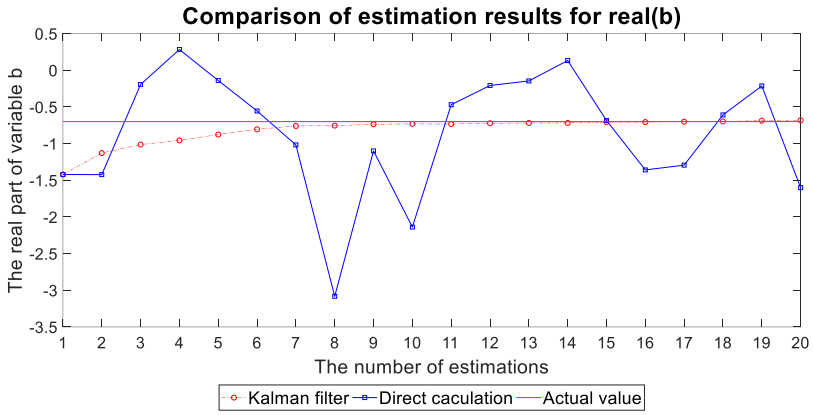

Figure 3.11 The estimation results for the real part of the variable b for one-end compensated line.

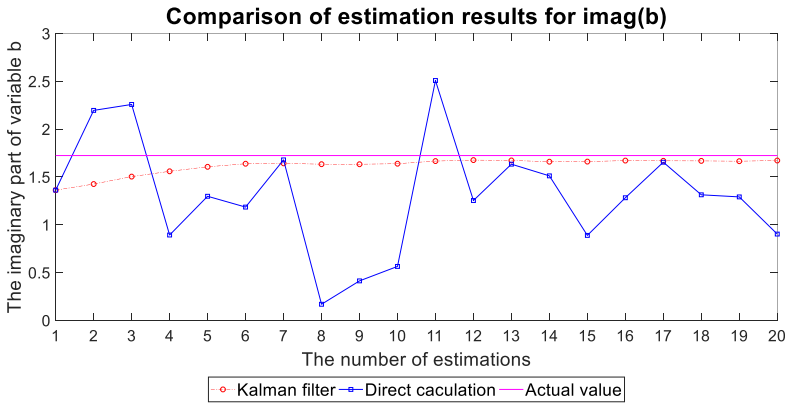

Figure 3.12 The estimation results for the imaginary part of the variable b for one-end compensated line.

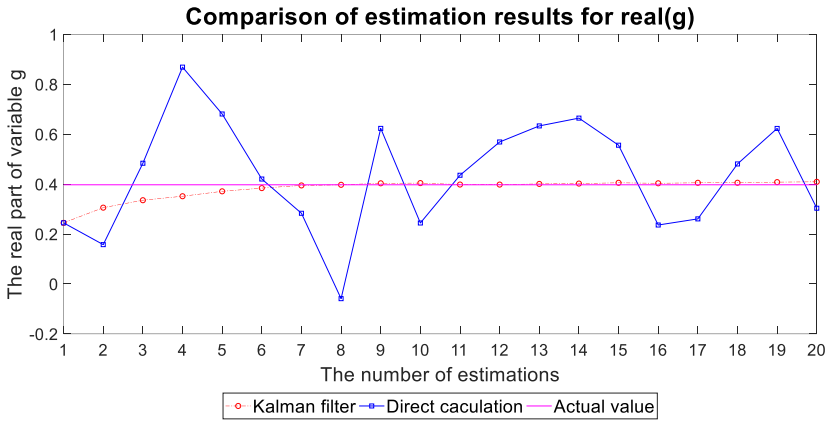

Figure 3.13 The estimation results for the real part of the variable g for one-end compensated line.

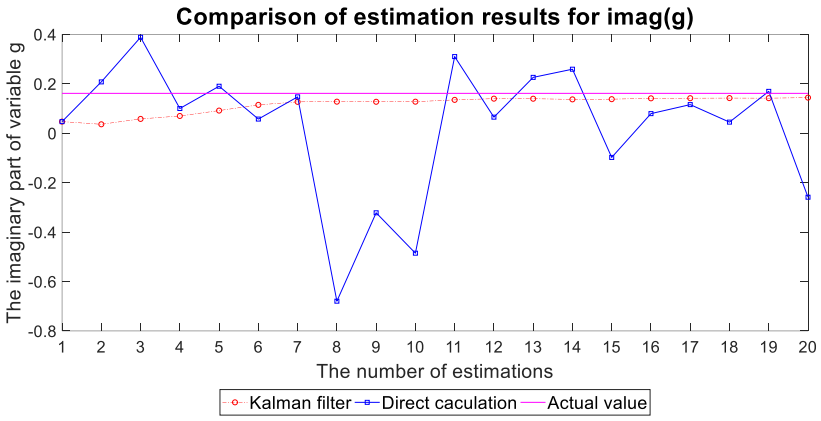

Figure 3.14 The estimation results for the imaginary part of the variable g for one-end compensated line.

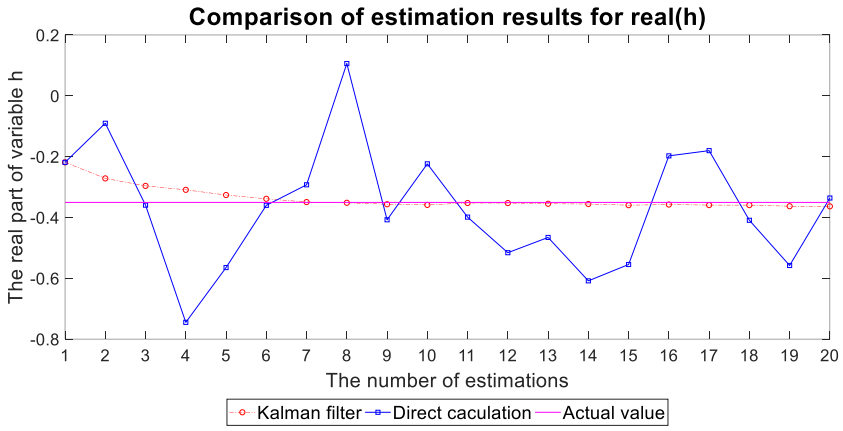

Figure 3.15 The estimation results for the real part of the variable h for one-end compensated line.

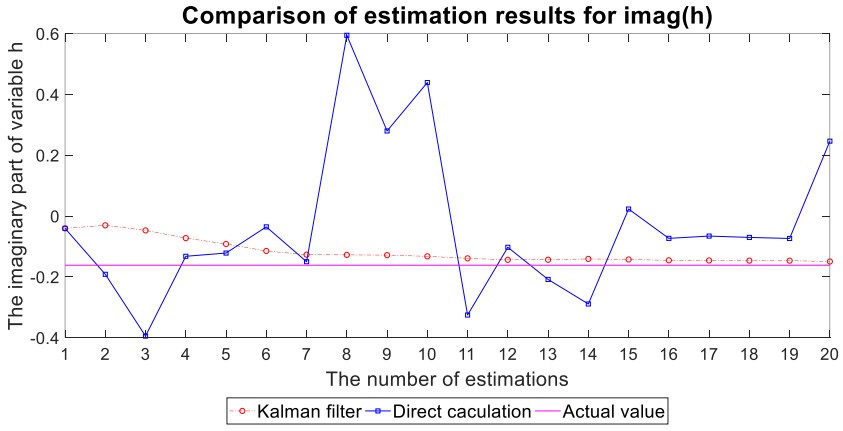

Figure 3.16 The estimation results for the imaginary part of the variable h for one-end compensated line.

The estimated line parameters are shown in Figure 3.17 – Figure 3.20. Evidently, the proposed Kalman filter method produces accurate estimates.

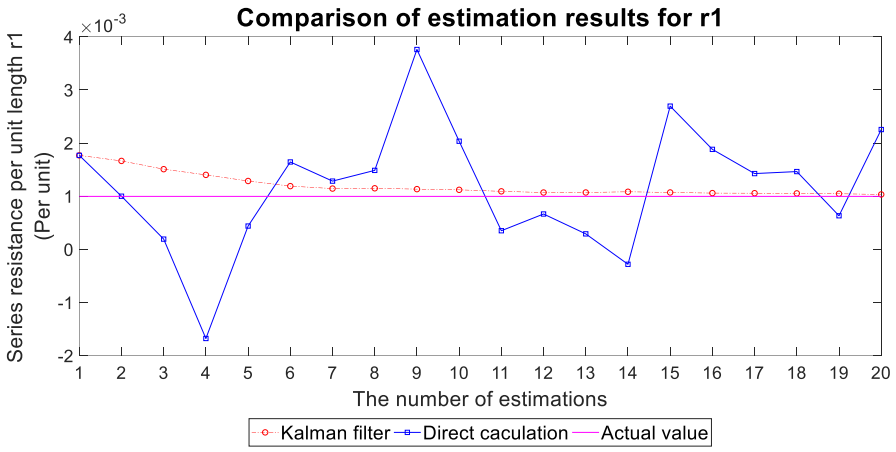

Figure 3.17 The estimation results for $r1$ of one-end compensated line.

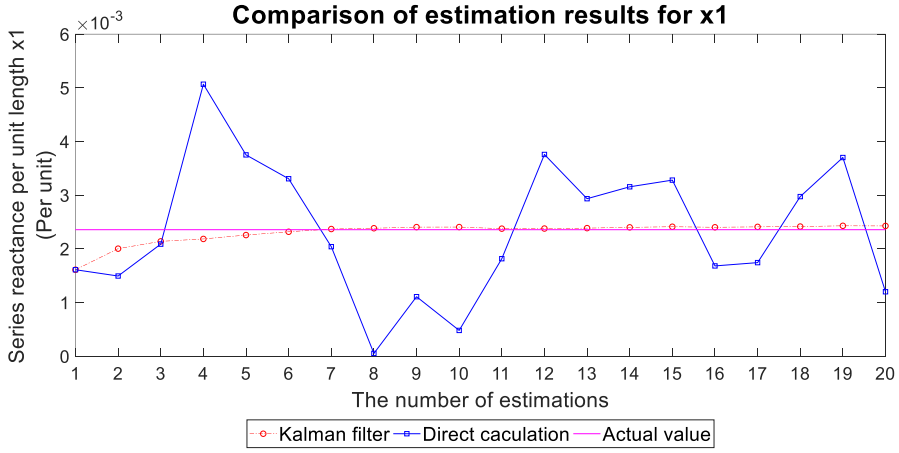

Figure 3.18 The estimation results for $x1$ of one-end compensated line.

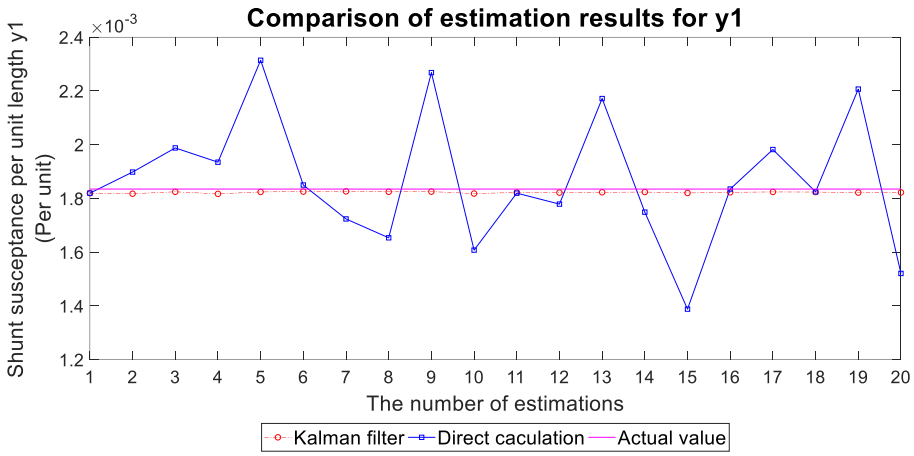

Figure 3.19 The estimation results for $y1$ of one-end compensated line.

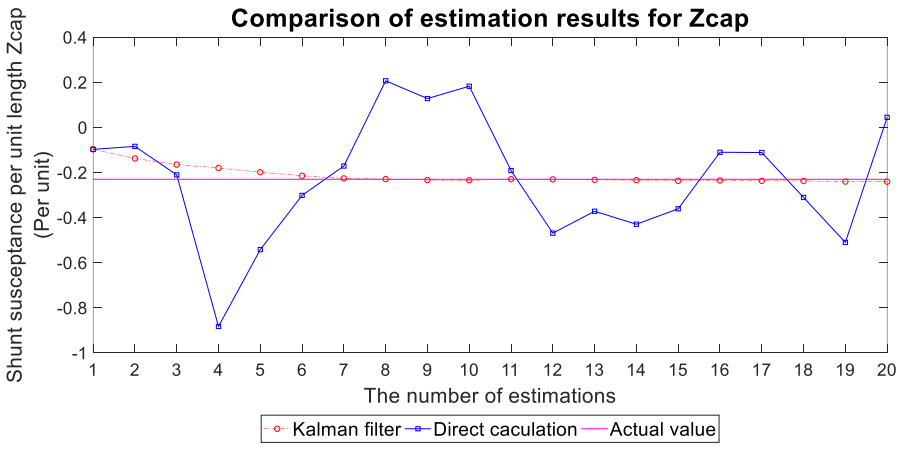

Figure 3.20 The estimation results for Z_{cap} of one-end compensated line.

The 20th estimation results details are shown in Table 3.12. As we can see, the estimation results of the proposed method for the one-end compensated line are very close to the actual values.

Table 3.12 Line parameters obtained from the 20th estimation results for the one-end compensated line with noises in measurements using the Kalman filter

Line Parameters	Actual Values	Estimated Values	Estimation Errors
Series Resistance (p.u./mile)	9.9667×10^{-4}	1.0332×10^{-3}	3.67%
Series Reactance (p.u./mile)	2.3566×10^{-3}	2.4271×10^{-3}	2.98%
Shunt Susceptance (p.u./mile)	1.8349×10^{-3}	1.8223×10^{-3}	-0.69%
Capacitance of Series Compensator (p.u./mile)	4.6006×10^{-5}	4.3905×10^{-5}	-4.57%

3.3.3 Kalman Filter Estimation Results for Mid-Compensated Line (Known Series compensator)

The proposed method for the mid-compensated line is studied in this section. First, the proposed method is used to perform estimation when there are no noises in the measurements. The estimation results are very accurate as shown in Table 3.13.

Table 3.13 Line parameters obtained from estimation results for the mid-compensated line without noise in measurements using the Kalman filter

Line Parameters	Actual Values	Estimated Values	Estimation Errors
Series Resistance (p.u./mile)	9.9667×10^{-4}	9.9455×10^{-4}	0.84%
Series Reactance (p.u./mile)	2.3566×10^{-3}	2.3571×10^{-3}	0.07%
Shunt Susceptance (p.u./mile)	1.8349×10^{-3}	1.8349×10^{-3}	0.00%

Then the voltage and current measurements are added with noise. The estimates for the variables A and B are shown in Figure 3.21 – Figure 3.24. It can be seen that the proposed method generates accurate results.

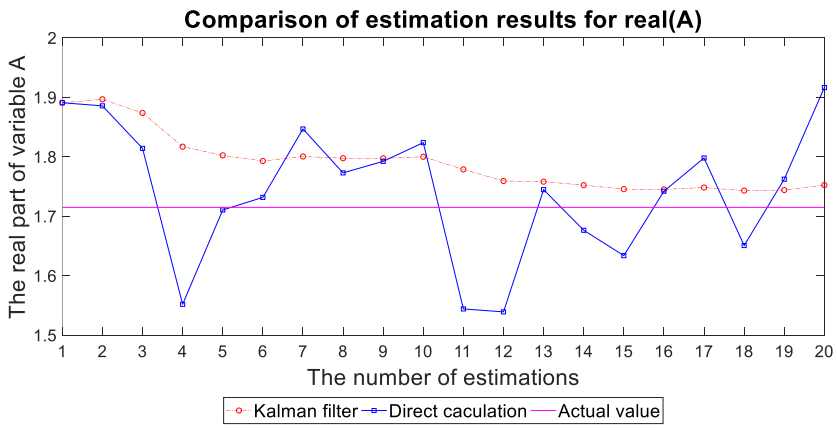

Figure 3.21 The estimation results for the real part of the variable A for the mid-compensated line.

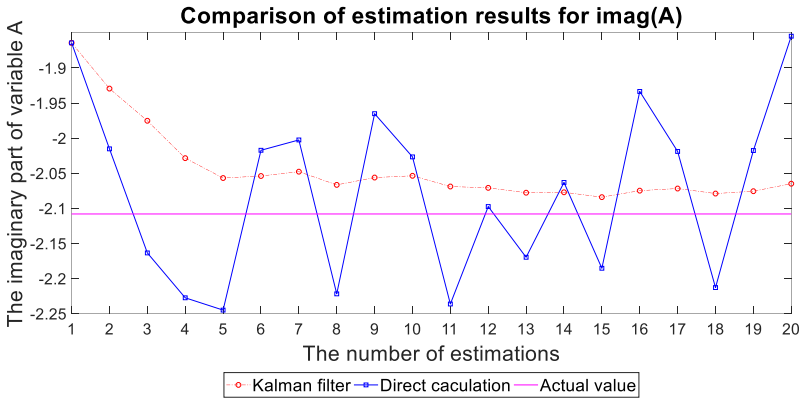

Figure 3.22 The estimation results for the imaginary part of the variable *A* for the mid-compensated line.

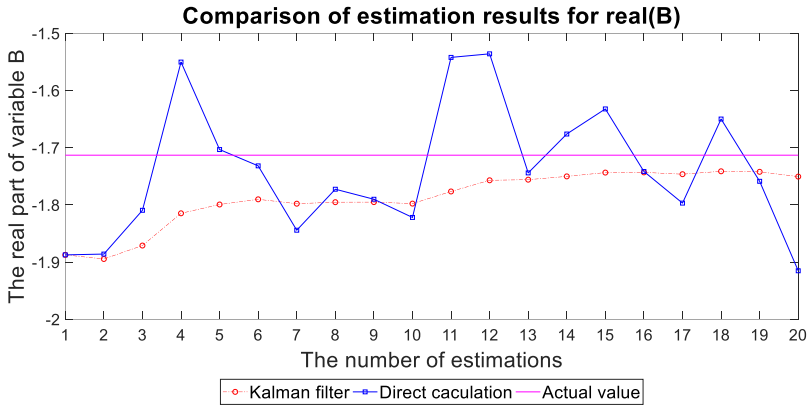

Figure 3.23 The estimation results for the real part of the variable *B* for the mid-compensated line.

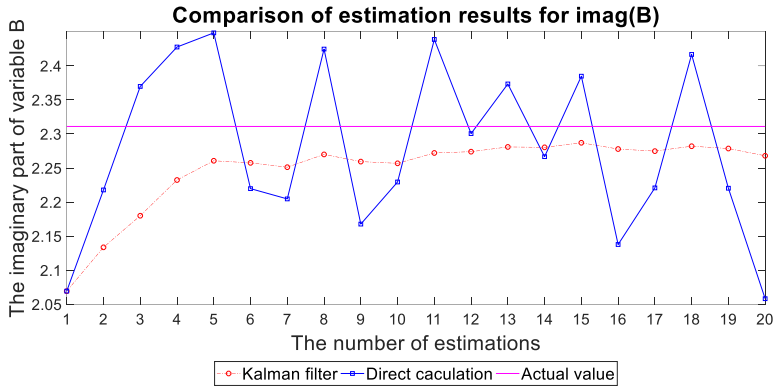

Figure 3.24 The estimation results for the imaginary part of the variable B for the mid-compensated line.

Figure 3.25 – Figure 3.27 show the estimates for the three line parameters. It is clear that the estimation results of the proposed method are more stable and accurate.

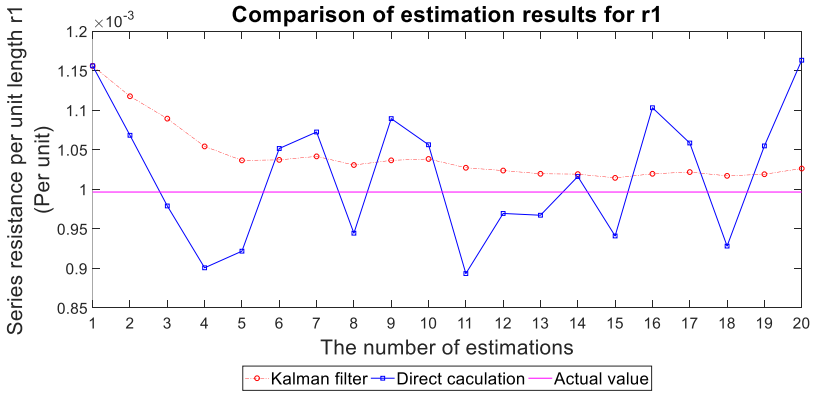

Figure 3.25 The estimation results for $r1$ for the mid-compensated line.

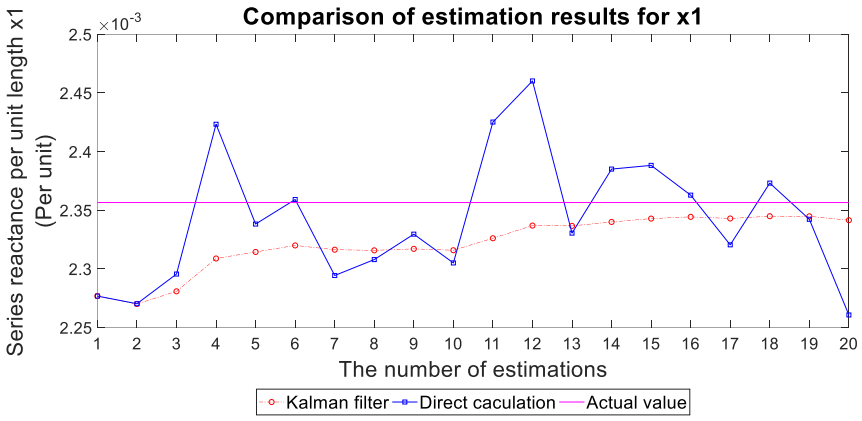

Figure 3.26 The estimation results for $x1$ for the mid-compensated line.

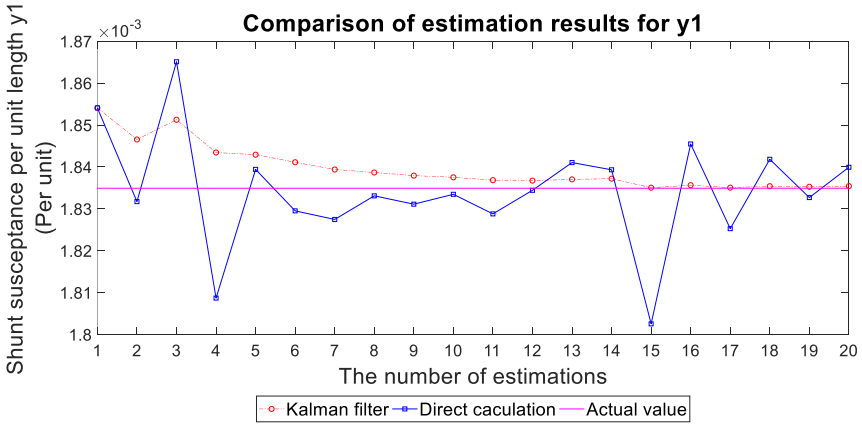

Figure 3.27 The estimation results for $y1$ for the mid-compensated line.

The 20th estimation results are shown in Table 3.14. All three line parameters can be estimated accurately under the effect of measurement noises.

Table 3.14 Line parameters obtained from the 20th estimation results for the mid-compensated line with noises in measurements using the Kalman filter

Line Parameters	Actual Values	Estimated Values	Estimation Errors
Series Resistance (p.u./mile)	9.9667×10^{-4}	1.0332×10^{-3}	2.98%
Series Reactance (p.u./mile)	2.3566×10^{-3}	2.4271×10^{-3}	-0.64%
Shunt Susceptance (p.u./mile)	1.8349×10^{-3}	1.8223×10^{-3}	0.03%

3.3.4 Kalman Filter Estimation Results for Mid-Compensated Line (Known Current Through Series Compensator)

The proposed method for the mid-compensated line is studied in this section. First, we add a magnitude noise with the standard deviation $\sigma_{magnitude}$ = 0.1% × magnitude of the measurement and an angle noise with the standard deviation $\sigma_{angle} = 0.2\,^{\circ}\,(= 10\,\mu s)$ to each measurement. The estimation results of the real and imaginary parts of the variables a and b are shown in Figure 3.28 – Figure 3.32. The estimation results of the proposed Kalman filter based method and direct calculation, and the actual values are compared in each plot.

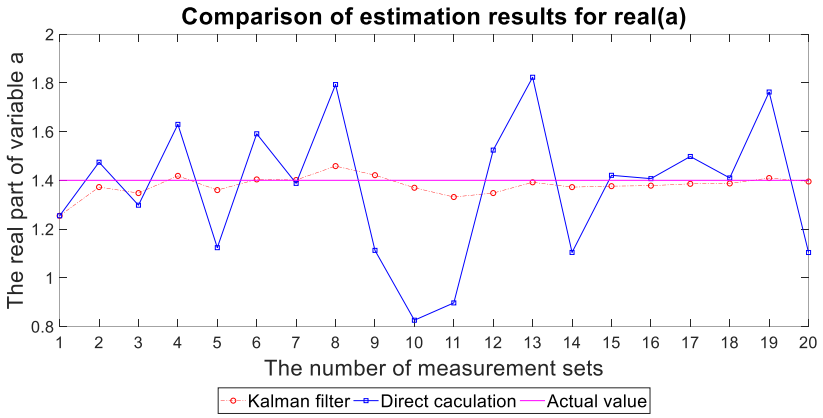

Figure 3.28 The estimation results for the real part of the variable a for the mid-compensated line.

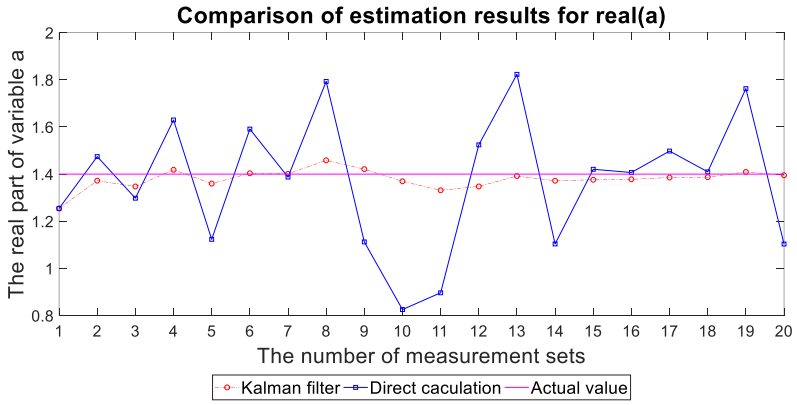

Figure 3.29 The estimation results for the real part of the variable a for the mid-compensated line.

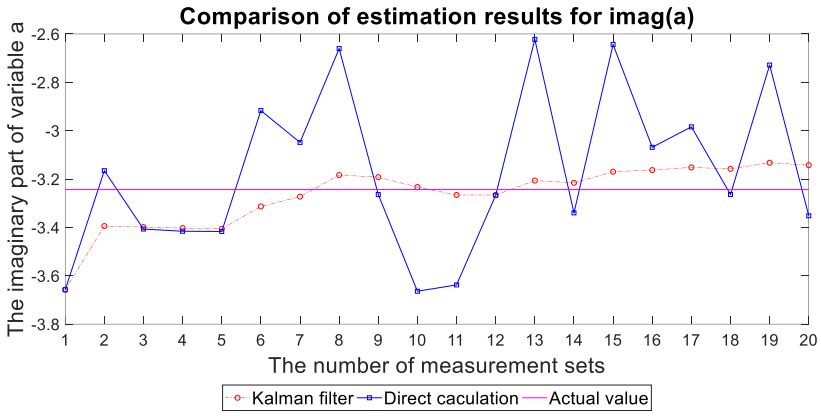

Figure 3.30 The estimation results for the imaginary part of the variable a for the mid-compensated line.

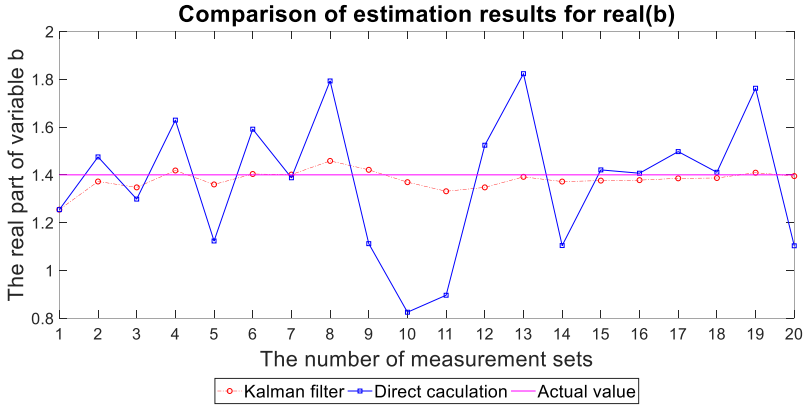

Figure 3.31 The estimation results for the real part of the variable b for the mid-compensated line.

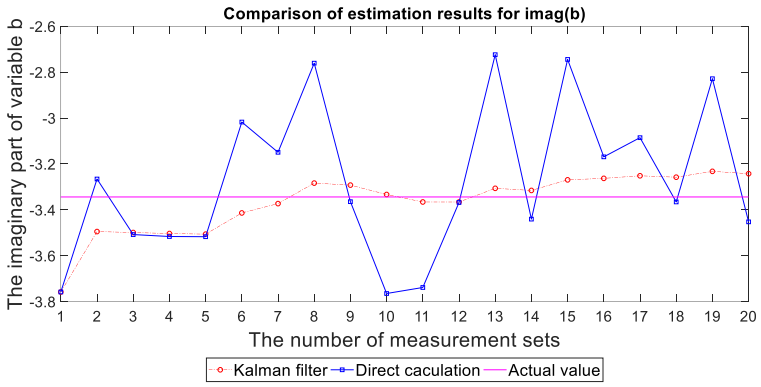

Figure 3.32 The estimation results for the imaginary part of the variable b for the mid-compensated line.

The estimation results for both the variables of the Kalman filter are getting closer to the actual values after several measurements. Based on the estimated variables, the three line parameters are calculated, and the results are shown in Figure 3.33–Figure 3.35.

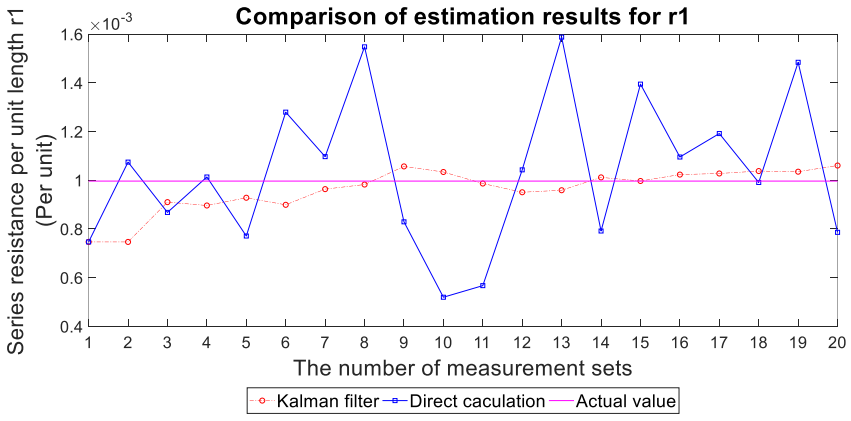

Figure 3.33 The estimation results for $r1$ for the mid-compensated line.

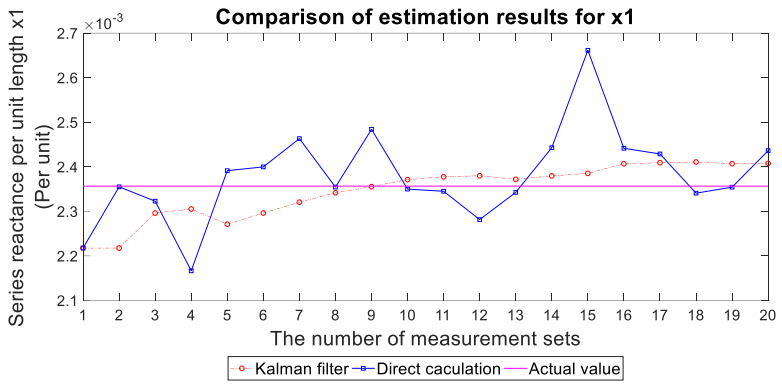

Figure 3.34 The estimation results for $x1$ for the mid-compensated line.

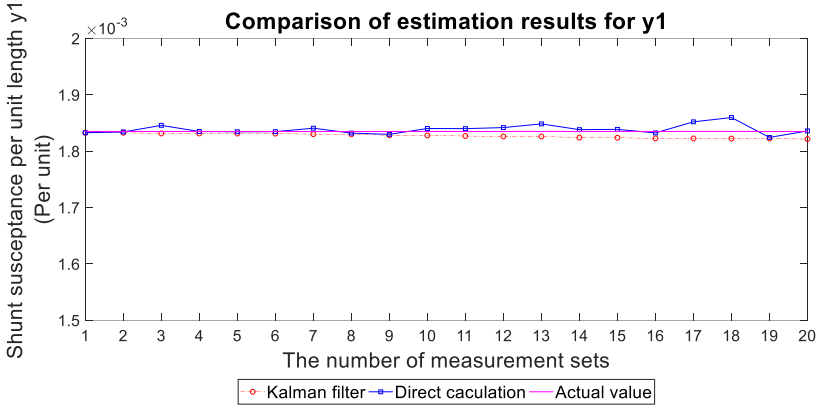

Figure 3.35 The estimation results for $y1$ for the mid-compensated line.

In Figure 3.33 and Figure 3.34, the proposed Kalman filter method has much better estimation accuracy than direct calculation after a few measurements. The estimation errors have been greatly reduced by the proposed method. From Figure 3.35, we can observe that both the Kalman filter method and the direct calculation method yield similarly accurate results for $y1$. Table II shows the results of the proposed method estimated at the 20^{th} measurements set.

Table 3.15 Line parameters obtained from estimation results for the mid-compensated line with noise in measurements using Kalman filter at the 20th measurements

Line Parameters	Actual Values	Estimated Values	Estimation Errors
Series Resistance (p.u./mile)	9.9667×10^{-4}	9.5204×10^{-4}	6.41%
Series Reactance (p.u./mile)	2.3566×10^{-3}	2.3694×10^{-3}	3.37%
Shunt Susceptance (p.u./mile)	1.8349×10^{-3}	1.8372×10^{-3}	0.05%

3.3.5 Kalman Filter Estimation Results for Two-End Compensated Line

In this section, the estimation results of the two-end compensated line are studied. Again, each measurement is added with a magnitude noise with the standard deviation $\sigma_{magnitude}$ = 0.1%× magnitude of the measurement and an angle noise with the standard deviation $\sigma_{angle} = 0.2\ °$. The estimation result of proposed methods and direct calculation for the variables A and B are shown in Figure 3.36 – Figure 3.39.

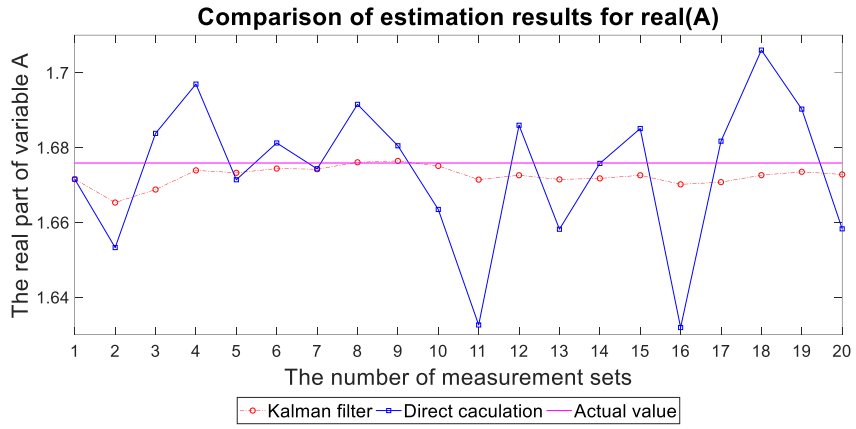

Figure 3.36 The estimation results for the real part of the variable *A* for the two-end compensated line.

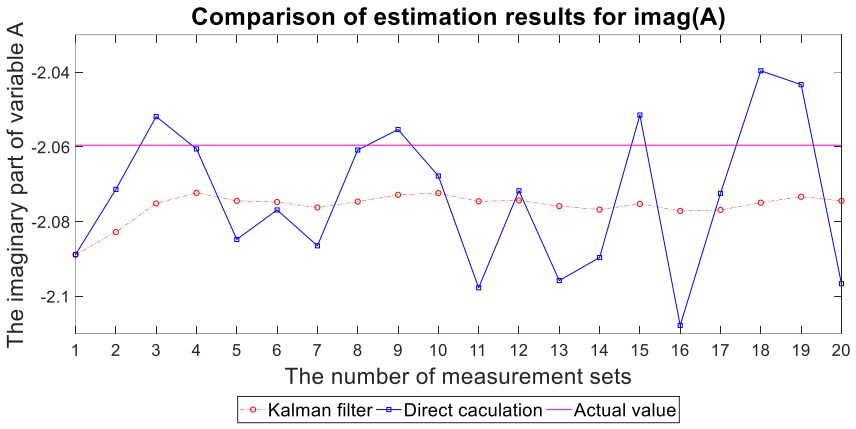

Figure 3.37 The estimation results for the imaginary part of the variable *A* for the two-end compensated line.

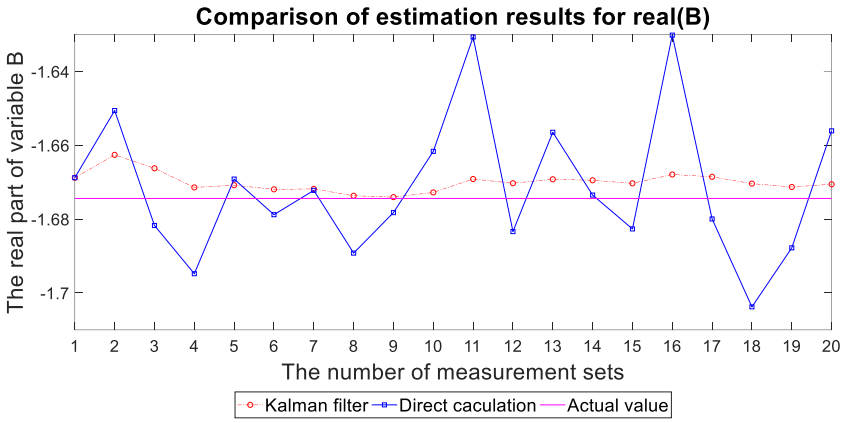

Figure 3.38 The estimation results for the real part of the variable B for the two-end compensated line.

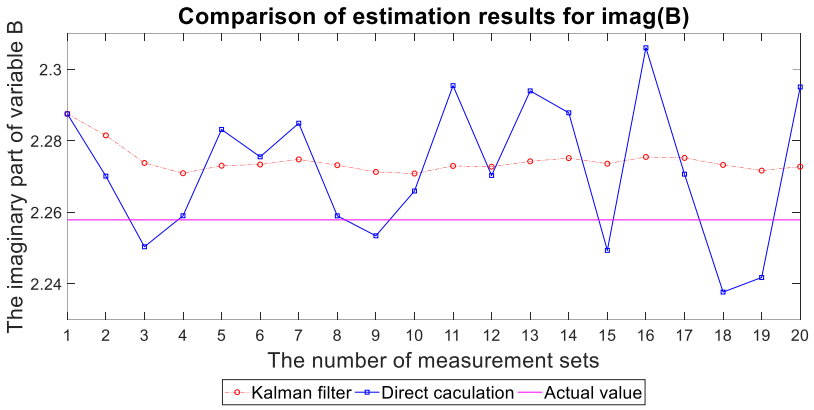

Figure 3.39 The estimation results for the imaginary part of the variable B for the two-end compensated line.

As these figures show, the estimates of the proposed method converge to the actual value while the estimates of direct calculation are sensitive to the added noise. Then the line parameters including $r1$, $x1$, $y1$, and Y_{cap} can be obtained by the proposed method. The results are shown in Figure 3.40 – Figure 3.43.

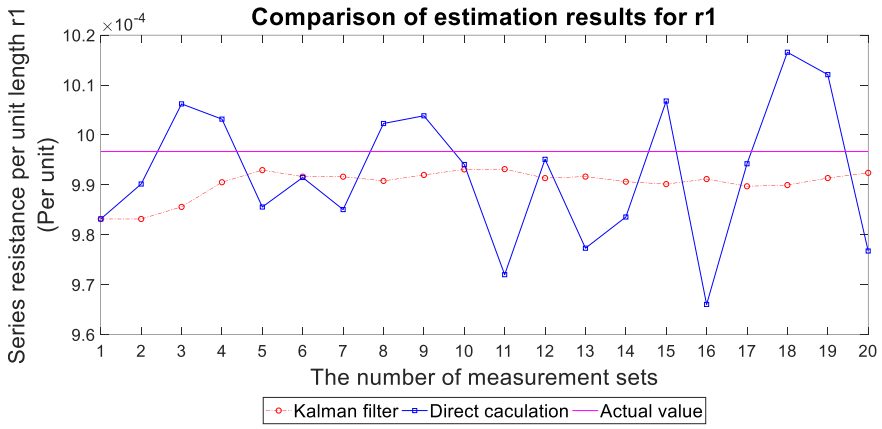

Figure 3.40 The estimation results for $r1$ for the two-end compensated line.

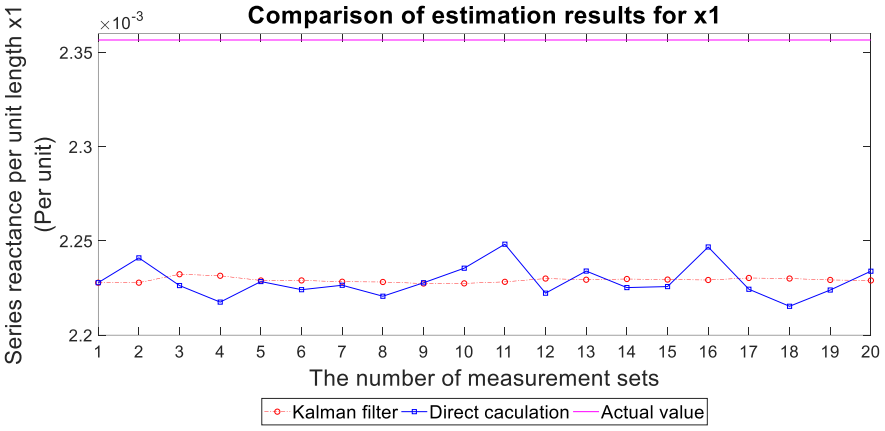

Figure 3.41 The estimation results for $x1$ for the two-end compensated line.

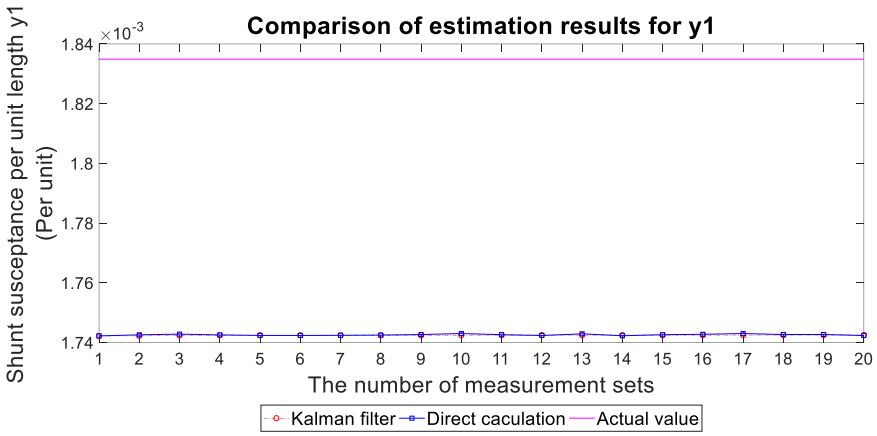

Figure 3.42 The estimation results for $y1$ for the two-end compensated line.

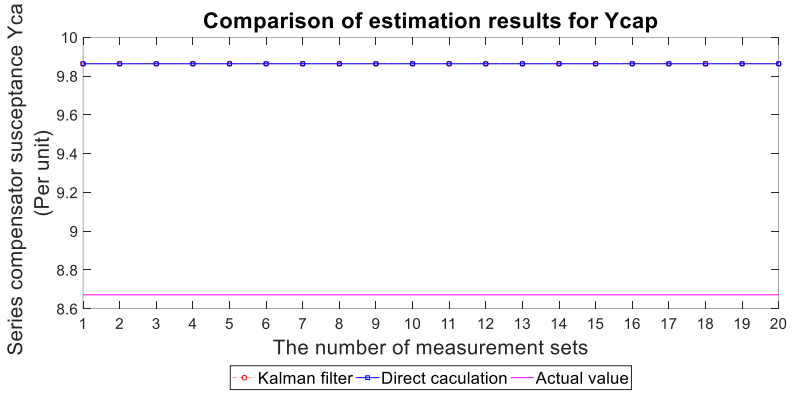

Figure 3.43 The estimation results for Y_{cap} for the two-end compensated line.

From Figure 3.40, we can see that the estimation accuracy for $r1$ has been improved greatly by the proposed method compared to the direct calculation. While in Figure 3.41 – Figure 3.43, both methods have the same estimation accuracy for estimating $x1$, $y1$, and Y_{cap}, which means the estimates for those three parameters are not very sensitive to the noise in the PMU measurements. The line parameters calculated from the Kalman filter at the 20th measurement sets are displayed in Table 3.16.

Table 3.16 Line parameters obtained from estimation results for the two-end compensated line with noise in measurements using Kalman filter at the 20th measurements

Line Parameters	Actual Values	Estimated Values	Estimation Errors
Series Resistance (p.u./mile)	9.9667×10^{-4}	9.9449×10^{-4}	-0.42%
Series Reactance (p.u./mile)	2.3566×10^{-3}	2.2229×10^{-3}	-5.41%
Shunt Susceptance (p.u./mile)	1.8349×10^{-3}	1.7426×10^{-3}	-5.03%
Capacitance of Series Compensator (p.u./mile)	8.6718×10^{-5}	9.8632×10^{-5}	13.74%

3.4 Kalman Filter Tracking Results for Transmission Line Parameters

This section presents evaluation studies based on simulated data. Different line configurations were built using Matlab Simscape Electrical and the proposed algorithms were implemented in Matlab. The actual parameters of the transmission line are shown in Table 3.1. Simulation studies were run to generate voltage and current phasor measurements during varying operating conditions. The measurements were added with normally distributed random noises. Each random noise consists of two parts: the magnitude noise and the angle noise. Both noises have their mean set to zero. For the magnitude noise, its mean $\mu_{mag} = 0$ and its standard deviation σ_{mag} varies for each case; for the angle noise, its mean $\mu_{angle} = 0$ and its standard deviation $\sigma_{angle} = 0.2°$.

Since the series resistance is more susceptible to the change of loading and weather conditions when compared to the series reactance and shunt susceptance, we only changed the series resistance dynamically while the series reactance and shunt susceptance were kept static. In

all the simulations, the series resistance was first set to its normal value and then changed to 120%, 150%, 100%, and 80% of its normal value during different periods.

For each case study, the estimation results of the normal Kalman filter method, adjusted Kalman filter method, and fast Kalman filter method (the parameter n is set to 2 for all cases) were compared.

3.4.1 Kalman Filter Tracking Results for Non-Compensated Transmission Line

The parameters used for the non-compensated line are shown in Table 3.17. The variables D, U_1, U_2 correspond to Adjusted Kalman gain method, Fast KF1 and Fast KF2 method, respectively.

Table 3.17 The parameters of the proposed methods and the random noise used for the non-compensated line

Parameter	D	U_1	U_2	σ_{mag}
Value	20	0.4	0.3	0.5%

The estimation results for the parameters of the non-compensated line are shown in Figure 3.44 –Figure 3.46. The adjusted Kalman gain method has the best performance among all the methods when tracking the dynamically changing series resistance.

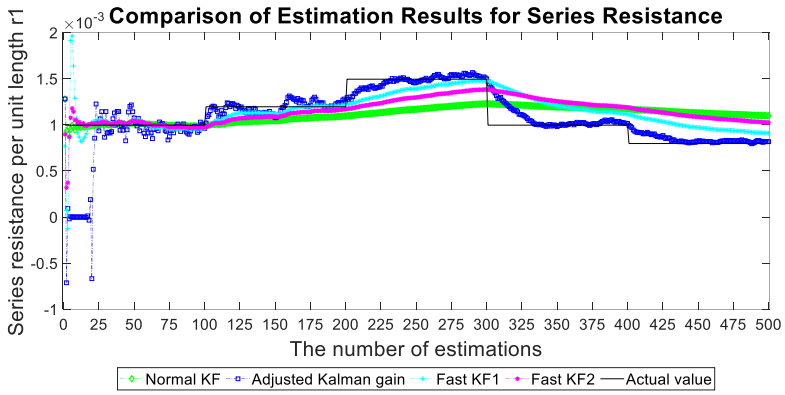

Figure 3.44 The tracking results for the positive sequence series resistance of the non-compensated line.

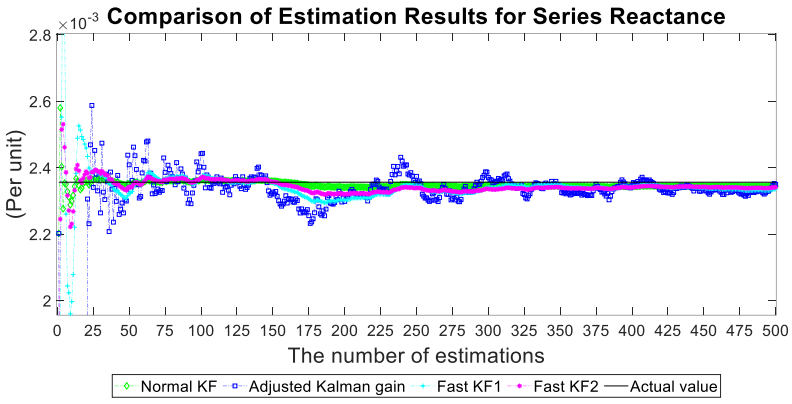

Figure 3.45 The tracking results for the positive sequence series reactance of the non-compensated line.

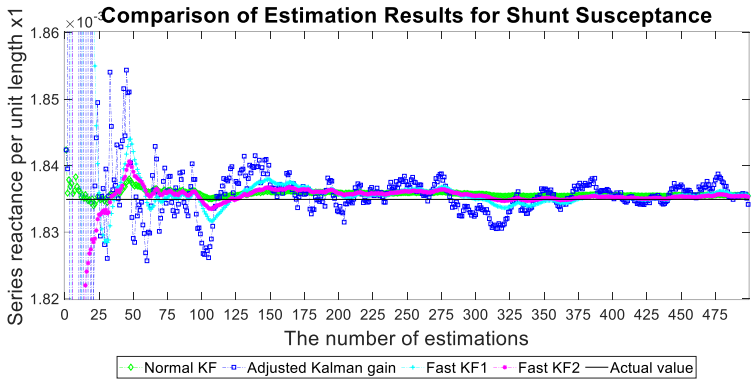

Figure 3.46 The tracking results for the positive sequence shunt susceptance of the non-compensated line.

3.4.2 Kalman Filter Tracking Results for One-End Compensated Line

The parameters used for the one-end compensated line are shown in Table 3.18.

Table 3.18 The parameters of the proposed methods and the random noise used for the one-end compensated line

Parameter	D	U_1	U_2	σ_{mag}
Value	10	0.4	0.3	0.1%

The tracking results for the positive sequence series resistance, series reactance, shunt susceptance, and the reactance of the series compensator of the one-end compensated line are shown in Figure 3.47–Figure 3.50. From the results, we can see that the proposed methods are able to track the dynamically changing line parameters accurately and quickly.

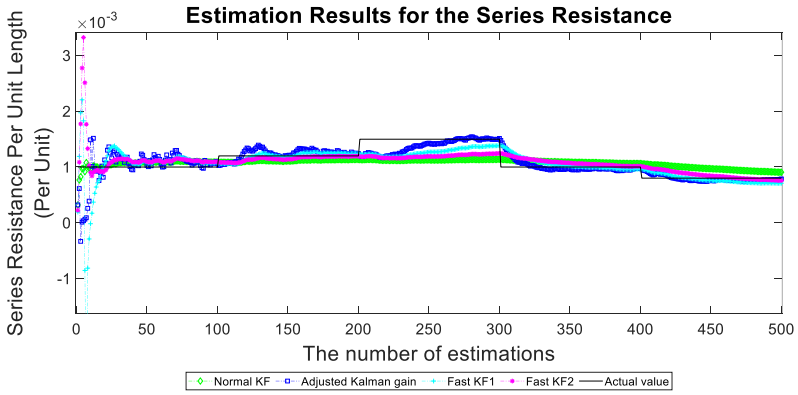

Figure 3.47 The tracking results for the positive sequence series resistance of the one-end compensated line.

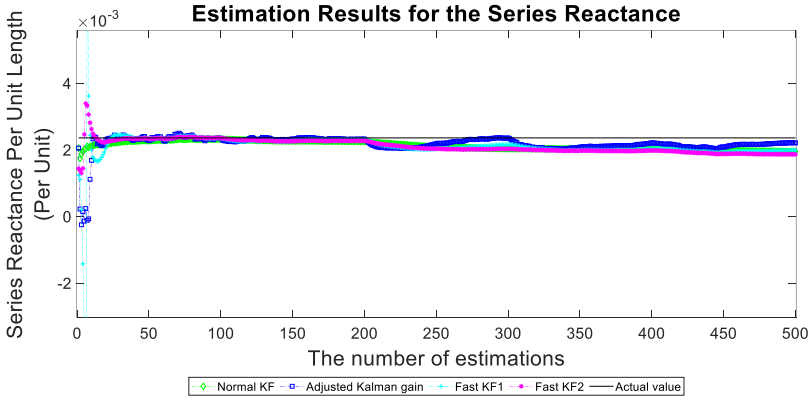

Figure 3.48 The tracking results for the positive sequence series reactance of the one-end compensated line.

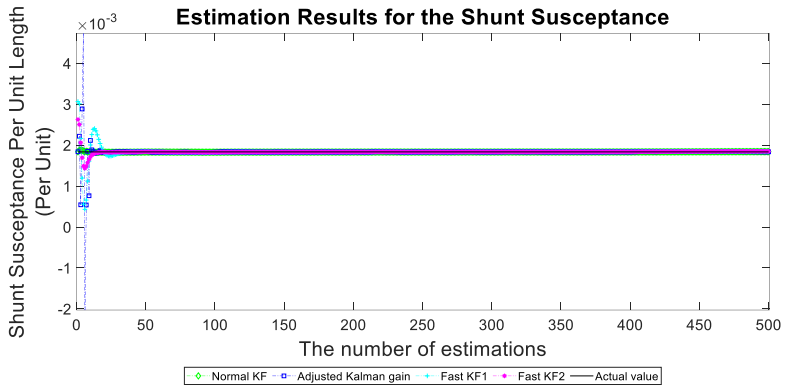

Figure 3.49 The tracking results for the positive sequence shunt susceptance of the one-end compensated line.

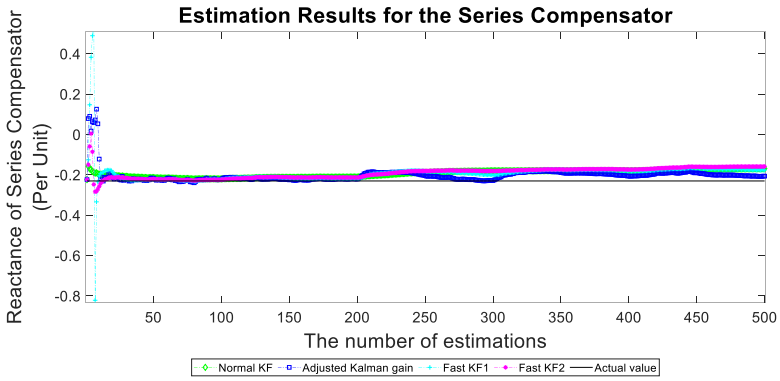

Figure 3.50 The tracking results for the positive sequence reactance of the series compensator of the one-end compensated line.

3.4.3 Kalman Filter Tracking Results for Mid-Compensated Line (Know Series Compensator)

The parameters used for the proposed method for the mid-compensated line are displayed in Table 4.

Table 3.19 The parameters of the proposed methods and the random noise used for the mid-compensated line with known series compensator

Parameter	D	U_1	U_2	σ_{mag}
Value	10	0.4	0.3	0.5%

The tracking results for the positive sequence series resistance, series reactance, and shunt susceptance of the mid-compensated line with known impedance of series compensator are shown in Figure 3.51–Figure 3.53. The results show that the proposed methods have the capability to track the changing line parameters.

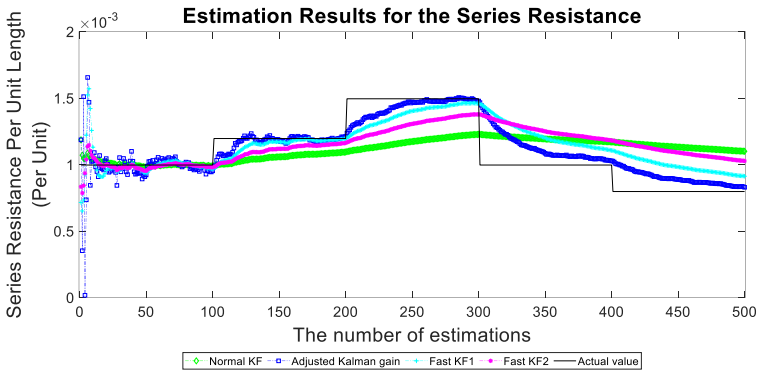

Figure 3.51 The tracking results for the positive sequence series resistance of the mid-compensated Line with known series compensator.

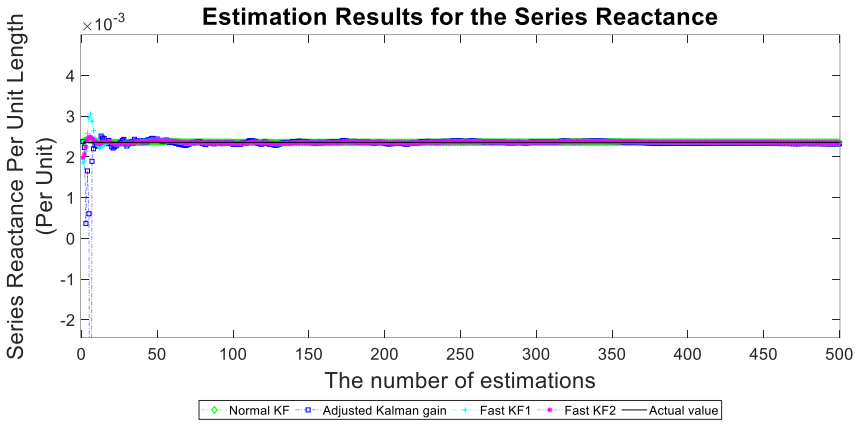

Figure 3.52 The tracking results for the positive sequence series reactance of the mid-compensated line with known series compensator.

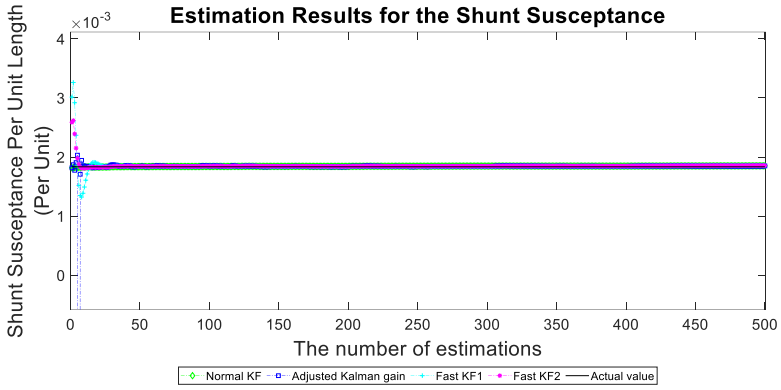

Figure 3.53 The tracking results for the positive sequence shunt susceptance of the mid-compensated line with known series compensator.

3.4.4 Kalman Filter Tracking Results for Mid-Compensated Line (Known Current Through Series Compensator)

The parameters used for the proposed method for the mid-compensated line with known current through series compensator are displayed in Table 3.20.

Table 3.20 The parameters of the proposed methods and the random noise used for the mid-compensated line with known current through series compensator

Parameter	D	U_1	U_2	σ_{mag}
Value	10	0.3	0.2	0.1%

The tracking results for the positive sequence series resistance, series reactance, and shunt susceptance of the one-end compensated line are shown in Figure 3.54–Figure 3.56. The proposed methods can successfully track the dynamic line parameters.

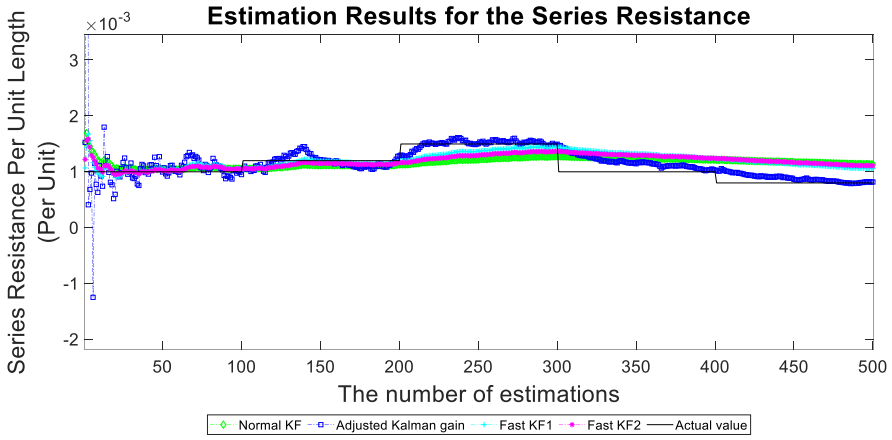

Figure 3.54 The tracking results for the positive sequence series resistance of the mid-compensated line with known current through series compensator.

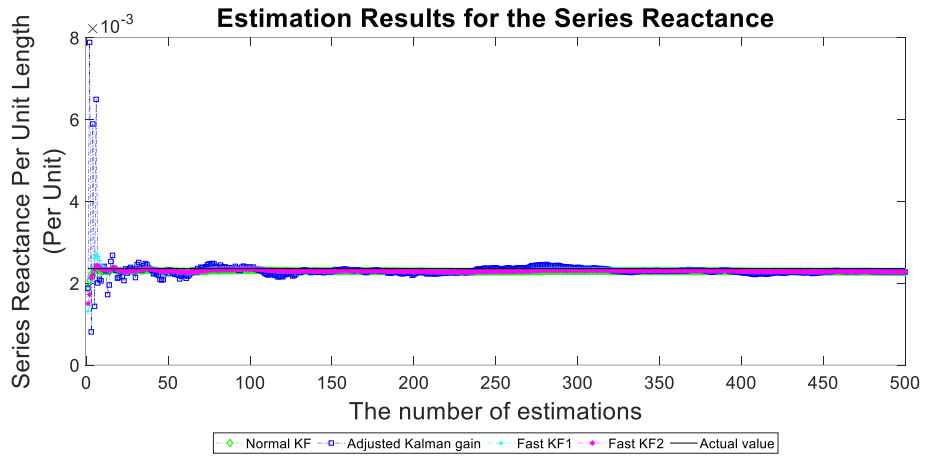

Figure 3.55 The tracking results for the positive sequence series reactance of the mid-compensated line with known current through series compensator.

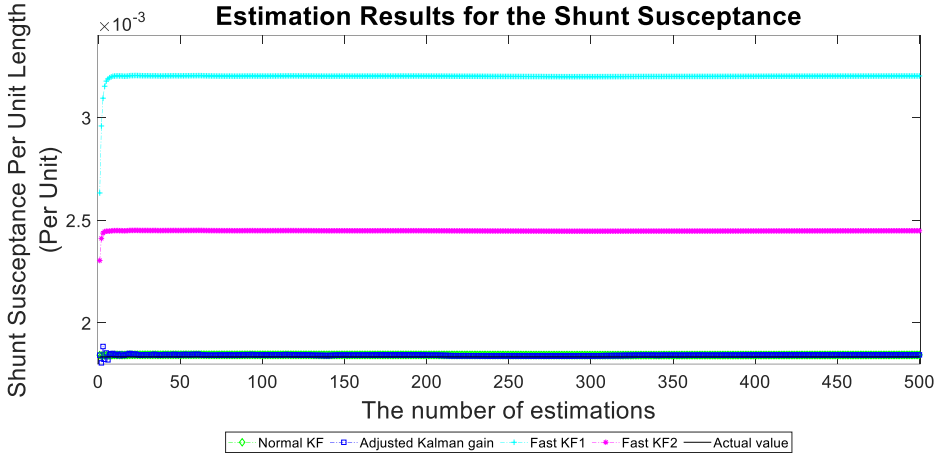

Figure 3.56 The tracking results for the positive sequence shunt susceptance of the mid-compensated line with known current through series compensator.

3.4.5 Kalman Filter Tracking Results for Two-end Compensated Line

The parameters used for the proposed tracking methods for the two-end compensated line are displayed in Table 3.21.

Table 3.21 The parameters of the proposed methods and the random noise used for the two-end compensated line

Parameter	D	U_1	U_2	σ_{mag}
Value	10	0.3	0.2	0.5%

The tracking results for the positive sequence series resistance, series reactance, shunt susceptance, and the reactance of the series compensator of the two-end compensated line are shown in Figure 3.57–Figure 3.58. All three line parameters can be tracked successfully by the proposed method.

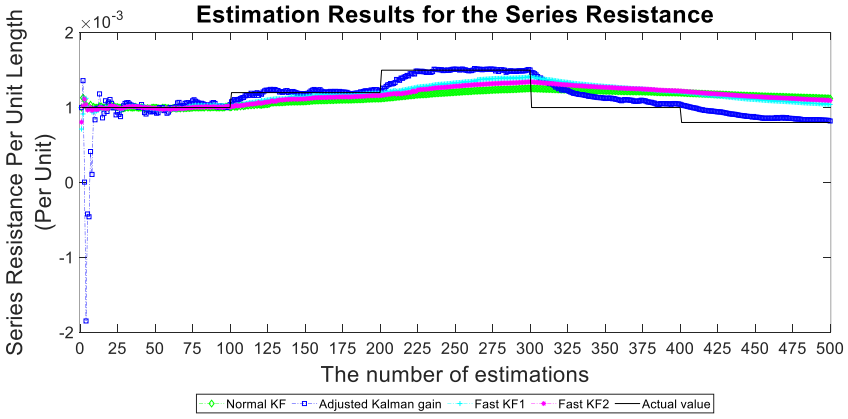

Figure 3.57 The tracking results for the positive sequence series resistance of the two-end compensated line.

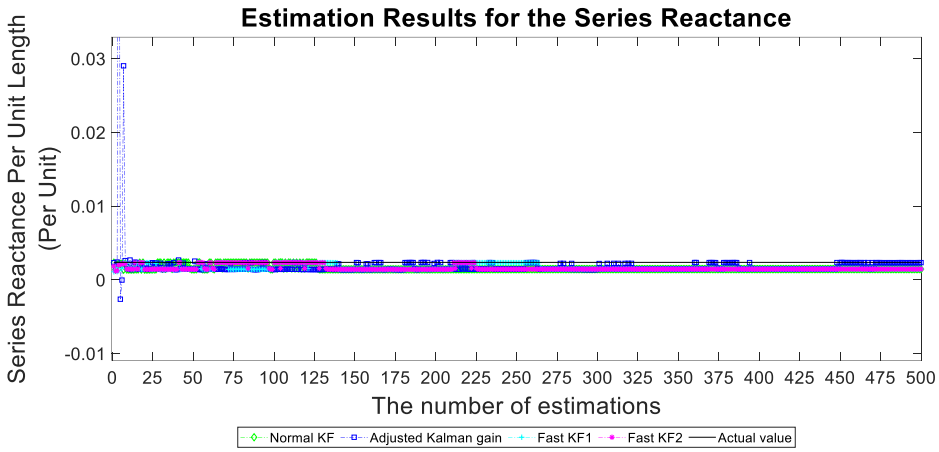

Figure 3.58 The tracking results for the positive sequence series reactance of the two-end compensated line.

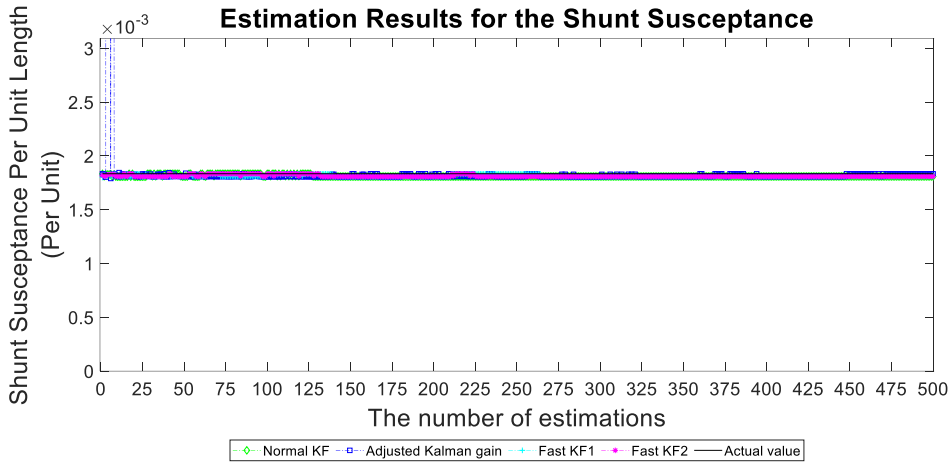

Figure 3.59 The tracking results for the positive sequence shunt susceptance of the two-end compensated line.

CHAPTER 4 ZIP LOAD MODEL PARAMETER ESTIMATION

4.1 ZIP Load Model and Parameter Estimation for a Single Load

A single load can have two possible connection types. One is star connected, which is connected between a phase and the neutral. Another type is delta connected, which is connected between two different phases.

The ZIP load model for a single load is described by (4.1) and (4.2), where $|V|$, P, and Q are the voltage magnitude, real power, reactive power, as measured.

$$P = P_0\left(a_p\left(\frac{|V|}{V_0}\right)^2 + b_p\left(\frac{|V|}{V_0}\right) + c_p\right) \tag{4.1}$$

$$Q = Q_0\left(a_q\left(\frac{|V|}{V_0}\right)^2 + b_q\left(\frac{|V|}{V_0}\right) + c_q\right) \tag{4.2}$$

where P_0 , Q_0, V_0 are the base real power, base reactive power, and base voltage. a, b, and c are the ZIP parameters and their sum is equal to 1. Subscripts p and q to the ZIP parameters indicate values for real and reactive power, respectively.

In (4.1) and (4.2), for a star-connected single load, V represents the phase to neutral voltage, and P and Q represent the phase real and reactive power; for a delta-connected single load, V should be the voltage difference between the two phases, and P and Q are the sums of the real and reactive power measured at each phase. For example, suppose that a load is connected between phase B and C. Equation (4.1) may be more explicitly written as

$$P_B + P_C = P_0\left(a_p\left(\frac{|V_{BC}|}{\sqrt{3}V_0}\right)^2 + b_p\left(\frac{|V_{BC}|}{\sqrt{3}V_0}\right) + c_p\right) \tag{4.3}$$

$$V_{BC} = V_B - V_C \tag{4.4}$$

where, P_B and P_C are phase B and C real power, $\sqrt{3}V_0$ denotes the base voltage of the delta load, and V_{BC} is phase B to C voltage.

However, in practical applications, the phase angle of voltage may not always be available, and only phase voltage magnitude is measured. Thus the line to line voltage cannot be calculated. In this case, the average voltage magnitude of phase B and C is often used in the ZIP load model, i.e., $|V_{BC_{avg}}|$ in (4.5). For balanced cases, $V_c = V_B\angle -120°$, we have

$$|V_{BC_{avg}}| = \frac{|V_B| + |V_c|}{2V_0} = \frac{|V_B|}{V_0} \tag{4.5}$$

which is the same as $\frac{|V_{BC}|}{\sqrt{3}V_0}$. Therefore, using average magnitude will get identical results as using line-to-line voltage in the ZIP model for balanced voltage cases. Different results may be yielded for unbalanced cases, which will be further explained later.

In the following sections, the three commonly used estimation methods for the ZIP load model are discussed. A window size n is selected for each estimation, i.e., n sets of measurements are used for each estimation. It is assumed that the ZIP load model parameters remain constant, i.e., a, b, c, P_0, and Q_0 stay unchanged during the period of taking the n sets of measurements, although ZIP parameters may change over time.

4.1.1 Least Squares Method

The least squares method has been described in [25], [29], [36], [37] to estimate ZIP parameters based on the matrix equation $Z = Hx$. In summary, we have

$$Z = [P_1, P_2, \dots, P_n]^T \tag{4.6}$$

$$H = \begin{bmatrix} \left(\frac{|V_1|}{V_0}\right)^2 & \frac{|V_1|}{V_0} & 1 \\ \left(\frac{|V_2|}{V_0}\right)^2 & \frac{|V_2|}{V_0} & 1 \\ \vdots & \vdots & \vdots \\ \left(\frac{|V_n|}{V_0}\right)^2 & \frac{|V_n|}{V_0} & 1 \end{bmatrix} \tag{4.7}$$

$$x = \begin{bmatrix} a_p P_0 \\ b_p P_0 \\ c_p P_0 \end{bmatrix} \tag{4.8}$$

where Z consists of measured real power, H is composed of voltage measurements, and x is the unknown vector. The solution of the least squares method is given by

$$x = (H^T H)^{-1} H^T Z \tag{4.9}$$

Once x is obtained, P_0 is calculated as the sum of x, which implies that the sum of a_p, b_p and c_p is one. The ZIP parameters a_p, b_p and c_p are calculated by dividing x by P_0.

4.1.2 Optimization Method

The optimization method has been used in [24] to estimate ZIP parameters and works similarly to the theory of the least squares method. For a window size of n, (4.10) can be written based on the ZIP load model.

$$\begin{bmatrix} f_1 \\ f_2 \\ \vdots \\ f_n \end{bmatrix} = \begin{bmatrix} P_1 \\ P_2 \\ \vdots \\ P_n \end{bmatrix} - \begin{bmatrix} \left(\frac{|V_1|}{V_0}\right)^2 & \frac{|V_1|}{V_0} & 1 \\ \left(\frac{|V_2|}{V_0}\right)^2 & \frac{|V_2|}{V_0} & 1 \\ \vdots & \vdots & \vdots \\ \left(\frac{|V_n|}{V_0}\right)^2 & \frac{|V_n|}{V_0} & 1 \end{bmatrix} \begin{bmatrix} a_p P_0 \\ b_p P_0 \\ c_p P_0 \end{bmatrix} \tag{4.10}$$

where f is the difference between the measured P and the estimated P(calculated by using the measured voltage and estimated ZIP parameters). The optimization method will produce the estimation results that minimize $f_1(x)^2 + f_2(x)^2 + \cdots + f_n(x)^2$. Constraints can be easily imposed including $a_p + b_p + c_p$=1 and $a_p, b_p,$ and c_p being non-negative for loads.

4.1.3 Extension to Least Squares and Optimization Method

For practical applications, if we only want to obtain an average set of ZIP parameters, then the following method can be used.

We assume that for every N_1 consecutive time points, e.g., 4 points, P_0 remains constant. Suppose we have a total of n sets of measurements, say 2 sets, each of which contains such N_1 points. Then the total number of measurements will be nN_1. We have

$$\begin{aligned} P_1 &= P_{0_1}\left[a_p\left(\frac{|V_1|}{V_0}\right)^2 + b_p\left(\frac{|V_1|}{V_0}\right) + c_p\right] \\ P_2 &= P_{0_1}\left[a_p\left(\frac{|V_2|}{V_0}\right)^2 + b_p\left(\frac{|V_2|}{V_0}\right) + c_p\right] \end{aligned} \tag{4.11}$$

...

$$P_{N_1} = P_{0N_1}\left[a_p\left(\frac{|V_{N_1}|}{V_0}\right)^2 + b_p\left(\frac{|V_{N_1}|}{V_0}\right) + c_p\right]$$

...

$$P_{(k-1)*N_1+i} = P_{0k}\left[a_p\left(\frac{|V_{(k-1)*N_1+i}|}{V_0}\right)^2 + b_p\left(\frac{|V_{(k-1)*N_1+i}|}{V_0}\right) + c_p\right]$$

where, $a_p + b_p + c_p = 1$, $k = 1, \dots, n$ is measurement set index, and $i = 1, \dots, N_1$ are time points within each measurement set. The number of equations: nN_1 and the number of the unknown variables is P_{0k}, a_p, b_p, c_p, a total of $n + 3$ unknowns. Then either the least squares or optimization method can be used to solve for the unknowns.

In another variant, one of the ZIP parameters can be eliminated, so that the power can be written using any two of the ZIP parameters. For example, in (4.12), c_p is eliminated and the ZIP load model is represented by a_p and b_p.

$$P_{N_1} = P_{01}\left\{a_p\left[\left(\frac{|V_{N_1}|}{V_0}\right)^2 - 1\right] + b_p\left[\left(\frac{|V_{N_1}|}{V_0}\right) - 1\right] + 1\right\} \tag{4.12}$$

4.1.4 Kalman Filter Method

Similar to the Kalman filter method used for estimating line parameters, the Kalman filter method for ZIP load model parameters is also based on the five questions (2.60)–(2.64), which have been explained in Section 2.3.6. In this section, we just need to define the state to be estimated

$x_k = \begin{bmatrix} a_p P_0 \\ b_p P_0 \\ c_p P_0 \end{bmatrix}$, the measurement vector $w_k = [P_1, P_2, \dots, P_n]^T$, and the measurement matrix $H_k =$

$$\begin{bmatrix} \left(\frac{|V_1|}{V_0}\right)^2 & \frac{|V_1|}{V_0} & 1 \\ \left(\frac{|V_2|}{V_0}\right)^2 & \frac{|V_2|}{V_0} & 1 \\ \vdots & \vdots & \vdots \\ \left(\frac{|V_n|}{V_0}\right)^2 & \frac{|V_n|}{V_0} & 1 \end{bmatrix}.$$

4.1.5 Neural Network Method

The neural network has been used in [26], [54] to estimate the ZIP parameters. The structure of the proposed neural network is shown in Figure 4.1. It has two inputs $\left(\left(\frac{V}{V_0}\right)^2, \frac{V}{V_0}\right)$ and one output P. The measured voltages and powers are used as training data to train the neural network. The neural network will be trained for every n sets of measurements. After training, the weights and bias can be extracted from the trained neural network, from which the ZIP parameters can be obtained.

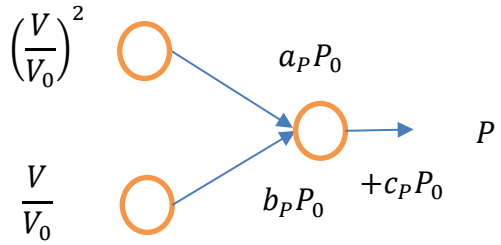

Figure 4.1 The structure of the neural network for ZIP load modeling.

4.1.6 Measurement Noises

In this section, the ZIP parameter estimation is studied under the effect of measurement noise. To this end, the ZIP parameters and base power are kept constant: $a_p = 0.25$, $b_p = 0.15$,

$c_p = 0.60$, $P_0 = 110$. The base voltage is $120\,V$. The estimation is performed using the least squares method. The noise is added to both power and voltage measurements and is defined as normally distributed random numbers with the mean $\mu = 0$ and the standard deviation $\sigma =$ 0.01% of the measurement magnitude. With very small measurement noises, the estimation error can be substantial as shown in Figure 4.2.

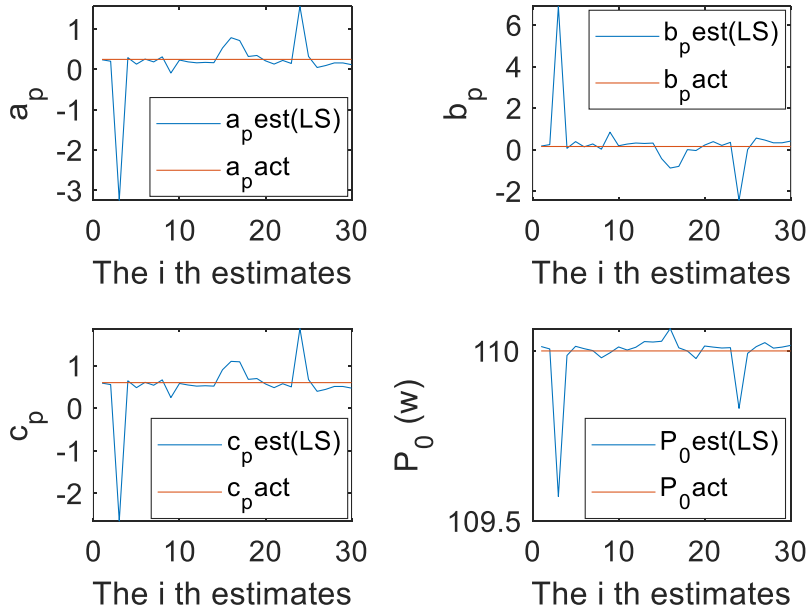

Figure 4.2 The ZIP estimation results for a single load with measurement noise (blue: estimated values; red: actual values).

For example, for the 3rd estimate, the voltage and power measurements without noises are: (114.6535, 114.3669, 117.1774, 116.7569) V and (106.8690, 106.7042, 108.3334, 108.0877) W. The estimated ZIP parameters and P_0 are: (0.2497, 0.1506, 0.5997) and 109.9998 W, which are very close to the actual ZIP parameters. The mean squared error (MSE) is 5.61×10^{-8}. Then, the ZIP parameters are estimated using voltage and power measurements with noises, which are: (114.6320, 114.3859, 117.1775, 116.7657) V and(106.8867, 106.6926, 108.3361, 108.0999) W.

The estimated ZIP parameters and P_0 are: (-3.2461, 6.8988, -2.6527) and 109.5718 W. The MSE is 2.24×10^{-4}. If we use the actual ZIP and base power value $(0.25, 0.15, 0.60, 110)$, the MSE is calculated as 3.67×10^{-4}. Therefore, the estimated values indeed yield smaller MSE than true values do, even though they deviate from true values.

4.2 ZIP Load Model and Parameter Estimation for Aggregate Load

In a power system, the measurement at a single load might not always be available. Therefore, there is the need of having a ZIP load model for several loads. Based on the modeling for a single load, we can also derive the ZIP load model for several loads connected together, i.e., aggregate load.

This section presents the ZIP load model and parameter estimation for aggregate load. Section 4.2.1 discusses a single delta load continuing from Section 4.1.

4.2.1 ZIP Load Model for a Single Delta Load

This section studies a single load connected between two phases. In this case, the load is connected between phase B and C, as shown in Figure 4.3. Suppose that the load has base power $P_0 = 100kW$, base line to line voltage $V_{0LL} = 4.16kV$, and the ZIP parameters $a_p = 0.2$, $a_p = 0.5$, and $c_p = 0.3$.

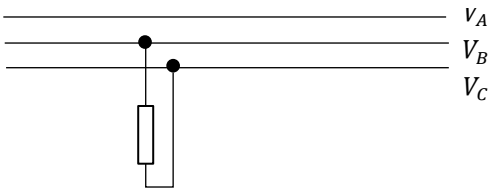

Figure 4.3 The circuit diagram of a single delta load.

The following subsections study the ZIP estimation for single delta under the balanced and different unbalanced voltage conditions. For each subsection, the ZIP parameters of the single delta load are estimated using the average voltage. The line-to-line voltage has also been used in estimation, but the results are not presented in each subsection since it always gives accurate results. All the estimation results are produced by using the least squares method.

4.2.1.1 Balanced Voltages Condition

In this section, the ZIP parameter estimation for a single delta load is studied under the balanced voltage condition. The voltage and power data used for estimation are shown in Table 4.1.

Table 4.1 Voltage and power data for the single delta load under the balanced voltage condition

$\lvert V_B \rvert$ (kV)	$\angle V_B$ (degree)	$\lvert V_C \rvert$ (kV)	$\angle V_C$ (degree)	P (kW)
2.2800	-120	2.2800	120	95.4882
2.4480	-120	2.4480	120	101.7395
2.5680	-120	2.5680	120	106.3245
2.6400	-120	2.6400	120	109.1235

If we use the line to line voltage magnitude, the estimated ZIP parameters are: $a_p = 0.2000$, $b_p = 0.5000$, and $c_p = 0.3000$. If we use the average voltage magnitudes, the estimated ZIP parameters are: $a_p = 0.1998$, $b_p = 0.5000$, and $c_p = 0.3002$. The results show that using average voltage for estimation can provide good estimation accuracy.

4.2.1.2 Unbalanced Voltages Condition (Unbalanced Magnitudes)

This section studies the effect of the unbalanced voltage magnitudes on ZIP parameter estimation for a single delta load. The estimated ZIP parameters are: $a_p = 0.1993$, $b_p = 0.5012$, and $c_p = 0.2995$.

Table 4.2 Voltage and power data for the single delta load under the unbalanced voltage magnitude condition

$\lvert V_B \rvert$ (kV)	$\angle V_B$ (degree)	$\lvert V_C \rvert$ (kV)	$\angle V_C$ (degree)	P (kW)	Voltage unbalance
2.2572	-120	2.2800	120	95.0714	0.50%
2.3998	-120	2.4480	120	100.8314	1.00%
2.5423	-120	2.5680	120	105.8296	0.50%
2.5898	-120	2.6400	120	108.1460	0.96%

4.2.1.3 Unbalanced Voltages Condition (Unbalanced Angles)

The effect of unbalanced voltage angle on ZIP parameter estimation is studied in this case. The four sets of measurements used for estimation are shown in Table 4.3. The estimated $a_p = 0.4171$, $b_p = 0.0488$, and $c_p = 0.5341$. Table 4.4 shows another set of measurements with voltage angle unbalance, and the estimated $a_p = 0.2020$, $b_p = 0.5005$, and $c_p = 0.2975$.

In the first case, the voltage angle unbalance is relatively small compared to the second case. But the unbalance is varying and the estimation results deviate a lot from the theoretical values. For the second case, as long as the voltage angle unbalance is invariant, the estimation results are promising although the voltage angle unbalance is large.

Table 4.3 Voltage and power data for the single delta load under the unbalanced voltage angle condition one

$\lvert V_B \rvert$ (kV)	$\angle V_B$ (degree)	$\lvert V_C \rvert$ (kV)	$\angle V_C$ (degree)	P (kW)
2.2800	-119	2.2800	120	95.9062
2.4480	-119.3	2.4480	120	102.0643
2.5680	-119.5	2.5680	120	106.5736
2.6400	-119.2	2.6400	120	109.5377

Table 4.4 Voltage and power data for the single delta load under the unbalanced voltage angle condition two

$\lvert V_B \rvert$ (kV)	$\angle V_B$ (degree)	$\lvert V_C \rvert$ (kV)	$\angle V_C$ (degree)	P (kW)
2.2800	-118	2.2800	120	95.9062
2.4480	-118	2.4480	120	102.1105
2.5680	-118	2.5680	120	106.7717
2.6400	-118	2.6400	120	109.4862

4.2.2 Aggregate ZIP Load Model for Three-Phase Star Load

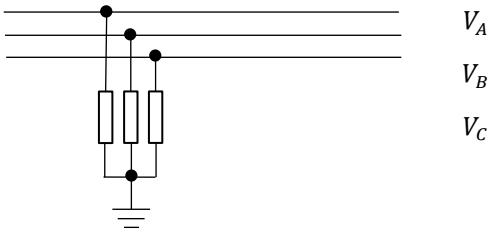

Figure 4.4 The circuit diagram for a three-phase star load.

In this section, the aggregate ZIP load model for the three-phase star-connected load is discussed. Figure 4.4 shows the circuit diagram. The individual ZIP load models for the real power of three single loads connected at phase A, B, and C can be described by (4.13)–(4.15)

$$P_A = P_{0_A}\left(a_{p_A}\left(\frac{|V_A|}{V_0}\right)^2 + b_{p_A}\left(\frac{|V_A|}{V_0}\right) + c_{p_A}\right) \tag{4.13}$$

$$P_B = P_{0_B}\left(a_{p_B}\left(\frac{|V_B|}{V_0}\right)^2 + b_{p_B}\left(\frac{|V_B|}{V_0}\right) + c_{p_B}\right) \tag{4.14}$$

$$P_C = P_{0_C}\left(a_{p_C}\left(\frac{|V_C|}{V_0}\right)^2 + b_{p_C}\left(\frac{|V_C|}{V_0}\right) + c_{p_C}\right) \tag{4.15}$$

It is hard to obtain an analytical form of ZIP load model for an aggregate ZIP load as in the single ZIP load model unless the three-phase voltages are balanced. So, if $|V_A| = |V_B| = |V_C| = V$, then we can obtain (4.16) by summing (4.13)–(4.15).

$$P_{Agg} = P_{0_{Agg}}\left(a_{p_{Agg}}\left(\frac{V}{V_0}\right)^2 + b_{p_{Agg}}\frac{V}{V_0} + c_{p_{Agg}}\right) \tag{4.16}$$

where

$$P_{Agg} = P_A + P_B + P_C \tag{4.17}$$

$$P_{0_{Agg}} = P_{0_A} + P_{0_B} + P_{0_C} \tag{4.18}$$

$$a_{p_{Agg}} = \frac{P_{0_A} a_{p_A} + P_{0_B} a_{p_B} + P_{0_C} a_{p_C}}{P_{0_A} + P_{0_B} + P_{0_C}} \tag{4.19}$$

$$b_{p_{Agg}} = \frac{P_{0_A} b_{p_A} + P_{0_B} b_{p_B} + P_{0_C} a_{p_C}}{P_{0_A} + P_{0_B} + P_{0_C}} \tag{4.20}$$

$$c_{p_{Agg}} = \frac{P_{0_A} c_{p_A} + P_{0_B} c_{p_B} + P_{0_C} c_{p_C}}{P_{0_A} + P_{0_B} + P_{0_C}} \tag{4.21}$$

The aggregate ZIP parameters are the weighted averages of the individual ZIP parameters of each load while the weights are the base power of each load. For the unbalanced system, the average three-phase voltage magnitude can be used:

$$V = \frac{|V_A| + |V_B| + |V_C|}{3} \tag{4.22}$$

Next, we studied the ZIP parameter estimation for the three-phase star load with four different configurations. The single loads at phase A, B, and C can have the same or different base power (P_0) and same or different ZIP parameters, which make up the four configurations. For each configuration, the ZIP parameter estimation is performed using the balanced and unbalanced voltage data shown in Table 4.5. The voltage unbalance [55] is calculated by

$$unbalance\ \% = \frac{max\ deviation\ from\ avg.V}{avg.V} \tag{4.23}$$

The estimation results are shown in Table 4.6–Table 4.9. The fourth row of every table is for the calculated theoretical ZIP parameters based on (4.19)–(4.21). It can be seen that the ZIP parameters can be estimated accurately under balanced voltages condition for all four configurations. However, under the condition of the unbalanced voltage, the ZIP parameters can only be estimated without much deviation for the three-phase loads with the same P_0 and the same ZIP parameters configuration.

Table 4.5 Three-phase balanced and unbalanced voltages

Balanced Voltages Case			Unbalanced Voltages Case			
$\|V_A\|$ (kV)	$\|V_B\|$ (kV)	$\|V_C\|$ (kV)	$\|V_A\|$ (kV)	$\|V_B\|$ (kV)	$\|V_C\|$ (kV)	Voltage unbalance
2.3040	2.3040	2.3040	2.3040	2.2560	2.3520	2.08%
2.4240	2.4240	2.4240	2.4240	2.3520	2.4720	2.64%
2.5200	2.5200	2.5200	2.5200	2.4480	2.5920	2.85%
2.6160	2.6160	2.6160	2.6160	2.5680	2.6400	1.53%

Table 4.6 The ZIP parameters of each load and the estimation results for the three-phase star load (same P_0 and same ZIP parameters)

	a_p	b_p	c_p	$P_0(kW)$
Load connected at phase A	0.4	0.2	0.4	120
Load connected at phase B	0.4	0.2	0.4	120
Load connected at phase C	0.4	0.2	0.4	120
Calculated Aggregate ZIP	0.4	0.2	0.4	360
Estimated Aggregate ZIP (balanced voltages case)	0.4	0.2	0.4	360
Estimated Aggregate ZIP (unbalanced voltages case)	0.36	0.27	0.37	360.07

Table 4.7 The ZIP parameters of each load and the estimation results for the three-phase star load (same P_0 and different ZIP parameters)

	a_p	b_p	c_p	$P_0(kW)$
Load connected at phase A	0.4	0.2	0.4	120
Load connected at phase B	0.6	0.3	0.1	120
Load connected at phase C	0.2	0.3	0.5	120
Calculated Aggregate ZIP	0.40	0.27	0.33	360
Estimated Aggregate ZIP (balanced voltages case)	0.40	0.27	0.33	360
Estimated Aggregate ZIP (unbalanced voltages case)	1.14	-1.25	1.10	357.37

Table 4.8 The ZIP parameters of each load and the estimation results for the three-phase star load (different P_0 and same ZIP parameters)

	a_p	b_p	c_p	$P_0(kW)$
Load connected at phase A	0.4	0.2	0.4	120
Load connected at phase B	0.4	0.2	0.4	150
Load connected at phase C	0.4	0.2	0.4	80
Calculated Aggregate ZIP	0.4	0.2	0.4	350
Estimated Aggregate ZIP (balanced voltages case)	0.4	0.2	0.4	350
Estimated Aggregate ZIP (unbalanced voltages case)	0.94	-0.90	0.96	348.12

Table 4.9 The ZIP parameters of each load and the estimation results for the three-phase star load (different P_0 and different ZIP parameters)

	a_p	b_p	c_p	$P_0(kW)$
Load connected at phase A	0.4	0.2	0.4	120
Load connected at phase B	0.6	0.3	0.1	150
Load connected at phase C	0.2	0.3	0.5	80
Calculated Aggregate ZIP	0.44	0.27	0.29	350
Estimated Aggregate ZIP (balanced voltages case)	0.44	0.27	0.29	350
Estimated Aggregate ZIP (unbalanced voltages case)	1.80	-2.52	1.71	345.32

4.2.3 Aggregate ZIP Load Model for Three-Phase Delta Load

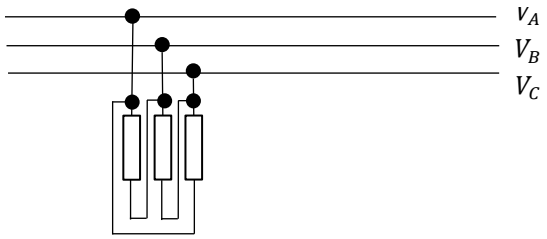

Figure 4.5 The circuit diagram for a three-phase delta load.

This section presents the aggregate ZIP load model for the real power of the three-phase aggregate delta loads. The circuit diagram is shown in Figure 4.5. The individual ZIP load model of the three loads can be expressed as in (4.24)–(4.26)

$$P_{AB} = P_{0_{AB}}\left(a_{p_{AB}}\left(\frac{|V_{AB}|}{\sqrt{3}V_0}\right)^2 + b_{p_{AB}}\left(\frac{|V_{AB}|}{\sqrt{3}V_0}\right) + c_{p_{AB}}\right) \quad (4.24)$$

$$P_{BC} = P_{0_{BC}}\left(a_{p_{BC}}\left(\frac{|V_{BC}|}{\sqrt{3}V_0}\right)^2 + b_{p_{BC}}\left(\frac{|V_{BC}|}{\sqrt{3}V_0}\right) + c_{p_{BC}}\right) \tag{4.25}$$

$$P_{AC} = P_{0_{AC}}\left(a_{p_{AC}}\left(\frac{|V_{AC}|}{\sqrt{3}V_0}\right)^2 + b_{p_{AC}}\left(\frac{|V_{AC}|}{\sqrt{3}V_0}\right) + c_{p_{AC}}\right) \tag{4.26}$$

If the three-phase voltages are balanced, i.e., $|V_A| = |V_B| = |V_C| = V$, then (4.24)–(4.26) can be rewritten as (4.27)–(4.29).

$$P_{AB} = P_{0_{AB}}\left(a_{p_{AB}}\left(\frac{V}{V_0}\right)^2 + b_{p_{AB}}\left(\frac{V}{V_0}\right) + c_{p_{AB}}\right) \tag{4.27}$$

$$P_{BC} = P_{0_{BC}}\left(a_{p_{BC}}\left(\frac{V}{V_0}\right)^2 + b_{p_{BC}}\left(\frac{V}{V_0}\right) + c_{p_{BC}}\right) \tag{4.28}$$

$$P_{AC} = P_{0_{AC}}\left(a_{p_{AC}}\left(\frac{V}{V_0}\right)^2 + b_{p_{AC}}\left(\frac{V}{V_0}\right) + c_{p_{AC}}\right) \tag{4.29}$$

Then an analytical form of aggregate ZIP load model can be obtained by summing (4.27)-(4.29)

$$P_{Agg} = P_{0_{Agg}}\left(a_{p_{Agg}}\left(\frac{V}{V_0}\right)^2 + b_{p_{Agg}}\frac{V}{V_0} + c_{p_{Agg}}\right) \tag{4.30}$$

where

$$P_{Agg} = P_{AB} + P_{BC} + P_{AC} \tag{4.31}$$

$$P_{0_{Agg}} = P_{0_{AB}} + P_{0_{BC}} + P_{0_{AC}} \tag{4.32}$$

$$a_{p_{Agg}} = \frac{P_{0_{AB}} a_{p_{AB}} + P_{0_{BC}} a_{p_{BC}} + P_{0_{AC}} a_{p_{AC}}}{P_{0_{AB}} + P_{0_{BC}} + P_{0_{AC}}} \tag{4.33}$$

$$b_{p_{Agg}} = \frac{P_{0_{AB}} a_{p_{AB}} + P_{0_{BC}} a_{p_{BC}} + P_{0_{AC}} a_{p_{AC}}}{P_{0_{AB}} + P_{0_{BC}} + P_{0_{AC}}} \tag{4.34}$$

$$c_{p_{Agg}} = \frac{P_{0_{AB}} a_{p_{AB}} + P_{0_{BC}} a_{p_{BC}} + P_{0_{AC}} a_{p_{AC}}}{P_{0_{AB}} + P_{0_{BC}} + P_{0_{AC}}} \tag{4.35}$$

For the case of unbalanced voltages, we can use the three-phase average voltage as the voltage variable for the ZIP load model for the three-phase delta load.

The ZIP parameter estimation for the three-phase delta load is also studied for the four different configurations under balanced and unbalanced voltages conditions using the voltage data in Table 4.5. The results are shown in Table 4.10–Table 4.13 From the results, we have similar observations: the voltage unbalance can cause the estimated ZIP parameters to deviate from the theoretical ZIP parameters, and the deviation is minimum for the three-phase load with the same base power and same ZIP parameters configuration.

Table 4.10 The ZIP parameters of each load and the estimation results for the three-phase delta load (same P_0 and same ZIP parameters)

	a_p	b_p	c_p	$P_0(kW)$
Load connected at phase A and B	0.4	0.2	0.4	120
Load connected at phase B and C	0.4	0.2	0.4	120
Load connected at phase A and C	0.4	0.2	0.4	120
Calculated Aggregate ZIP	0.4	0.2	0.4	360
Estimated Aggregate ZIP (balanced voltages case)	0.40	0.20	0.40	359.73

Estimated Aggregate ZIP (unbalanced voltages case)	0.38	0.24	0.38	359.77

Table 4.11 The ZIP parameters of each load and the estimation results for the three-phase delta load (same P_0 and different ZIP parameters)

	a_p	b_p	c_p	$P_0(kW)$
Load connected at phase A and B	0.4	0.2	0.4	120
Load connected at phase B and C	0.6	0.3	0.1	120
Load connected at phase A and C	0.2	0.3	0.5	120
Calculated Aggregate ZIP	0.40	0.27	0.33	360
Estimated Aggregate ZIP (balanced voltages case)	0.40	0.27	0.33	359.71
Estimated Aggregate ZIP (unbalanced voltages case)	0.53	0.00	0.47	359.20

Table 4.12 The ZIP parameters of each load and the estimation results for the three-phase delta load (different P_0 and same ZIP parameters)

	a_p	b_p	c_p	$P_0(kW)$
Load connected at phase A and B	0.4	0.2	0.4	120
Load connected at phase B and C	0.4	0.2	0.4	150
Load connected at phase A and C	0.4	0.2	0.4	80
Calculated Aggregate ZIP	0.4	0.2	0.4	350
Estimated Aggregate ZIP (balanced voltages case)	0.40	0.20	0.40	349.74
Estimated Aggregate ZIP (unbalanced voltages case)	0.55	-0.10	0.55	349.19

Table 4.13 The ZIP parameters of each load and the estimation results for the three-phase delta load (different P_0 and same ZIP parameters)

	a_p	b_p	c_p	$P_0(kW)$
Load connected at phase A and B	0.4	0.2	0.4	120
Load connected at phase B and C	0.6	0.3	0.1	150
Load connected at phase A and C	0.2	0.3	0.5	80
Calculated Aggregate ZIP	0.44	0.27	0.29	350
Estimated Aggregate ZIP (balanced voltages case)	0.44	0.27	0.30	349.70
Estimated Aggregate ZIP (unbalanced voltages case)	0.69	-0.24	0.55	348.76

4.2.4 Aggregate ZIP Load Model for Multiple Three-Phase Star Loads

This section studies the aggregate ZIP load model for multiple three-phase star-connected balanced loads in power systems. Suppose there are n three-phase balanced star loads connected together. Assume that $|V_A| = |V_B| = |V_C| = V$. The real power of each three-phase load are P_i ($i = 1, 2, \dots, n$); the ZIP parameters and base power of the ZIP model for three each load are P_{0_i} and (a_{p_i}, b_{p_i}, c_{p_i}). The power of each three-phase star-connected load can be expressed as

$$P_i = P_{0_i}\left(a_{p_i}\left(\frac{|V|}{V_0}\right)^2 + b_{p_i}\frac{|V|}{V_0} + c_{p_i}\right) \tag{4.36}$$

Then the aggregate ZIP load model for the multiple three-phase loads can be expressed as

$$P_{Agg} = P_{0_{Agg}}\left(a_{p_{Agg}}\left(\frac{|V|}{V_0}\right)^2 + b_{p_{Agg}}\frac{|V|}{V_0} + c_{p_{Agg}}\right) \tag{4.37}$$

where

$$P_{Agg} = \sum_{i=1}^{n} P_i \tag{4.38}$$

$$P_{0_{Agg}} = \sum_{i=1}^{n} P_{0_i} \tag{4.39}$$

$$a_{p_{Agg}} = \frac{\sum_{i=1}^{n} P_{0_i} a_{p_i}}{\sum_{i=1}^{n} P_{0_i}} \tag{4.40}$$

$$b_{p_{Agg}} = \frac{\sum_{i=1}^{n} P_{0_i} b_{p_i}}{\sum_{i=1}^{n} P_{0_i}} \tag{4.41}$$

$$c_{p_{Agg}} = \frac{\sum_{i=1}^{n} P_{0_i} c_{p_i}}{\sum_{i=1}^{n} P_{0_i}} \tag{4.42}$$

If the ZIP parameters of all loads are the same, then the aggregate ZIP parameters will also be the same as the ZIP parameters of each load despite what the base power of each load is and how the base power of each load changes with time.

If all loads do not have the same ZIP parameters, the aggregate ZIP parameters will only keep constant if the base power of each load is constant or the ratio between the base powers of all loads are constant. For unbalanced system, we can use the three-phase average voltage as the voltage variable for the ZIP load model.

4.2.5 Aggregate ZIP Load Model for Multiple Three-Phase Delta Loads

The aggregate ZIP load model for multiple three-phase delta connected loads is the same as the aggregate ZIP load model for multiple three-phase star loads as given by (4.37) under the assumption that the system voltages are balanced.

4.2.6 Aggregate ZIP Load Model for Multiple Three-Phase Star and Delta Loads

The aggregate ZIP load model for multiple three-phase star and delta loads can also be described by (4.37) since the aggregate ZIP load model for both multiple star loads and multiple delta loads can be described by (4.37).

4.2.7 Aggregate ZIP Load Model for Multiple Star Loads

In this case, the aggregate ZIP load model for multiple three-phase and single-phase star connected loads are studied. Figure 4.6 shows the circuit diagram.

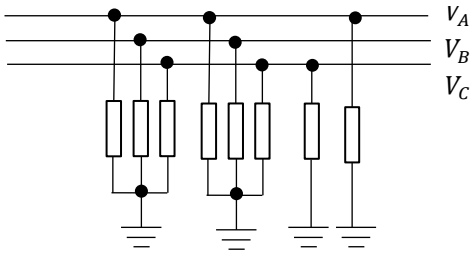

Figure 4.6 The circuit diagram of three-phase and single-phase star loads.

First, the aggregate ZIP load model can be obtained for each phase. Suppose that n single loads are connected to phase A and the voltage drop on the line is ignored. Thus all loads will have the same voltage, and the general form of load i ($i = 1, 2, \dots, n$) connected to Phase A can be described by (4.43)

$$P_{A_i} = P_{0_{A_i}} \left(a_{p_{A_i}} \left(\frac{|V_A|}{V_0} \right)^2 + b_{p_{A_i}} \frac{|V_A|}{V_0} + c_{p_{A_i}} \right) \tag{4.43}$$

Then the aggregate ZIP load model can be obtained

$$P_{A_{Agg}} = P_{0_{A_{Agg}}} \left(a_{p_{A_{Agg}}} \left(\frac{|V_A|}{V_0} \right)^2 + b_{p_{A_{Agg}}} \frac{|V_A|}{V_0} + c_{p_{A_{Agg}}} \right) \tag{4.44}$$

where

$$P_{A_{Agg}} = \sum_{i=1}^{n} P_{A_i} \tag{4.45}$$

$$P_{0_{A_{Agg}}} = \sum_{i=1}^{n} P_{0_{A_i}} \tag{4.46}$$

$$a_{p_{A_{Agg}}} = \frac{\sum_{i=1}^{n} P_{0_{A_i}} a_{p_{A_i}}}{\sum_{i=1}^{n} P_{0_{A_i}}} \tag{4.47}$$

$$b_{p_{A_{Agg}}} = \frac{\sum_{i=1}^{n} P_{0_{A_i}} b_{p_{A_i}}}{\sum_{i=1}^{n} P_{0_{A_i}}} \tag{4.48}$$

$$c_{p_{A_{Agg}}} = \frac{\sum_{i=1}^{n} P_{0_{A_i}} c_{p_{A_i}}}{\sum_{i=1}^{n} P_{0_{A_i}}} \tag{4.49}$$

The aggregate ZIP load model can be derived similarly for the loads connected at phase B to neutral and phase C to neutral. Suppose $V_A = V_B = V_C = V$ and there are m loads and k loads connected at Phase B and C, respectively, the ZIP load model for multiple star aggregate loads can be represented by (4.50)

$$P_{Agg} = P_{0_{Agg}} \left(a_{p_{Agg}} \left(\frac{V}{V_0} \right)^2 + b_{p_{Agg}} \frac{V}{V_0} + c_{p_{Agg}} \right) \tag{4.50}$$

where

$$P_{Agg} = \sum_{i=1}^{n} P_{A_i} + \sum_{i=1}^{m} P_{B_i} + \sum_{i=1}^{k} P_{C_i} \tag{4.51}$$

$$P_{0_{Agg}} = \sum_{i=1}^{n} P_{0_{A_i}} + \sum_{i=1}^{m} P_{0_{B_i}} + \sum_{i=1}^{k} P_{0_{C_i}} \tag{4.52}$$

$$a_{p_{Agg}} = \frac{\sum_{i=1}^{n} P_{0_{A_i}} a_{p_{A_i}} + \sum_{i=1}^{m} P_{0_{B_i}} a_{p_{B_i}} + \sum_{i=1}^{k} P_{0_{C_i}} a_{p_{C_i}}}{P_{0_{Agg}}} \tag{4.53}$$

$$b_{p_{Agg}} = \frac{\sum_{i=1}^{n} P_{0_{A_i}} b_{p_{A_i}} + \sum_{i=1}^{m} P_{0_{B_i}} b_{p_{B_i}} + \sum_{i=1}^{k} P_{0_{C_i}} b_{p_{C_i}}}{P_{0_{Agg}}} \tag{4.54}$$

$$c_{p_{Agg}} = \frac{\sum_{i=1}^{n} P_{0_{A_i}} c_{p_{A_i}} + \sum_{i=1}^{m} P_{0_{B_i}} c_{p_{B_i}} + \sum_{i=1}^{k} P_{0_{C_i}} c_{p_{C_i}}}{P_{0_{Agg}}} \tag{4.55}$$

The aggregate base power is the sum of the base power of each load, and the aggregate ZIP parameters are the weighted averages of the ZIP parameters of each load while the weights are the base power of each load. If all loads have the same ZIP parameters, the aggregate ZIP load model will have the same ZIP parameters regardless of the base power of each load.

4.2.8 Aggregate ZIP Load Model for Multiple Delta Loads

In this case, the aggregate ZIP load model for multiple delta-connected loads (three-phase and single delta loads) are studied. The circuit diagram is shown in Figure 4.7.

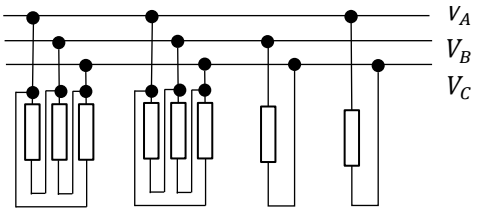

Figure 4.7 The circuit diagram of three-phase delta loads.

First, the aggregate ZIP load model can be obtained for every two phases. Suppose that n single delta loads are connected between Phase A and B. Thus, all loads will have the same line-

to-line voltage and the general form of load i ($i = 1, 2, \dots, n$) connected to Phase A and B can be described by (4.56)

$$P_{AB_i} = P_{0_{AB_i}} \left(a_{p_{AB_i}} \left(\frac{|V_{AB}|}{\sqrt{3}V_0} \right)^2 + b_{p_{AB_i}} \frac{|V_{AB}|}{\sqrt{3}V_0} + c_{p_{AB_i}} \right) \tag{4.56}$$

Then the aggregate ZIP load model can be obtained

$$P_{AB_{Agg}} = P_{0_{AB_{Agg}}} \left(a_{p_{AB_{Agg}}} \left(\frac{|V_{AB}|}{\sqrt{3}V_0} \right)^2 + b_{p_{AB_{Agg}}} \frac{|V_{AB}|}{\sqrt{3}V_0} + c_{p_{AB_{Agg}}} \right) \tag{4.57}$$

where

$$P_{AB_{Agg}} = \sum_{i=1}^{n} P_{AB_i} \tag{4.58}$$

$$P_{0_{AB_{Agg}}} = \sum_{i=1}^{n} P_{0_{AB_i}} \tag{4.59}$$

$$a_{p_{AB_{Agg}}} = \frac{\sum_{i=1}^{n} P_{0_{AB_i}} a_{p_{AB_i}}}{\sum_{i=1}^{n} P_{0_{AB_i}}} \tag{4.60}$$

$$b_{p_{AB_{Agg}}} = \frac{\sum_{i=1}^{n} P_{0_{AB_i}} b_{p_{AB_i}}}{\sum_{i=1}^{n} P_{0_{AB_i}}} \tag{4.61}$$

$$c_{p_{AB_{Agg}}} = \frac{\sum_{i=1}^{n} P_{0_{AB_i}} c_{p_{AB_i}}}{\sum_{i=1}^{n} P_{0_{AB_i}}} \tag{4.62}$$

The aggregate ZIP load model can be derived similarly for the loads connected at phase BC and phase AC loads. Then if we can assume $|V_A| = |V_B| = |V_C| = V$ (consequently $\frac{|V_{AB}|}{\sqrt{3}V_0} = \frac{V}{V_0}$)

the aggregate ZIP load model for all three phases can be obtained by summing phase AB, BC, and AC loads. If there are m and k loads connected at phase BC and phase AC, the aggregate ZIP load model for all three-phase can be expressed as

$$P_{Agg} = P_{0_{Agg}} \left(a_{p_{Agg}} \left(\frac{V}{V_0} \right)^2 + b_{p_{Agg}} \frac{V}{V_0} + c_{p_{Agg}} \right) \tag{4.63}$$

where

$$P_{Agg} = \sum_{i=1}^{n} P_{AB_i} + \sum_{i=1}^{m} P_{BC_i} + \sum_{i=1}^{k} P_{AC_i} \tag{4.64}$$

$$P_{0_{Agg}} = \sum_{i=1}^{n} P_{0_{AB_i}} + \sum_{i=1}^{m} P_{0_{BC_i}} + \sum_{i=1}^{k} P_{0_{AC_i}} \tag{4.65}$$

$$a_{p_{Agg}} = \frac{\sum_{i=1}^{n} P_{0_{AB_i}} a_{p_{AB_i}} + \sum_{i=1}^{m} P_{0_{BC_i}} a_{p_{BC_i}} + \sum_{i=1}^{k} P_{0_{AC_i}} a_{p_{AC_i}}}{P_{0_{Agg}}} \tag{4.66}$$

$$b_{p_{Agg}} = \frac{\sum_{i=1}^{n} P_{0_{AB_i}} b_{p_{AB_i}} + \sum_{i=1}^{m} P_{0_{BC_i}} b_{p_{BC_i}} + \sum_{i=1}^{k} P_{0_{AC_i}} b_{p_{AC_i}}}{P_{0_{Agg}}} \tag{4.67}$$

$$c_{p_{Agg}} = \frac{\sum_{i=1}^{n} P_{0_{AB_i}} c_{p_{AB_i}} + \sum_{i=1}^{m} P_{0_{BC_i}} c_{p_{BC_i}} + \sum_{i=1}^{k} P_{0_{AC_i}} c_{p_{AC_i}}}{P_{0_{Agg}}} \tag{4.68}$$

The aggregate base power is the sum of the base power of each load, and the aggregate ZIP parameters are the weighted averages of the ZIP parameters of each load while the weight is the

base power of each load. If all loads have the same ZIP parameters, the aggregate ZIP load model will have the same ZIP parameters despite what base power each load has.

4.2.9 Aggregate ZIP Load Model for Multiple Star and Delta Loads

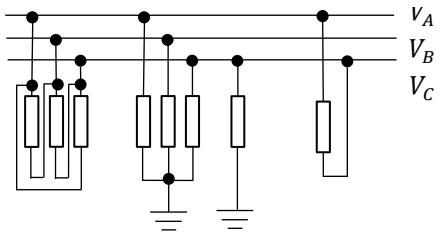

Figure 4.8 The circuit diagram of three-phase star and delta loads.

The circuit diagram of star and delta connected loads is shown in Figure 4.8. As we can learn from the previous derivation from Section 4.2.7 and 4.2.8, the analytical form of the aggregate ZIP load model can only be obtained if we assume the three-phase voltages are balanced. Based on this assumption, we can express the aggregate ZIP load model as

$$P_{Agg} = P_{0_{Agg}}\left(a_{p_{Agg}}\left(\frac{V}{V_0}\right)^2 + b_{p_{Agg}}\frac{V}{V_0} + c_{p_{Agg}}\right) \tag{4.69}$$

where

$$P_{Agg} = \sum_{i=1}^{n} P_{A_i} + \sum_{i=1}^{m} P_{B_i} + \sum_{i=1}^{k} P_{C_i} + \sum_{i=1}^{n2} P_{AB_i} + \sum_{i=1}^{m2} P_{BC_i} + \sum_{i=1}^{k2} P_{AC_i} \tag{4.70}$$

$$P_{0_{Agg}} = \sum_{i=1}^{n} P_{0_{A_i}} + \sum_{i=1}^{m} P_{0_{B_i}} + \sum_{i=1}^{k} P_{0_{C_i}} + \sum_{i=1}^{n2} P_{0_{AB_i}} + \sum_{i=1}^{m2} P_{0_{BC_i}} + \sum_{i=1}^{k2} P_{0_{AC_i}} \tag{4.71}$$

(4.72)

$$a_{p_{Agg}} =$$

$$\frac{\sum_{i=1}^{n} P_{0_{A_i}} a_{p_{A_i}} + \sum_{i=1}^{m} P_{0_{B_i}} a_{p_{B_i}} + \sum_{i=1}^{k} P_{0_{C_i}} a_{p_{C_i}}}{P_{0_{Agg}}}$$

$$+ \frac{\sum_{i=1}^{n2} P_{0_{AB_i}} a_{p_{AB_i}} + \sum_{i=1}^{m2} P_{0_{BC_i}} a_{p_{BC_i}} + \sum_{i=1}^{k2} P_{0_{AC_i}} a_{p_{AC_i}}}{P_{0_{Agg}}}$$

$$b_{p_{Agg}} =$$

$$\frac{\sum_{i=1}^{n} P_{0_{A_i}} b_{p_{A_i}} + \sum_{i=1}^{m} P_{0_{B_i}} b_{p_{B_i}} + \sum_{i=1}^{k} P_{0_{C_i}} b_{p_{C_i}}}{P_{0_{Agg}}} \tag{4.73}$$

$$+ \frac{\sum_{i=1}^{n2} P_{0_{AB_i}} b_{p_{AB_i}} + \sum_{i=1}^{m2} P_{0_{BC_i}} b_{p_{BC_i}} + \sum_{i=1}^{k2} P_{0_{AC_i}} b_{p_{AC_i}}}{P_{0_{Agg}}}$$

$$c_{p_{Agg}} =$$

$$\frac{\sum_{i=1}^{n} P_{0_{A_i}} c_{p_{A_i}} + \sum_{i=1}^{m} P_{0_{B_i}} c_{p_{B_i}} + \sum_{i=1}^{k} P_{0_{C_i}} c_{p_{C_i}}}{P_{0_{Agg}}} \tag{4.74}$$

$$+ \frac{\sum_{i=1}^{n2} P_{0_{AB_i}} c_{p_{AB_i}} + \sum_{i=1}^{m2} P_{0_{BC_i}} c_{p_{BC_i}} + \sum_{i=1}^{k2} P_{0_{AC_i}} c_{p_{AC_i}}}{P_{0_{Agg}}}$$

For the circuit with three-phase balanced voltages, the aggregate ZIP parameters are the weighted averages of the ZIP parameters of each load while the weight is the base power of each load; the weight of each load solely depends on the base power of that load no matter what the connection type (delta or wye) is. If all loads have the same ZIP parameters, the aggregate ZIP load model will have the same ZIP parameters despite what base power each load has.

4.2.10 Aggregate ZIP Load Model for Reactive Power

Since Equation (4.1) and (4.2) are completely analogous, all the previous discussions regarding the ZIP load model for real power are applicable to the ZIP model for reactive power.

Special attention is given to reactive power compensating devices as follows, when calculating the aggregate ZIP for a load together with the reactive power compensating device.

4.2.10.1 Reactive Power Compensating Device Modeled as Constant Q

In this scenario, the reactive compensating device is modeled as a constant Q source. An example will be a power electronics based reactive power compensator that is capable of regulating its reactive power output.

Suppose there is a single load connected between phase B and neutral; the load has base power $Q_{0_1} = 100\text{kVar}$, ZIP parameter $a_{q_1} = 0.2$, $b_{q_1} = 0.5$, and $c_{q_1} = 0.3$. A constant Q source is connected in parallel to the load with $Q_{0_2} = -30$ kVar, $a_{q_2} = 0$, $b_{q_2} = 0.0$, and $c_{q_2} = 1.0$. The aggregate ZIP parameters are found to be $a_q = 0.2857$, $b_q = 0.7143$, and $c_q = 0$. If $Q_{0_2} = -120$ kVar, $a_{q_2} = 0.0$, $b_{q_2} = 0.0$, and $c_{q_2} = 1.0$, The aggregate ZIP parameters are found to be $a_q = -1$, $b_q = -2.5$, and $c_q = 4.5$.

The examples manifest that the aggregate ZIP parameters can be negative for reactive power when there is a large capacitor bank connected with loads.

4.2.10.2 Reactive Power Compensating Device Modeled as Constant Impedance

In this scenario, the reactive compensating device is modeled as a constant impedance load. An example will be a regular capacitor bank, whose reactive power is proportional to the square of the terminal voltage.

Suppose there is a single load connected between phase B and neutral. Suppose the load has base power $Q_{0_1} = 100\text{kVar}$, ZIP parameter $a_{q_1} = 0.2$, $b_{q_1} = 0.5$, and $c_{q_1} = 0.3$. A Q source is connected in parallel to the load with $Q_{0_2} = -30$ kVar, $a_{q_2} = 1.0$, $b_{q_2} = 0.0$, and $c_{q_2} = 0.0$.

The aggregate ZIP parameters are found to be: $a_q = 0.2857$, $b_q = 0.7143$, and $c_q = 0$. If $Q_{02} = -120$ kVar, $a_{q2} = 1.0$, $b_{q2} = 0.0$, and $c_{q2} = 0.0$, The combined ZIP parameters are found to be: $a_q = 5$, $b_q = 2.5$, and $c_q = -1.5$.

4.2.11 Aggregate ZIP Load Model for a Load Combined with Real Power Source

This section discusses the calculation for the aggregate ZIP parameters for a load together with the real power injecting device such as a PV generator. The real power injecting device is modeled as a constant P.

Suppose there is a single load connected between phase B and neutral. Suppose the load has base power $P_{01} = 100$kW, ZIP parameter $a_{p1} = 0.2$, $b_{p1} = 0.5$, and $c_{p1} = 0.3$. A constant P source is connected in parallel to the load with $P_{02} = -40\ kW$, $a_{p2} = 0.0$, $b_{p2} = 0.0$, and $c_{p2} = 1.0$. The combined ZIP parameters are found to be: $a_p = 0.3333$, $b_p = 0.8333$, and $c_p = -0.1666$. If the real power source has $P_{02} = -120\ kW$, $a_{p2} = 0.0$, $b_{p2} = 0.0$, and $c_{p2} = 1.0$. The combined ZIP parameters are found to be: $a_p = -1$, $b_p = -2.5$, and $c_p = 4.5$.

CHAPTER 5 ZIP LOAD MODEL PARAMETER ESTIMATION CASE STUDIES

We choose the IEEE 13 and 34 bus systems for the case studies. The configuration of the 13-bus system is displayed in Figure 5.1. The ZIP parameters of loads are predefined in the OpenDSS simulation program. Thus the estimation performance can not only be assessed by the estimation error for the power but also be evaluated by comparing the estimated ZIP parameters with the preset ZIP parameters.

The measurements data used in estimation are generated using OpenDSS Simulation. The base power P_0 and Q_0 are changing hourly while the ZIP load model coefficients (a, b, c) are kept constant. The window size of each estimation n is set to 4. The measurements are taken every 15 minutes for a day. Some cases will only show the estimation results for the ZIP load model for P since the results for Q are similar.

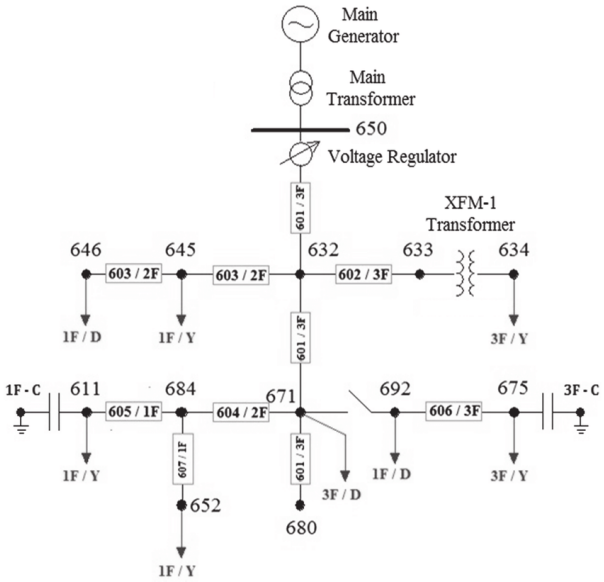

Figure 5.1 Configuration of IEEE 13-bus test feeder. [56]

5.1 IEEE 13-Bus Test Feeder

5.1.1 Single Load

5.1.1.1 Single Star Load

In this case, the single star loads in the IEEE 13-bus system, i.e., loads at bus 645, 611, 652, which are connected between one phase and neutral, are studied. The estimated ZIP parameters for real power using the three different methods are shown in Figure 5.2. We can see that all three methods can estimate the ZIP parameters accurately. Based on the estimated ZIP parameters, the estimated power is computed. The estimated power is then compared with the measured power to compute the absolute percentage error. The errors are also shown in Figure 5.2. The estimation results for reactive power are similar and thus are not shown here.

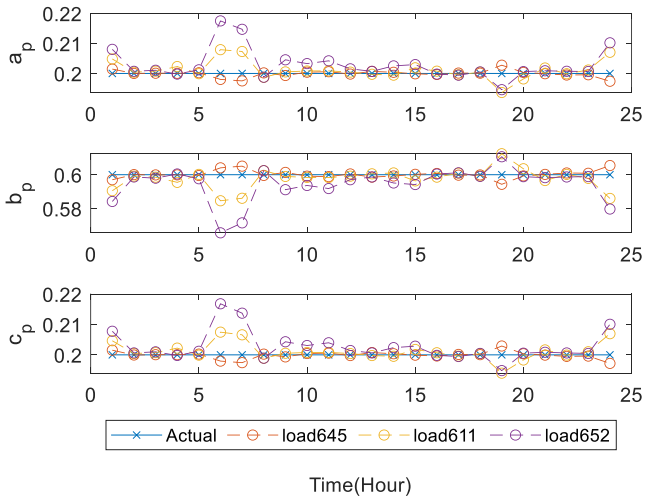

(a) Least squares method

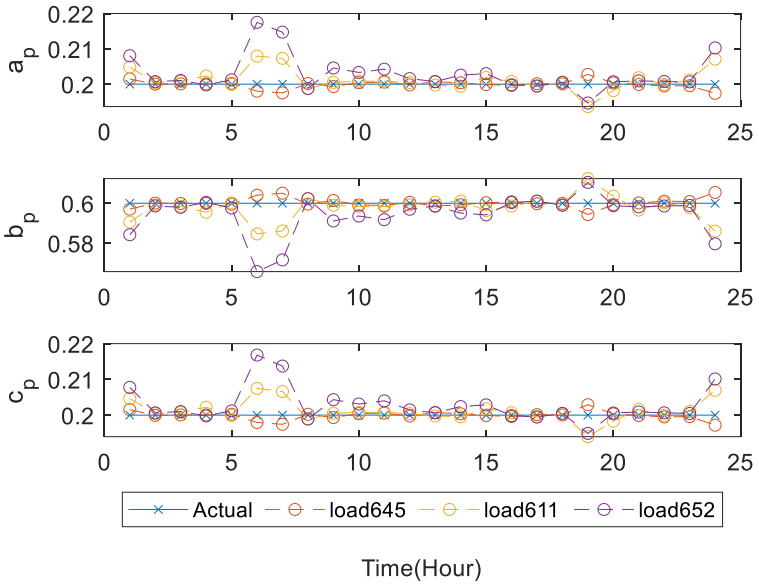

(b) Optimization method

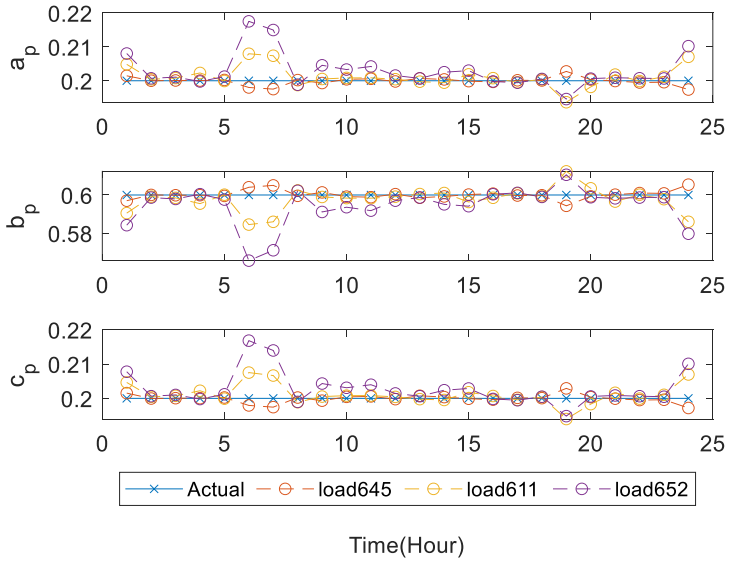

(c) Neural network method

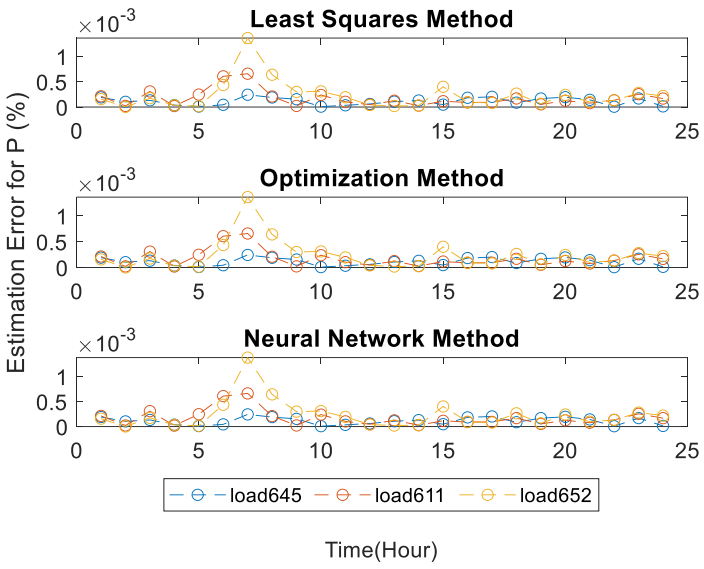

(d) Estimation error

Figure 5.2 ZIP load model estimation results for the real power of the single star loads.

5.1.1.2 Single Delta Load

In this case, the single delta loads connected between 2 different cases are studied. They are the loads at bus 646 and 692. In Figure 5.3, lines “load 646” and “load 692” are estimated using the average voltage of the 2 phases while “load 646 2” and “load 692 2” are estimated using the line-to-line voltage. From the figure, we can see that the estimation results using line-to-line voltage are more accurate than using the average phase voltage.

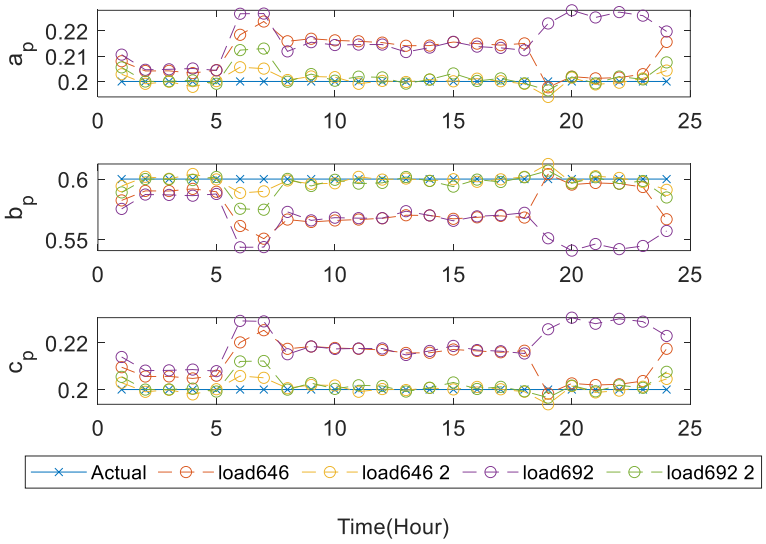

(a) Least squares method

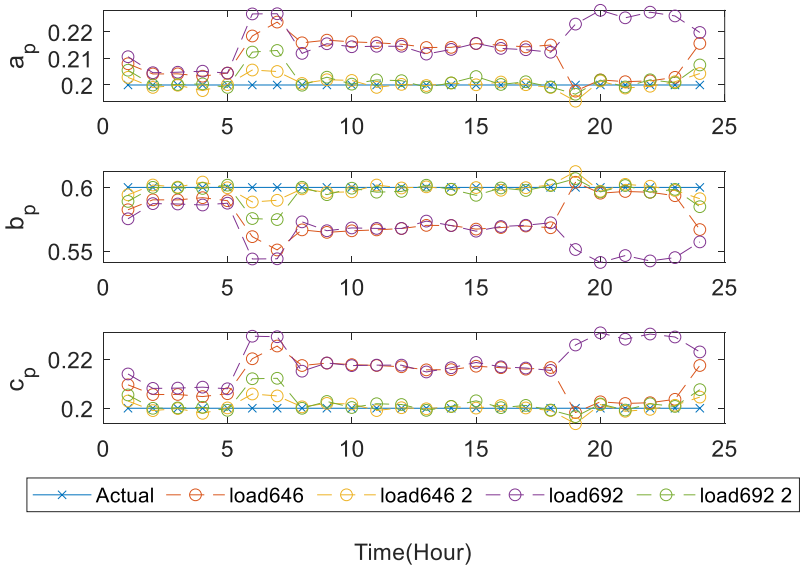

(b) Optimization method

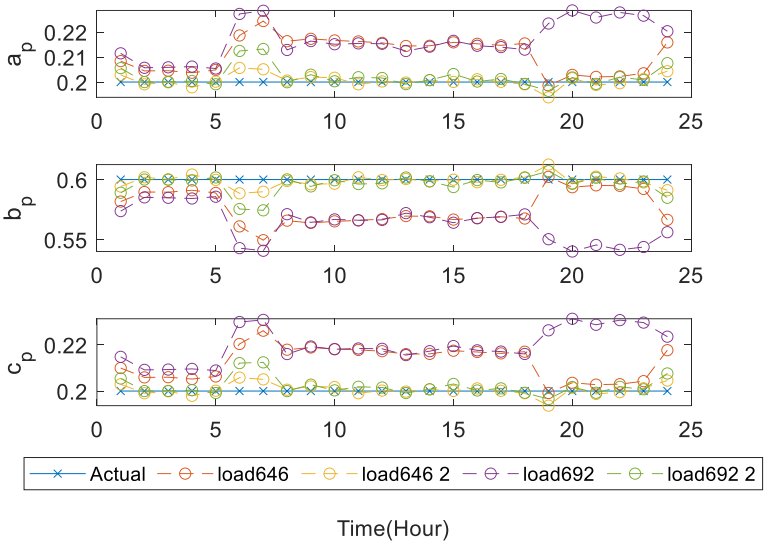

(c) Neural network method

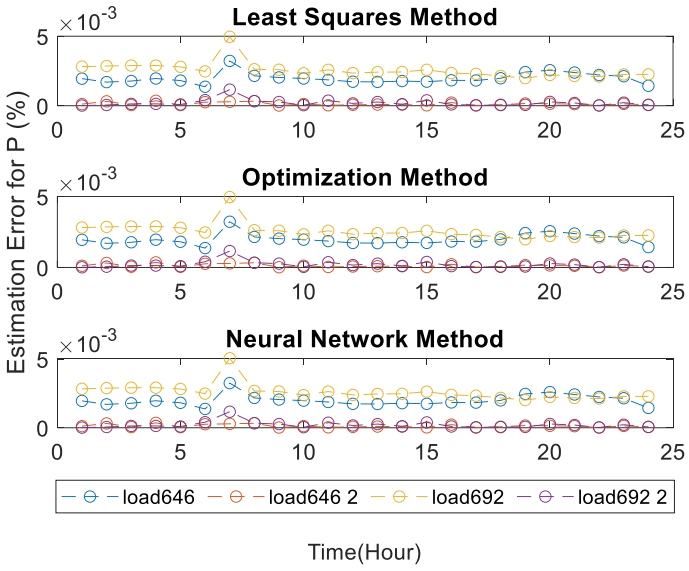

(d) Estimation error

Figure 5.3 ZIP load model estimation results for the real power of the phase-to-phase loads.

5.1.2 Aggregate Load

5.1.2.1 Three-Phase Star Load

In this case, the ZIP load model for the three-phase star loads at bus 634, 670, and 675 are estimated using the average phase voltage and the sum of three-phase power.

The base real and reactive power of all three loads at each phase are shown in Table 5.1 and Table 5.2, respectively. Among the three three-phase star loads, load 634 is the most balanced while load 670 is the most unbalanced.

Table 5.1 The base real power of the three-phase star loads of the IEEE 13-bus system

Load	Phase A $P_0(kW)$	Phase B $P_0(kW)$	Phase C $P_0(kW)$
634	160	120	120
670	17	66	117
675	485	68	290

Table 5.2 The base reactive power of the three-phase star loads of the IEEE 13-bus system

Load	Phase A $Q_0\ (kVar)$	Phase B $Q_0\ (kVar)$	Phase C $Q_0\ (kVar)$
634	110	90	90
670	10	38	68
675	190	60	212

The estimation results using the three methods are shown in Figure 5.4. As expected, we can see that the estimated results differ from the calculated results due to load unbalanced. For bus 634, the estimated results are close to the calculated results, as it has the smallest load unbalance.

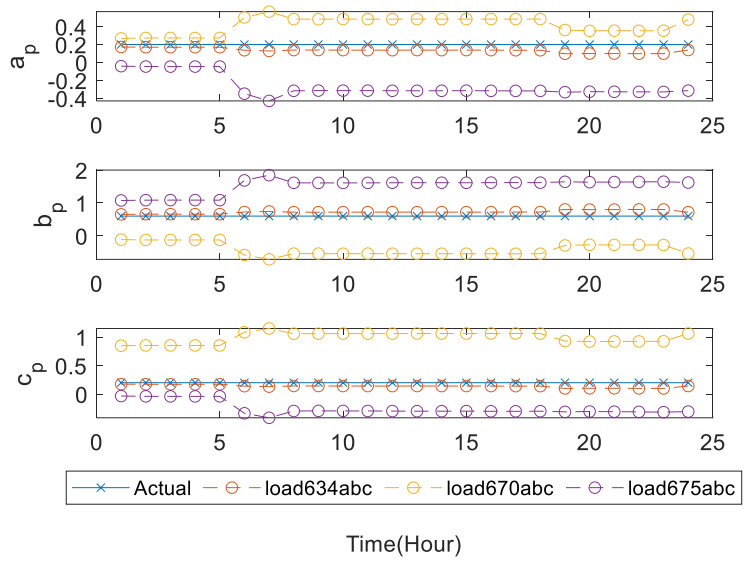

(a) Least squares method

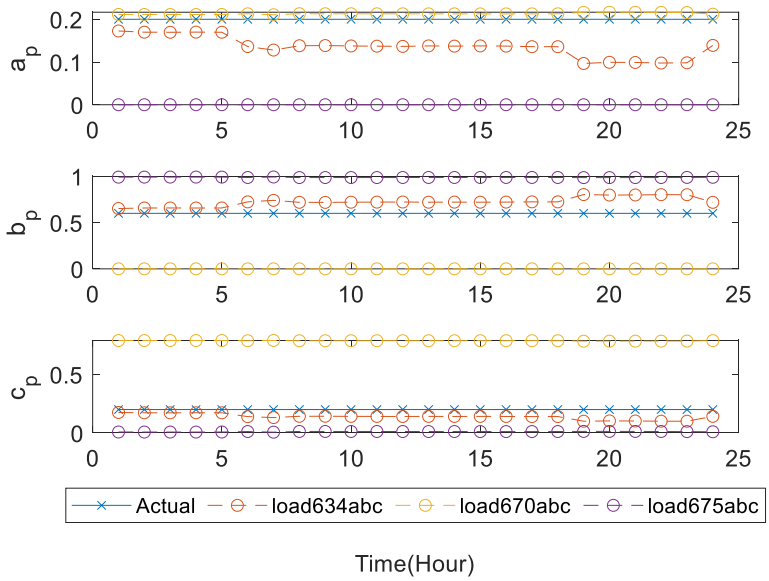

(b) Optimization method

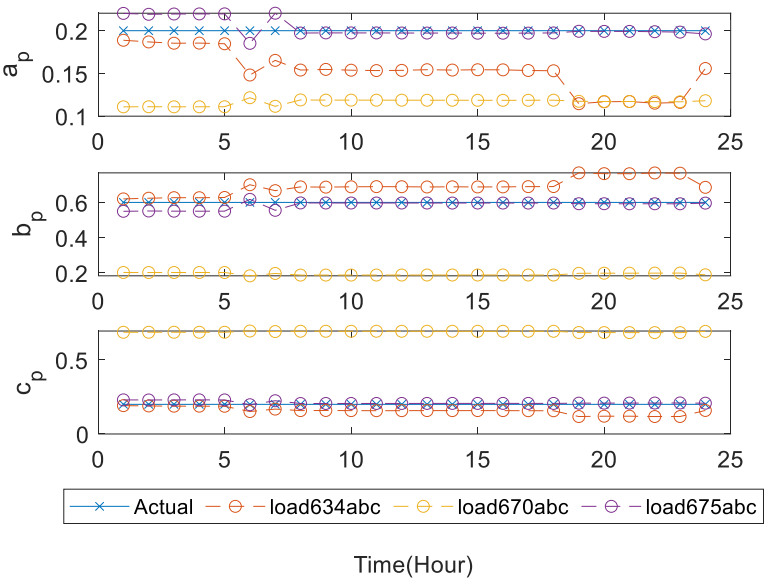

(c) Neural network method

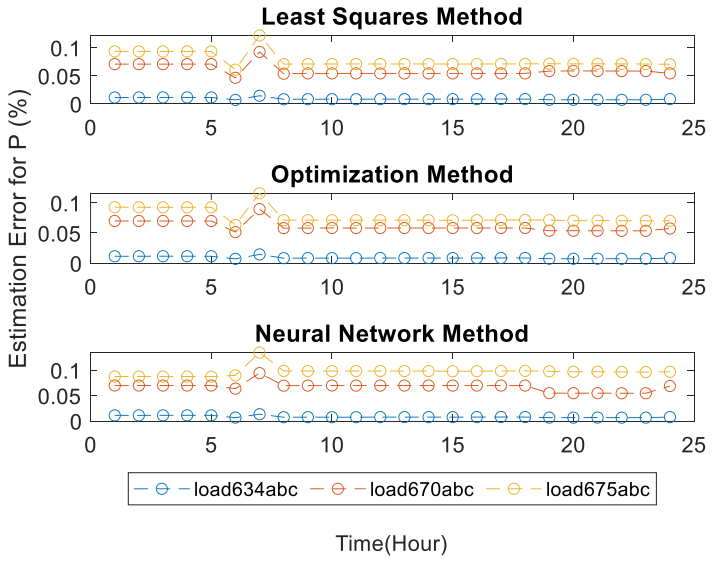

(d) Estimation error

Figure 5.4 ZIP load model estimation results for the real power of the three-phase Y-connected loads.

5.1.2.2 Three-Phase Delta Load

In this case, the load at bus 671, which is the only three-phase Δ-connected load in the IEEE 13-bus system, is studied. The estimation results are shown in Figure 5.5. The actual ZIP parameters are computed using (4.30). All three methods can estimate the aggregate ZIP parameters accurately.

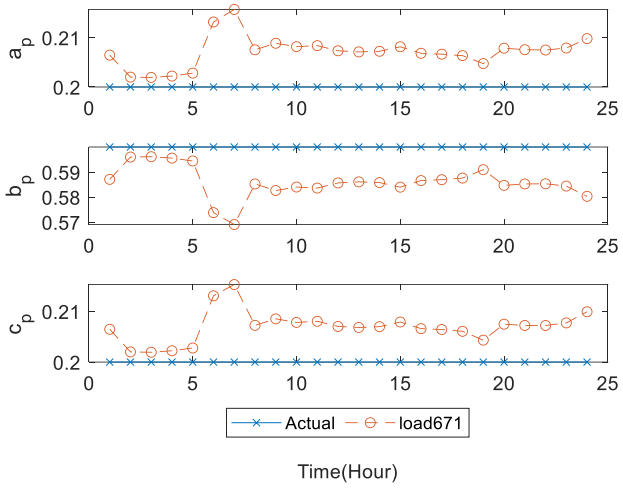

(a) Least squares method

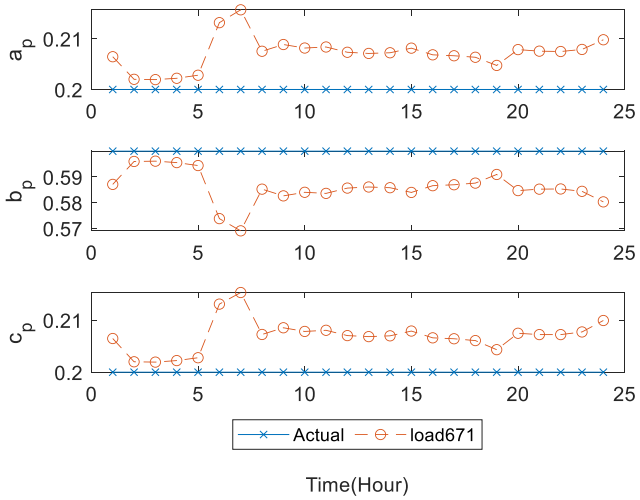

(b) Optimization method

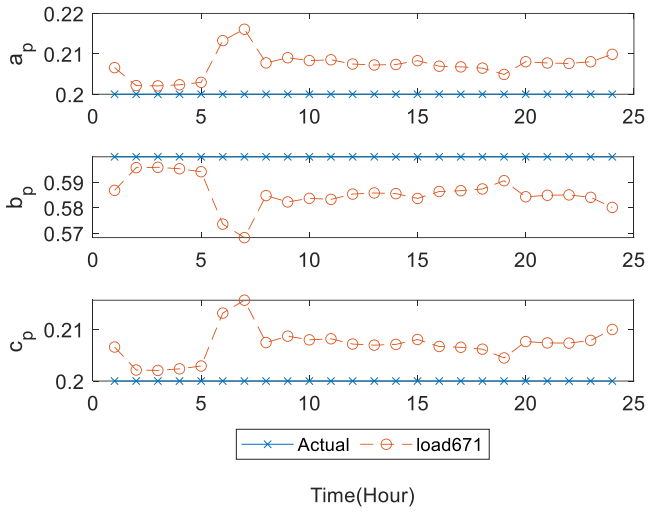

(c) Neural network method

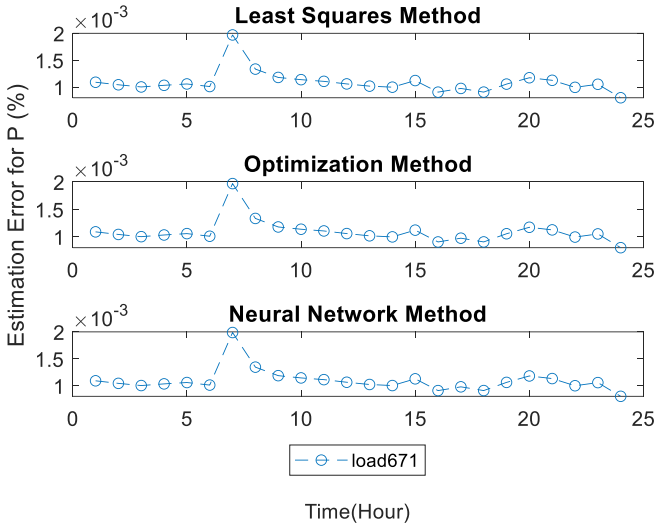

(d) Estimation error

Figure 5.5 ZIP load model estimation results for the real power of the three-phase Δ-connected loads.

5.1.2.3 Multiple Loads 1

In this case, the aggregate load models for the loads at bus 645 and 646 are studied. Load 645 is a single star load, which is connected between phase B and neutral, while load 646 is a single delta load, which is connected between phase B and C. The aggregate load is estimated using the average voltage of phase B and C at bus 632 and the power from bus 632 to 645. The (a_p, b_p, c_p) for 645 and 646 are both set to $(0.2, 0.6, 0.2)$, with their P_0 set to $170kW$ and $230kW$.

The estimation results are shown in Figure 5.6. From the results, we can see that the estimation for each load is accurate while the estimated aggregate ZIP parameters deviate from our expectations. The reason is that this aggregate load consists of both phase-to-neutral and phase-to-phase loads, which means the ZIP load model for the first load is a function of phase B and C voltage while the second load only depends on phase B. Thus using the phase B and C average voltage as the voltage for the aggregate ZIP load model is inappropriate. But we also cannot choose only phase B voltage as the voltage for the aggregate ZIP load model as the load at bus 646 is also dependent on phase C.

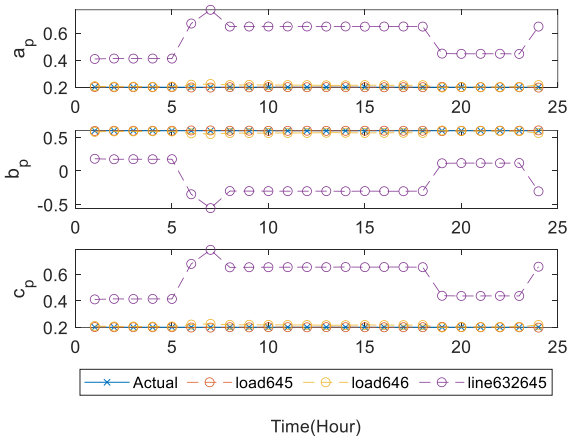

(a) Least squares method

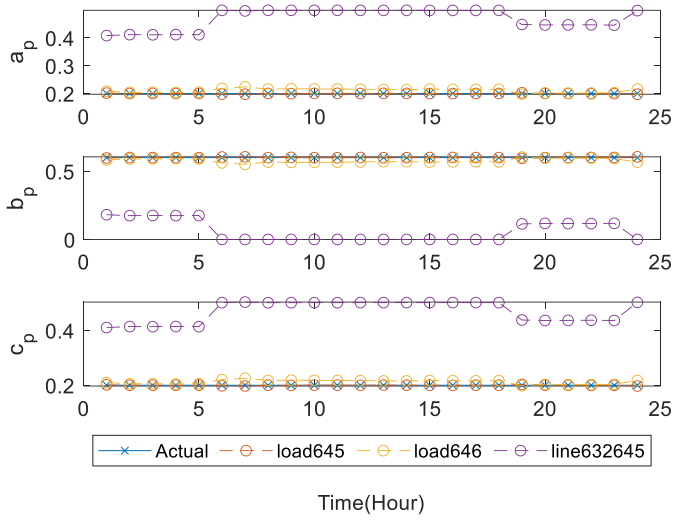

(b) Optimization method

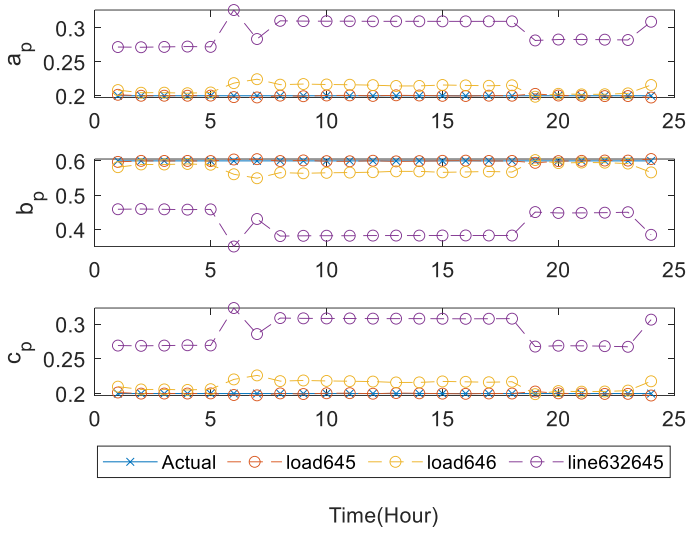

(c) Neural network method

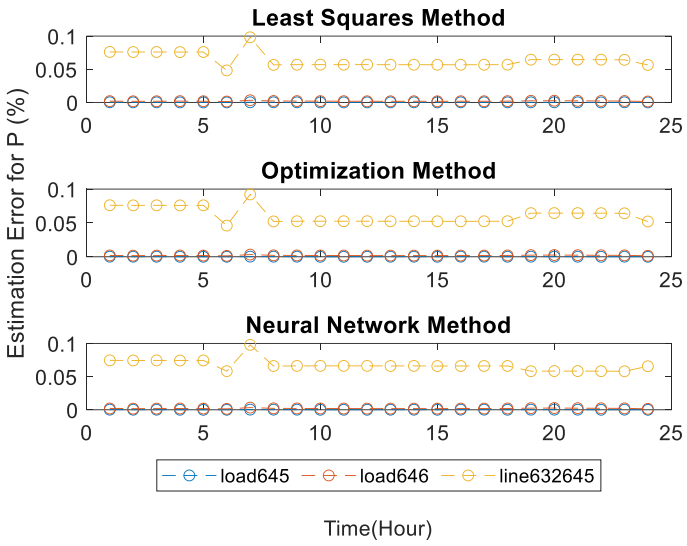

(d) Estimation error

Figure 5.6 ZIP load model estimation results for the real power of the aggregate load .

5.1.2.4 Multiple Loads 2

In this case, we changed the load at 646 from phase-to-phase (BC) load to phase-B-to-neutral load. The purpose of this case study is to demonstrate that the aggregate load can be estimated more accurately when they are all phase-to-neutral connected especially at the same phase. The load at bus 645 is also a phase-B-to-neutral load. The (a_p, b_p, c_p) for 645 and 646 are set to $(0.2, 0.6, 0.2)$ and $(0.5, 0.2, 0.3)$, respectively. The loads have their P_0 set to 170 kW and 230 kW, respectively. For the easiness of demonstration, both P_0 will change hourly but according to the same set of multipliers. In this way, the aggregate (a_p, b_p, c_p) can remain at $(0.3725, 0.37, 0.2575)$. However, if P_{0_1} and P_{0_2} vary based on different multipliers, then the aggregate (a_p, b_p, c_p) will not be static.

The estimation results are shown in Figure 5.7. As expected, the aggregate ZIP parameters, as well as the ZIP parameters of each load, can be estimated accurately. The estimation results for

each load are based on the voltage and power measured at each load. The aggregate ZIP parameters are estimated using the phase B power flowing from bus 632 to bus 645 and the phase B voltage at bus 632.

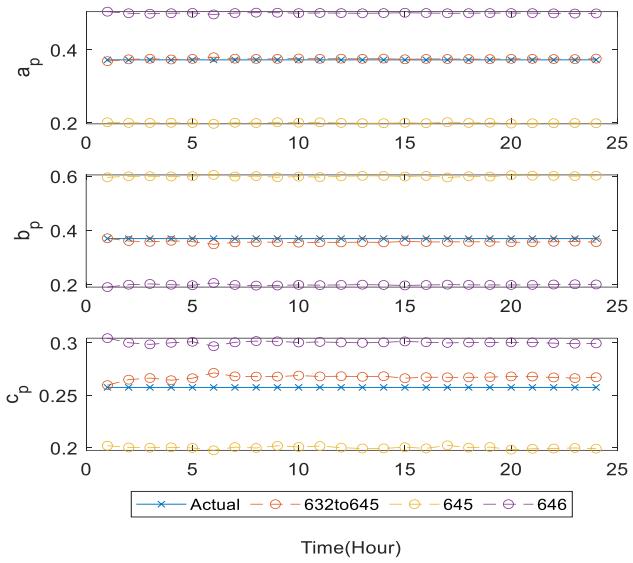

(a) Least squares method

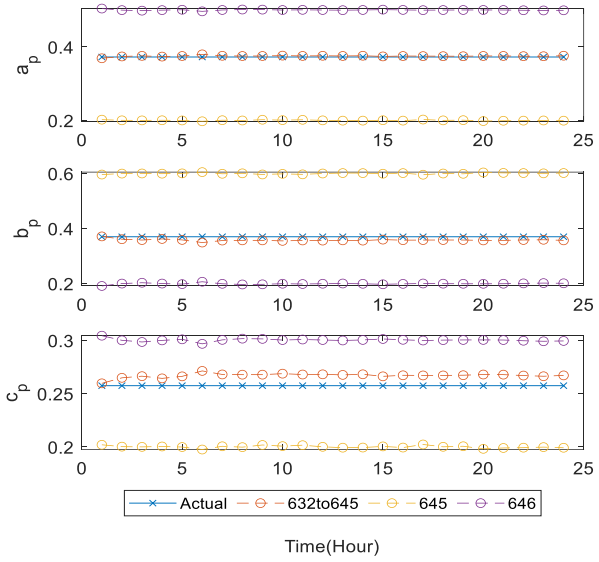

(b) Optimization method

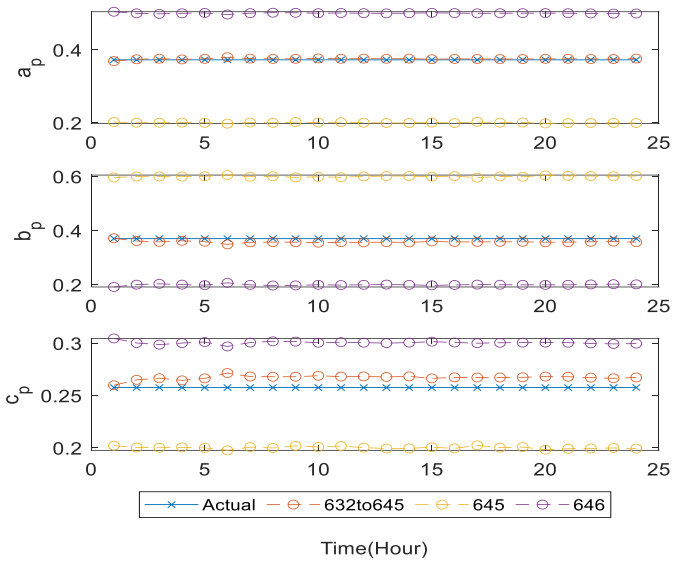

(c) Neural network method

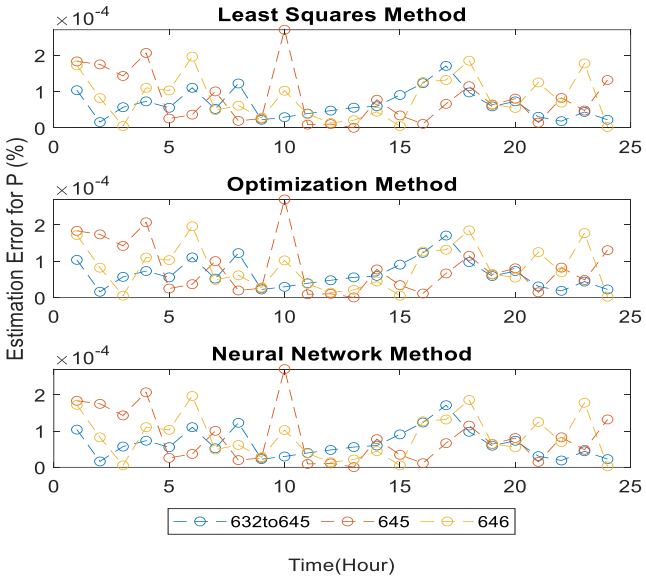

(d) Estimation error

Figure 5.7 ZIP load model estimation results for the real power of the case aggregate load.

5.2 IEEE 34-Bus Test Feeder

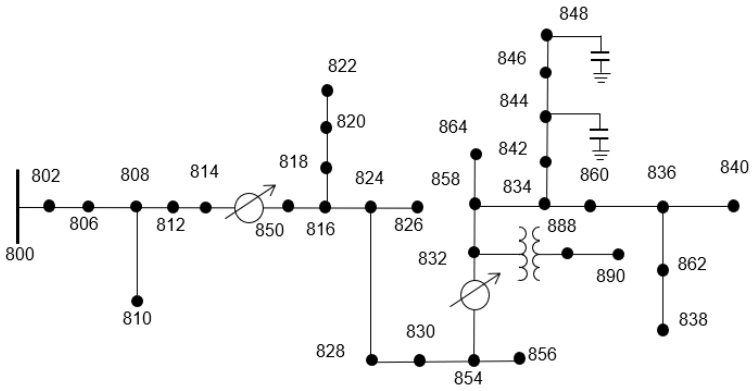

Figure 5.8 Configuration of IEEE 34-bus test feeder.

The case studies are also performed based on the IEEE 34-bus system. The distributed loads along the lines in the system are modeled as a load located at the middle of those lines. Since there is just one three-phase delta load in the IEEE 13-bus system, the ZIP parameter estimation for the three-phase delta load is also studied in the IEEE 34-bus system. The configuration of the IEEE 34-bus system is shown in Figure 5.8.

5.2.1 Aggregate Load

5.2.1.1 Three-Phase Delta Load

The ZIP parameter estimation for the three-phase delta loads in the 34-bus system, i.e., loads 848, 890, and 830, is studied in this section. The ZIP parameter estimation results for real power are shown in Figure 5.9. The estimation results for reactive power are similar and thus are not shown. The ZIP parameters of load 848 and 890 can be estimated accurately while the results for load 830 deviate from the theoretically calculated ZIP parameters. The average voltage magnitude unbalance for load 848, 890, and 830 in the 24 hours are 1.66%, 1.54%, and 1.64%. Voltage unbalance is not the only reason for the deviation of estimated ZIP parameters. The other

reason is the load unbalance. Among the three loads, loads 848 and 890 are balanced while load 830 is unbalanced as shown in Table 5.3 and Table 5.4, respectively. The results are consistent with our findings in Section 4.2.3.

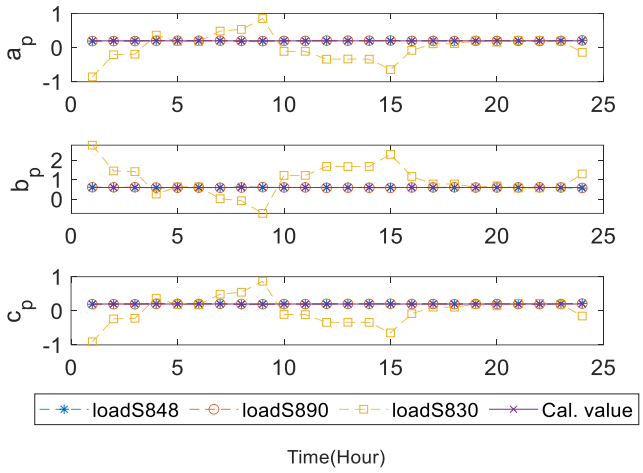

(a) Least squares method

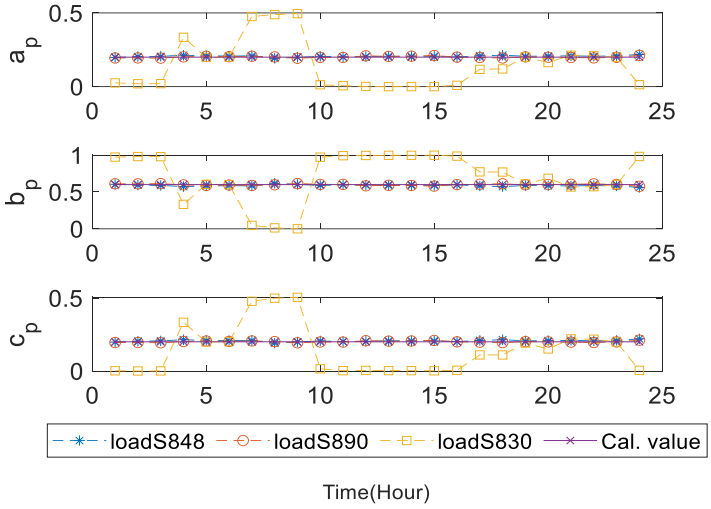

(b) Optimization method

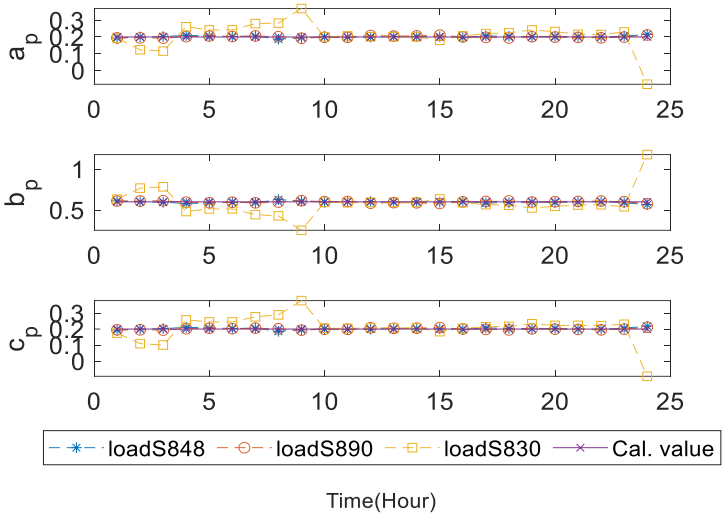

(c) Neural network method

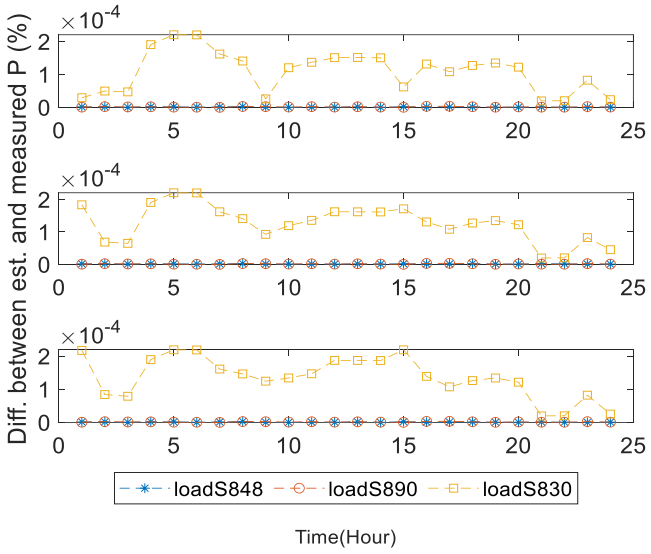

(d) Estimation error

Figure 5.9 ZIP load model estimation results for the real power of load 848, 890, and 890.

Table 5.3 The base real power of the three-phase delta loads of the IEEE 34-bus system

Load	Phase A $P_0(kW)$	Phase B $P_0(kW)$	Phase C $P_0(kW)$
848	20	20	20
890	150	150	150
830	10	10	25

Table 5.4 The base reactive power of the three-phase delta loads of IEEE 34-bus system

Load	Phase A $Q_0\ (kVar)$	Phase B $Q_0\ (kVar)$	Phase C $Q_0\ (kVar)$
848	16	16	16
890	75	75	75
830	5	5	10

CHAPTER 6 CONCLUSION

Transmission line and load model parameters are essential inputs to power system modeling and simulation, control, protection, operation, optimization, and planning. The accuracy of those parameters can determine the quality of those power system studies. The two common power system estimation problems – transmission line parameter and ZIP load model parameter – have been studied in detail in this research.

For the transmission line parameter part, a linear estimation method and an optimal estimator method were proposed for estimating transmission line parameters. Considering the potential presence of bad measurements, a bad data detection and identification method is considered to eliminate the bad data. For improving estimating accuracy under noise conditions, Kalman filter based methods were proposed to estimate line parameters for transmission lines with different series compensation configurations.

Moreover, considering that the resistance of line parameters can change dynamically due to changing ambient environment in real-world, two modified Kalman based filter approaches were proposed to track the changing line parameters. The estimation results based on the simulation data show that both methods are able to track the varying line parameters even under the effect of measurement noise.

For ZIP load parameter estimation, the aggregate ZIP load model has been comprehensively studied with respect to the connection types of loads in this research. The estimation for the aggregate ZIP load model is studied under load unbalance and voltage unbalance conditions. Factors that affect estimation accuracy for different scenarios have been investigated.

Simulated data based on the IEEE 13-bus and the IEEE 34-bus system have been used to demonstrate and evaluate the proposed methods.

REFERENCES

[1] L. Mustafa and L. Yuan, "Development of Efficient and Robust Methods for Estimation of Transmission Line Parameters Using Synchronized PMU Data," SoutheastCon 2018, 2018, pp. 1-6, doi: 10.1109/SECON.2018.8479175.

[2] W. Fan and Y. Liao, “Power system NERC reliability compliance study and violation mitigation,” International Review of Modelling and Simulations, vol. 13, no. 1, January 2020, doi: 10.15866/iremos.v13i1.17204.

[3] Q. Wang et al., “Integrated protection based on multi-frequency domain information for UHV half-wavelength AC transmission line,” Protection and Control of Modern Power Systems, vol. 1, no. 1. Springer Science and Business Media LLC, Dec. 2016. doi: 10.1186/s41601-016-0027-8.

[4] S. Das, S. Navalpakkam Ananthan, and S. Santoso, “Relay performance verification using fault event records,” Protection and Control of Modern Power Systems, vol. 3, no. 1. Springer Science and Business Media LLC, Jul. 16, 2018. doi: 10.1186/s41601-018-0094-0.

[5] W. Fan and Y. Liao, “Fault location techniques for simultaneous faults in power distribution systems with distributed generations,” International Energy & Sustainability Conference 2017, October 19 - 20, 2017, Farmingdale, NY, USA. doi: 10.1109/iesc.2017.8167480.

[6] W. Fan and Y. Liao, “Fault identification and location for distribution network with distributed generations,” International Journal of Emerging Electric Power Systems, vol. 19, no. 3, May 2018. doi: 10.1515/ijeeps-2018-0048

[7] W. Fan and Y. Liao, “Fault location for distribution systems with distributed generations without using source impedances,” 51st North American Power Symposium, Wichita, Kansas, October 13-15, 2019. doi: 10.1109/NAPS46351.2019.9000284

[8] W. Fan, “Advanced fault area identification and fault location for transmission and distribution systems”, Theses and Dissertations--Electrical and Computer Engineering, 144, University of Kentucky , 2019. doi: 10.13023/etd.2019.396

[9] W. Fan and Y. Liao, “Wide area measurements based fault detection and location method for transmission lines,” Protection and Control of Modern Power Systems, vol. 4, March 2019. doi: 10.1186/s41601-019-0121-9

[10] P. Kundur, Power System Stability and Control (The EPRI Power System Engineering Series). New York, NY, USA: McGraw-Hill, 1994.

[11] Y. Liao, “Some algorithms for transmission line parameter estimation,” 2009 41st Southeastern Symposium on System Theory, Tullahoma, TN, 2009, pp. 127-132. doi: 10.1109/SSST.2009.4806781

[12] X. Jiao and Y. Liao, “A linear estimator for transmission line parameters based on distributed parameter line model,” 2017 IEEE Power and Energy Conference at Illinois (PECI), Champaign, IL, 2017, pp. 1-8. doi: 10.1109/PECI.2017.7935724

[13] Y. Liao and M. Kezunovic, “Online optimal transmission line parameter estimation for relaying applications,” in IEEE Transactions on Power Delivery, vol. 24, no. 1, pp. 96-102, Jan. 2009. doi: 10.1109/TPWRD.2008.2002875

[14] M. Lahmar and Y. Liao, “Accurate methods for estimating transmission line parameters using synchronized and unsynchronized data,” 2017 International Energy and Sustainability Conference (IESC), Farmingdale, NY, 2017, pp. 1-5. doi: 10.1109/IESC.2017.8167474

[15] Y. Liao, “Power transmission line parameter estimation and optimal meter placement,” Proceedings of the IEEE SoutheastCon 2010 (SoutheastCon), Concord, NC, 2010, pp. 250-254. doi: 10.1109/SECON.2010.5453876

[16] PSC North America. Review of Series Compensation for Transmission Lines. 2014.

[17] A. Arif, Z. Wang, J. Wang, B. Mather, H. Bashualdo, and D. Zhao, "Load modeling—a review," IEEE Trans. Smart Grid, vol. 9, no. 6, pp. 5986–5999, Nov. 2018, doi: 10.1109/tsg.2017.2700436cccc.

[18] M. Usman, A. Cervi, M. Coppo, F. Bignucolo, and R. Turri, "Centralized OPF in unbalanced multi-phase neutral equipped distribution networks hosting ZIP loads," IEEE Access, vol. 7, pp. 177890–177908, 2019, doi: 10.1109/access.2019.2958695.

[19] D. He, T. Habetler, M. J. Mousavi, and N. Kang, "A ZIP model-based feeder load modeling and forecasting method," presented at the 2013 IEEE Power & Energy Society General Meeting, 2013, doi: 10.1109/pesmg.2013.6672997.

[20] M. K. Dosoglu and M. Dursun, "Investigation with ZIP load model of voltage stability analysis in wind turbine integrated power system," presented at the 2018 2nd International Symposium on Multidisciplinary Studies and Innovative Technologies (ISMSIT), Oct. 2018, doi: 10.1109/ismsit.2018.8567310.

[21] W. Fan et al., "Distribution system voltage and var optimization," 2012 IEEE Power and Energy Society General Meeting. IEEE, Jul. 2012. doi: 10.1109/pesgm.2012.6345208.

[22] W. Fan et al., "A CVR On/Off Status Detection Algorithm for Measurement and Verification," presented at the 2021 IEEE Power & Energy Society Innovative Smart Grid Technologies Conference (ISGT), Feb. 2021, doi: 10.1109/isgt49243.2021.9372257.

[23] Z. S. Hossein et al., "Conservation voltage reduction and volt-var optimization: measurement and verification benchmarking," IEEE Access, vol. 8. Institute of Electrical and Electronics Engineers (IEEE), pp. 50755–50770, 2020. doi: 10.1109/access.2020.2979242.

[24] M. Sadeghi and G. Abdollahi sarvi, “Determination of ZIP parameters with least squares optimization method,” presented at the Energy Conference (EPEC), Oct. 2009, doi: 10.1109/epec.2009.5420883.

[25] A. Bokhari et al., “Experimental determination of the zip coefficients for modern residential, commercial, and industrial loads,” IEEE Trans. Power Delivery, vol. 29, no. 3, pp. 1372–1381, Jun. 2014, doi: 10.1109/tpwrd.2013.2285096.

[26] K. Wang, H. Huang, and C. Zang, “Research on time-sharing ZIP load modeling based on linear BP network,” presented at the 2013 5th International Conference on Intelligent Human-Machine Systems and Cybernetics (IHMSC), Aug. 2013, doi: 10.1109/ihmsc.2013.16.

[27] H. Fan, T. Zhang, H. Yu, and G. Geng, “Identifying ZIP coefficients of aggregated residential load model using AMI data,” presented at the 2019 IEEE 3rd International Electrical and Energy Conference (CIEEC), Sep. 2019, doi: 10.1109/cieec47146.2019.cieec-2019582.

[28] H. Bai, P. Zhang, and V. Ajjarapu, “A novel parameter identification approach via hybrid learning for aggregate load modeling,” IEEE Trans. Power Syst., vol. 24, no. 3, pp. 1145–1154, Aug. 2009, doi: 10.1109/tpwrs.2009.2022984.

[29] A. Shahsavari, M. Farajollahi, and H. Mohsenian-Rad, “Individual load model parameter estimation in distribution systems using load switching events,” IEEE Trans. Power Syst., vol. 34, no. 6, pp. 4652–4664, Nov. 2019, doi: 10.1109/tpwrs.2019.2919901.

[30] M. Bircan, A. Durusu, B. Kekezoglu, O. Elma, and U. S. Selamogullari, “Experimental determination of ZIP coefficients for residential appliances and ZIP model based appliance identification: The case of YTU Smart Home,” Electric Power Systems Research, vol. 179, p. 106070, Feb. 2020, doi: 10.1016/j.epsr.2019.106070.

[31] J. J. Grainger and W. D. Stevenson. Power System Analysis. New York: McGraw-Hill, 1994.

[32] Y. Huang, Y. Zhang, Y. Zhao, P. Shi, and J. A. Chambers, “A novel outlier-robust Kalman filtering framework based on statistical similarity measure,” IEEE Transactions on Automatic Control, vol. 66, no. 6. Institute of Electrical and Electronics Engineers (IEEE), pp. 2677–2692, Jun. 2021. doi: 10.1109/tac.2020.3011443.

[33] Y. Huang, Y. Zhang, B. Xu, Z. Wu, and J. A. Chambers, “A new adaptive extended Kalman filter for cooperative localization,” IEEE Transactions on Aerospace and Electronic Systems, vol. 54, no. 1. Institute of Electrical and Electronics Engineers (IEEE), pp. 353–368, Feb. 2018. doi: 10.1109/taes.2017.2756763.

[34] Y. Huang, Y. Zhang, Z. Wu, N. Li, and J. Chambers, “A novel adaptive Kalman filter with inaccurate process and measurement noise covariance matrices,” IEEE Transactions on Automatic Control, vol. 63, no. 2. Institute of Electrical and Electronics Engineers (IEEE), pp. 594–601, Feb. 2018. doi: 10.1109/tac.2017.2730480.

[35] A. Kaba and E. Kıyak, “Optimizing a Kalman filter with an evolutionary algorithm for nonlinear quadrotor attitude dynamics,” Journal of Computational Science, vol. 39. Elsevier BV, p. 101051, Jan. 2020. doi: 10.1016/j.jocs.2019.101051.

[36] Y. Ji et al., “An equivalent modeling method for multi-port area load based on the extended generalized ZIP load model,” presented at the 2018 International Conference on Power System Technology (POWERCON), Nov. 2018, doi: 10.1109/powercon.2018.8601588.

[37] H. Ren, N. N. Schulz, V. Krishnan, and Y. Zhang, “Online Static Load Model Estimation in Distribution Systems,” 2019 IEEE 28th International Symposium on Industrial Electronics (ISIE). IEEE, Jun. 2019. doi: 10.1109/isie.2019.8781530.

[38] C. Mishra, V. A. Centeno, and A. Pal, “Kalman-filter based recursive regression for three-phase line parameter estimation using synchrophasor measurements,” 2015 IEEE Power & Energy Society General Meeting. IEEE, Jul. 2015. doi: 10.1109/pesgm.2015.7285678.

[39] S. Gajare, A. K. Pradhan, and V. Terzija, “A Method for Accurate Parameter Estimation of Series Compensated Transmission Lines Using Synchronized Data,” IEEE Transactions on Power Systems, vol. 32, no. 6. Institute of Electrical and Electronics Engineers (IEEE), pp. 4843–4850, Nov. 2017. doi: 10.1109/tpwrs.2017.2679542.

[40] F. R. C. Soldevilla and F. A. C. Huerta, “Estimation of transmission lines parameters using particle swarm optimization,” *2018 IEEE PES Transmission & Distribution Conference and Exhibition - Latin America (T&D-LA)*, Lima, 2018, pp. 1-5. doi: 10.1109/tdc-la.2018.8511793.

[41] S. V. Unde and S. S. Dambhare, “Double circuit transmission line parameter estimation using PMU,” *2016 IEEE 6th International Conference on Power Systems (ICPS)*, New Delhi, 2016, pp. 1-4. doi: 10.1109/ICPES.2016.7584163

[42] D. Yildiz, S. Karagol and O. Ozgonenel, “Estimation of online transmission line parameters and fault location by using different differential Equation algorithms,” *2015 9th International Conference on Electrical and Electronics Engineering (ELECO)*, Bursa, 2015, pp. 1034-1038. doi: 10.1109/ELECO.2015.7394500

[43] A. M. Dán and D. Raisz, “Estimation of transmission line parameters using wide-area measurement method,” *2011 IEEE Trondheim PowerTech*, Trondheim, 2011, pp. 1-6. doi: 10.1109/ptc.2011.6019406.

[44] R. Rubesa, V. Kirincic and S. Skok, “Transmission line positive sequence impedance estimation based on multiple scans of Phasor Measurements,” *2014 IEEE International Energy Conference (ENERGYCON)*, Cavtat, 2014, pp. 644-651. doi: 10.1109/ENERGYCON.2014.6850495

[45] L. Ding, T. Bi and D. Zhang, “Transmission line parameters identification based on moving-window TLS and PMU data,” *2011 International Conference on Advanced Power System Automation and Protection*, Beijing, 2011, pp. 2187-2191. doi: 10.1109/APAP.2011.6180790

[46] C. Li, Y. Zhang, H. Zhang, Q. Wu and V. Terzija, “Measurement-based transmission line parameter estimation with adaptive data selection scheme,” in *IEEE Transactions on Smart Grid*, vol. 9, no. 6, pp. 5764-5773, Nov. 2018. doi: 10.1109/APAP.2011.6180790

[47] X. Bian, X. R. Li, H. Chen, D. Gan and J. Qiu, “Joint estimation of state and parameter with synchrophasors—part I: state tracking,” in *IEEE Transactions on Power Systems*, vol. 26, no. 3, pp. 1196-1208, Aug. 2011. doi: 10.1109/TPWRS.2010.2098422

[48] C. Ye, S. Feng, P. Xu and J. Liu, “Transmission line parameter identification considering non-synchronized time of fault recording information,” *2018 2nd IEEE Advanced Information Management,Communicates,Electronic and Automation Control Conference (IMCEC)*, Xi'an, 2018, pp. 1749-1753. doi: 10.1109/IMCEC.2018.8469344

[49] M. Zhan, S. Zhou, B. Li, L. Li, G. Lin and J. Yi, “Parameter estimation of transmission line based on GATS,” *2010 International Symposium on Computational Intelligence and Design*, Hangzhou, 2010, pp. 179-182. doi: 10.1109/ISCID.2010.134

[50] P. Ren, H. Lev-Ari and A. Abur, “Tracking three-phase untransposed transmission line parameters using synchronized measurements,” in *IEEE Transactions on Power Systems*, vol. 33, no. 4, pp. 4155-4163, July 2018. doi: 10.1109/TPWRS.2017.2780225

[51] X. Chen, Y. Li and J. Luo, “An extraction method of distributed parameters for one type of unparallel transmission lines,” *2014 IEEE International Conference on Signal Processing, Communications and Computing (ICSPCC)*, Guilin, 2014, pp. 767-770. doi: 10.1109/ICSPCC.2014.6986300

[52] Z. Wu, L. T. Zora and A. G. Phadke, “Simultaneous transmission line parameter and PMU measurement calibration,” *2015 IEEE Power & Energy Society General Meeting*, Denver, CO, 2015, pp. 1-5. doi: 10.1109/PESGM.2015.7286115

[53] I. Ivanov and A. Murzin, “Synchrophasor-based transmission line parameter estimation algorithm taking into account measurement errors,” *2016 IEEE PES Innovative Smart Grid Technologies Conference Europe (ISGT-Europe)*, Ljubljana, 2016, pp. 1-6. doi: 10.1109/ISGTEurope.2016.7856301

[54] S. He and S. K. Starrett, “Modeling power system load using adaptive neural fuzzy logic and artificial neural networks,” presented at the 2009 North American Power Symposium - NAPS, Oct. 2009, doi: 10.1109/naps.2009.5483985.

[55] “IEEE recommended practice for electric power distribution for industrial plants,” IEEE Standard 141-1993, pp. 1–768, April 1994.

[56] H. E. Rojas-Cubides, A. S. Cruz-Bernal, and H. D. Rojas-Cubides, “Analysis of voltage sag compensation in distribution systems using a multilevel DSTATCOM in ATP/EMTP,” DYNA, vol. 82, no. 192, pp. 26–36, Aug. 2015. doi: 10.15446/dyna.v82n192.48566

[57] Y. Zhang and Y. Liao, “Kalman filter approach for line parameter estimation for long transmission lines,” 2020 IEEE Power and Energy Conference at Illinois (PECI). IEEE, Feb. 2020. doi: 10.1109/PECI48348.2020.9064634

[58] Y. Zhang, Y. Liao, E. Jones, N. Jewell, and D. M. Ionel, “Kalman filter based approach for ZIP load modeling for aggregate loads,” 2021 IEEE Kansas Power and Energy Conference (KPEC). IEEE, Apr. 19, 2021. doi: 10.1109/KPEC51835.2021.9446202

[59] Y. Zhang and Y. Liao, “Optimal line parameter estimation method for mid-compensated transmission lines,” 2019 North American Power Symposium (NAPS). IEEE, Oct. 2019. doi: 10.1109/naps46351.2019.9000274.

[60] Y. Zhang and Y. Liao, “Series compensated transmission line parameter estimation based on Kalman filter,” 2020 SoutheastCon. IEEE, Mar. 28, 2020. doi: 10.1109/SoutheastCon44009.2020.9249656

[61] Y. Zhang and Y. Liao, “Kalman filter based method for tracking dynamic transmission line parameters,” SN Applied Sciences, vol. 3, no. 1. Springer Science and Business Media LLC, Jan. 2021. doi: 10.1007/s42452-020-04036-8

[62] Y. Zhang, Y. Liao, E. Jones, N. Jewell, D. M Ionel, “ZIP load modeling for single and aggregate loads and CVR factor estimation,” PAC World Conference, August 31-September 1, 2021. https://uknowledge.uky.edu/ece_present/1.

[63] P. Ren, A. Abur, and H. Lev-Ari, “Tracking transmission line parameters in power grids observed by PMUs,” 2019 IEEE Milan PowerTech. IEEE, Jun. 2019. doi: 10.1109/PTC.2019.8810838

[64] P. Ren, H. Lev-Ari, and A. Abur, “Tracking three-phase untransposed transmission line parameters using synchronized measurements,” IEEE Transactions on Power Systems, vol. 33, no. 4. Institute of Electrical and Electronics Engineers (IEEE), pp. 4155–4163, Jul. 2018. doi: 10.1109/TPWRS.2017.2780225

[65] X. Wang et al., “Evaluating load models and their impacts on power transfer limits,” 2020 IEEE 16th International Conference on Control & Automation (ICCA). IEEE, Oct. 09, 2020. doi: 10.1109/ICCA51439.2020.9264570

VITA

Education

01/2017 – 12/2021

Ph.D. Student

Department Electrical and Computer Engineering, University of Kentucky,

Lexington, Kentucky, USA

09/2013 – 05/2015

Master of Engineering

Department of Electrical and Computer Engineering, University of Maryland,

College Park, Maryland, USA

10/2009 – 06/2013

Bachelor of Engineering

College of Electrical and Electronic Engineering, Shanghai Institute of Technology

Shanghai, China

Awards

07/2020 – 05/2021

Research Assistant, University of Kentucky, Lexington, KY, USA

08/2017 – 05/2020

Teaching Assistant, University of Kentucky, Lexington, KY, USA

09/2009 – 06/2013

Awarded Scholarships for seven semesters, Shanghai Institute of Technology, Shanghai, China